Hydrogen storage in salt caverns

Chemical modelling and analysis of large-scale hydrogen storage in underground salt caverns.

by

Maarten Pieter Laban

to obtain the degree of Master of Science
at the Delft University of Technology,
to be defended publicly on 16-07-20

Student number:	4228650	
Project duration:	September 2, 2019 – Mei 1, 2020	
Thesis committee:	Prof.dr.Ir. P. Herder	TU Delft, chair
	Assoc.prof.Ir. H. Hajibeygi	TU Delft
	Prof.dr.Ir. S. Klein,	TU Delft
	Ir. E. van Ruijven	Vattenfall

TU Delft

Acknowledgements

First and foremost, I would like to thank Prof. dr. ir. P.M. Herder and Prof. dr. ir. S. Klein for supervising my master thesis. Thank you for challenging me to get it right and for the more then insightful feedback on my work.
Secondly I would like to thank Assoc.prof. H. Hajibeygi, for allowing me, as a mechanical engineer, to participate in the many meetings of the geo-science oriented ADMIRE group. You are an inspiring teacher and the possibility for me to present my work and to reflect have been very helpful.
I would like to thank both my supervisors from Vattenfall, Ir. E. van Ruijven and Ir. C. Nijhof for their costly time and insightful meetings. I would also like to thank Ir. S. Bojert for answering my many questions, allowing me access to the cavern data and accompanying me to the HYPOS convention.

I would like to dedicate this work to young Ozzy. By doing so, I hope he will become an engineer as well.

Nomenclature

Abbreviations

MDEA	-	3,4-Methylenedioxy-N-ethylamphetamine
TEG	-	Triethylene glycol
H2	-	Hydrogen gas
H2S	-	Hydrogensulfide
CO2	-	Carbon Dioxide
CO	-	Carbon-Monoxide
NaCl	-	Halite/ Rocksalt
CaSO4	-	Anhydrite
OPEX	-	Operating Expenditures
CAPEX	-	Capital Expenditures
EU	-	European Union
NL	-	the Netherlands
PHREEQC	-	pH-REactive-EQuilibrium-C
SMR	-	Steam Methane Reforming
CCS	-	Carbon Capture Storage
UV	-	Ultra-Violet
PEM	-	Proton Exchange Membrane
GTS	-	Gasunie Transport Services
HHV	-	Higher Heating Value
TNO	-	the Netherlands Organisation for applied scientific research
BRR	-	Bacterial Reduction Rate
BSR	-	Bacterial Sulfate Reduction
SRB	-	Sulfate Reducing Bacteria
OGE	-	Open Grid Europe

Abstract

In this paper the suitability of compressed hydrogen gas storage in salt caverns is analysed. The presence of microbial sulfate reducing bacteria create a contamination risk of H2S inside the cavern. Key cavern parameters that influence the production of H2S are highlighted by a chemical model. The model uses empirical data provided by Vattenfall, in order to predict what would happen inside cavern S43, would it be contaminated by sulfate reducing bacteria. By doing so, it can be understood what cavern conditions are suitable for the storage of hydrogen. An analysis is done on the above ground process of a salt cavern storage plant to determine what extra separation steps are required to reach ISO limitations for hydrogen gas. The research is done by answering the following research questions:

What are key cavern conditions that influence the suitability of hydrogen storage in salt caverns and for what purpose can the storage plant be implemented?

The sub-research objectives are formulated as follows:

1. *What are the potential process risks when storing hydrogen in salt caverns?*
2. *Are there substantial risks of contamination with subsurface hydrogen storage? What are the defining variables that contribute to said contamination?*
3. *How do these impurities build up when the salt cavern is used?*
4. *Is the equipment currently used in the gas storage facility in Epe useable for hydrogen gas storage? What changes should be made to the current storage process?*

When analysing future utilisation demands of hydrogen, one of the primary applications is energy conversion by fuel cells. There are severe limitations set by the International Organization for Standardization on the maximum amount of H2S in hydrogen gas used by fuel cells. This paper uses a chemical model based on PHREEQC to predict the chemical reactions in the cavern. In order to get close to actual results, the model input is constructed following empirical data of an existing salt cavern. With the chemical model different cases can be constructed each highlighting an important cavern constraint. What are the positive and negative forces on the production of H2S in salt caverns and what could be theoretically done to prevent H2S contamination? Primary aspects that positively contribute to H2S production, when the cavern is modelled as a batch reactor, sorted by significance are:

- Bacterial growth and reduction rate
- Brine volume and sulfate concentration.
- Brine pH and ionic strength.
- Cavern pressure and temperature.
- Fe2+ and Fe3+ concentration.

The chemical model only predicts what will happen in the cavern when there is no gas coming in or out, like a batch reactor. For this reason a dynamic model is constructed which predicts H2S outflow in the gas when applying different demand-cases to the cavern. The model results showed that with applying a maximum use case, which fluctuates between the maximum pressure and minimum pressure, there is still a minimum H2S output that is higher then the allowed limits. A demand curve is simulated where the cavern is used to power a hydrogen gas-turbine to profit from seasonal energy price changes. In this demand curve the cavern produces significantly less and less often, giving time for the H2S to build up. In two years, the H2S production reaches levels above the allowable limits set for hydrogen gas turbines.

A gas process facility is required to eliminate H2S contamination, in order to size such a facility it was modelled in Aspen Hysys. The model is validated by using data from literature. After analyses of resulting process equipment and gas streams, the absorber tower's efficiency is most dependant on its temperature its pressure and the absorbent flow rate. The water concentration is above ISO levels when withdrawn from the cavern. So to follow these limitations, an additional dehydration step is required. In conclusion the process is capable of accurately separating the H2S to below ISO limits. The process works using 3% of the potential chemical energy of hydrogen. The process is unable to purify the water concentrations.

As a result of this research some conclusions can be made. When using salt caverns for long term hydrogen storage can be a significant risk of H2S contamination as a result of microbial sulfate reduction. For the reference case the H2S concentrations reach above the levels set for fuel cell use and concentrations will increase in significance when utilisation of the cavern is decreased. For fuel cell application, a separation process based on MDEA gas sweetening can be used to get the hydrogen up to the demanded H_2S purity. But a more economical solution would involve extensive testing of the cavern soil for any microbial activity. If there are no sulfate reducing bacteria there will be no problem. Other pre-process steps could involve increasing the pH of the brine in the cavern to avoid H2S production. As well as increasing the iron concentration in the brine.

Contents

List of Figures

List of Tables

1 Introduction

In this report, a study on the suitability of large scale underground salt cavern storage for hydrogen gas is presented as a project created by Vattenfall Amsterdam and supervised by the Delft University of Technology. This chapter illustrates the problem at hand. It gives valuable background information required to understand the vastly changing world of hydrogen energy and it highlights both the positives as the challenges that arise in this new world. Next, the research question is outlined in section 1.3. Its approach is described in section 1.4. Finally, to narrow the research area, the scope is defined in section 1.5.

1.1. Problem background

To create a complete view of the potential of hydrogen gas, this chapter will take a closer look at the (potential) benefits and challenges that accompany the use of the smallest molecule in the universe. An illustration on the use of hydrogen is given in figure 1.1

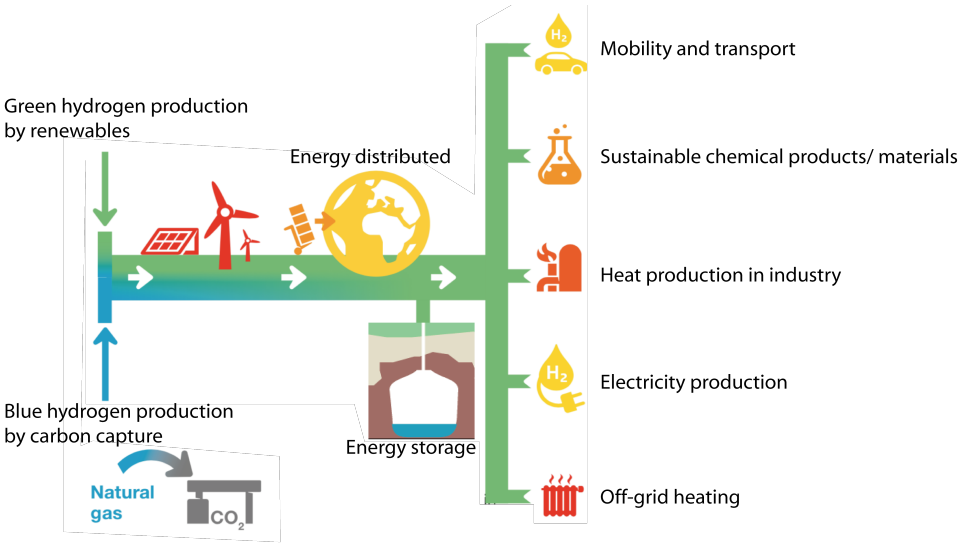

Figure 1.1: Roadmap of hydrogen, from production to storage to potential use.

1.1.1. The potential of hydrogen

One of the great benefits of hydrogen is the diversity of industries in which it can be applied. One of these advances is the possible use of hydrogen in 'deep' emissions in hard-to-abate sectors. These emissions are in industries where electricity is not the applied form of energy, or where electricity-based solution have high costs and drawbacks. Hard-to-abate emissions include aviation, shipping, iron and steel production, chemical manufacturing, high-temperature industrial heat, long-distance road transport and off-grid heat

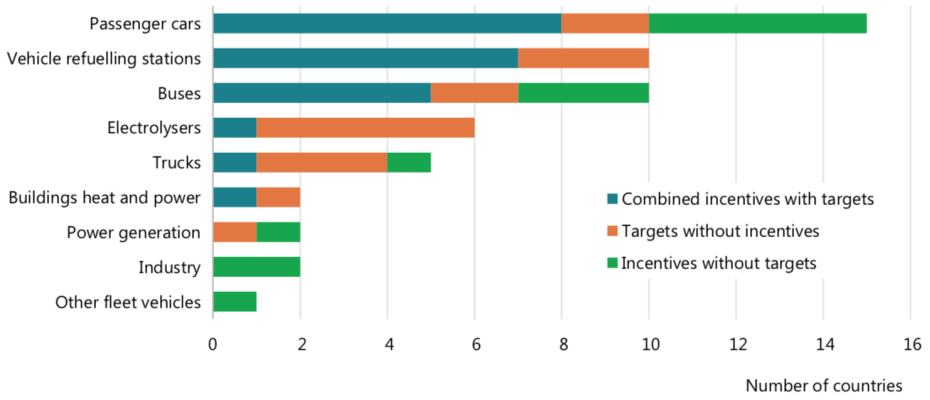

Figure 1.2: Policies directly supporting hydrogen deployment by target application[47]

for buildings. As a low-carbon chemical energy carrier, hydrogen is a leading prospect for reducing these hard-to-abate emissions as it can be stored, combusted and combined in chemical reactions, using processes that are similar to natural gas, oil and coal. [47]
Another benefit of hydrogen is its ability to supplement other technologies. As the declining renewable energy costs enables competitiveness of the production of clean hydrogen, converting electricity to hydrogen can positively influence the way these renewable energy technologies are being used. For example by optimising down time of solar and wind energy production, or by supporting energy security on the imbalance market. International hydrogen trade could, in an ambitious low-carbon context, provide the possibility of trade and storage of solar and wind energy between different countries to overcome seasonal and environmental differences.
The versatility of hydrogen is not only found in its appliances, also the way it is stored, transported and produced are highly adaptable. Hydrogen can be stored in the ground, as is the primary subject of this report, but also in metal containers, as a liquid, gas, or attached to solids. It can be transformed to electricity, methane or ammonia. Produced using renewables, nuclear, natural gas, coal and oil. Transported by pipeline or in bulk. The possibilities for hydrogen gas seem endless, but first there are some substantial challenges that need to be remedied.

- *Production:*
  Currently the production of hydrogen is almost entirely supplied from natural gas and coal, as is illustrated in the Sankey diagram of figure 1.4. To overcome this challenge on this scale will require a larger portion of hydrogen to be produced by renewables. Supplementary to this 'green' hydrogen production, it will require a larger portion of 'grey' hydrogen, produced from fossil fuels, to implement CO2 capturing technology. This way making the process carbon neutral. More depth in to the production of hydrogen will be specified in chapter A.1.1.

- *Cost:*
  Following on from the challenges that arise from the method of hydrogen production is the cost of hydrogen. The production price of hydrogen is highly dependant on the method of production, the location of production and the quantity produced. Looking at the estimated price progression of green hydrogen production by renewable energy, as displayed in figure 1.3, it is seen that theoretically the price of green hydrogen produced in Germany (blue line in the left figure) will be able to compete with large scale grey hydrogen production, from fossil fuels, from 2026 onward [92].

- *Molecular properties of hydrogen*
  The biggest challenge when processing hydrogen gas are related to the chemical properties of the gas. Hydrogen gas has the lowest density of all gasses, which means it will take up more space when it is compressed, which results in a larger storage volume. Another problem comes with the small size of the molecule, which makes it very difficult to contain. Especially when pressurised, the gas molecule can slip through the cracks or porosity of the containment material, creating possible hazardous situations and an overall loss of material. This creates a challenge, both for the transportation as well for the

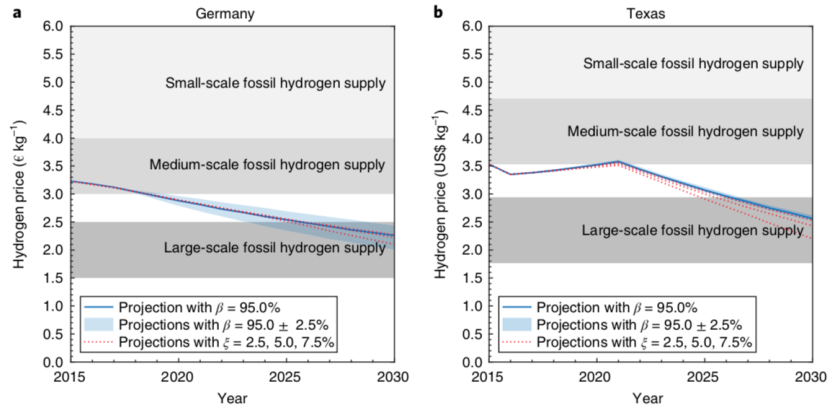

Figure 1.3: Prospects for renewable hydrogen production. a,b, The break-even price of renewable hydrogen for Germany (a) and Texas (b) relative to the benchmark prices for fossil hydrogen supply. β= adjustment rate, ξ= energy price differentiation. [39]

storage of hydrogen gas. Operationally, hydrogen embrittlement can prove to be big concern. Hydrogen embrittlement refers to a variety of effects hydrogen has on the mechanical properties of metals. The presence of hydrogen can cause metals to crack, blister and lose its strength an ductility, especially in the use of high strength steel.[58]. Another possible issue to consider is the interaction of hydrogen with chemical species present in underground reservoirs. The possible chemical reactions could cause the production of toxic gas as well as the loss of hydrogen. [33].

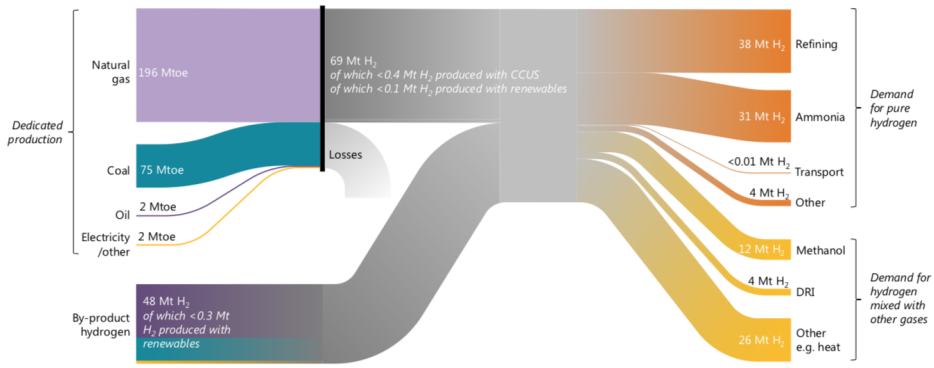

Figure 1.4: Today's hydrogen value chains Sankey diagram[47]

With the positives and negatives of hydrogen technology explained, the next section will shortly discuss different methods of storing it.

1.1.2. Storage methods

Transport and storage costs play an essential role in the competitiveness of hydrogen. The economic potential of hydrogen arises from the fact that it can be stored in large quantities for a long time and that with the right infrastructure hydrogen is available for long-distance transport. This results in a technology that is both beneficial to energy transportation and energy storage. Methods for storing hydrogen are appropriated based on the stored volume, the duration of storage, the required speed of discharge and the geographic availability of the various alternatives. The current perspective is to store hydrogen as a gas or liquid in tanks for stationary or mobile applications.

Liquidised hydrogen is cooled to approximately −253°C[77], where the hydrogen reaches its liquid form. This way the hydrogen can be stored in atmospheric pressure. However, the hydrogen has to be heavily insulated to minimise any boil off. Typical liquefied hydrogen boil-off rate can reach up to 0.2% per day [7].

The process of liquefication of hydrogen is costly and not very efficient. However, liquefied hydrogen can be a cost-effective solution when transporting large amounts over vast distances. For long term storage, the energy requirements needed to keep the hydrogen liquefied will prove to be the limiting factor. For this reason this report will focus entirely on pressurised hydrogen gas.

Pressurised hydrogen can be stored in vessels or underground storage facilities. When comparing hydrogen gas to natural gas, the difference in energy per volume is paramount. The low volumetric density of hydrogen makes it necessary to store it in containers with maximised pressure to minimise storage or transportation volume. Pressurised hydrogen at 700 bar for example still only has 15% of the volumetric energy density of natural gas. For this reason, hydrogen fuel refilling station would need seven times the space of a current natural gas refuelling station.

When handling significant amounts of hydrogen, as is necessary for continuous operations in an international value chain, pressurised tanks or liquid storage vessels do not suffice. Substantially sized hydrogen storage can take place in underground storage facilities. Salt caverns, depleted natural gas reservoirs and aquifers are all viable options.[56] Differences between the three are primarily found in the propriety of their use with hydrogen. Unlike gas reservoirs and aquifers, where difficulties can arise with the permeability of the storage environment, salt caverns have been used to store pure hydrogen in the United Kingdom since the 1970s and in the United States since the 1980s [59].
Salt cavern storage produces high efficiencies and competitive storage costs, as is seen in figure 1.5. Figure 1.6 further explains the hydrogen storing process, as well as defining the positive aspects of salt cavern storage in comparison to alternative large scale storage options. Radosław Tarkowski sums it up in his review on the potential of hydrogen storage in Poland: "Rock salt is chemically neutral to hydrogen, the walls of a salt cavern are impermeable for hydrogen and plasticity of salt prevents formation and propagation of fractures that could compromise the reservoir's tightness." [86] A salt cavern in the European Union on average has a volume of around 680.000m^3 and can reach pressures of up to 250 bar, depending on the depth of the cavern. The salt caverns are primarily used for natural gas storage, as 112 billion m^3, or 987 TWh, of methane is currently stored in salt caverns in the EU alone.[75]
The large volume of methane stored gives high hopes for hydrogen salt cavern storage. The only apparent limitation being possible geographic locations of these man-made underground salt domes.

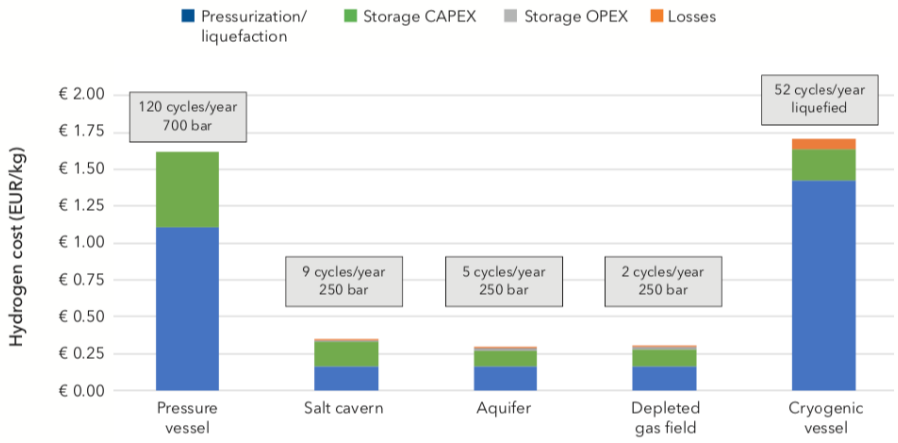

Figure 1.5: Overview of storage costs of hydrogen based on throughput[75]

1.2. Problem statement

When the diverse spectrum of hydrogen related technologies will be implemented in the near future, great interest will follow towards efficient long term, large scale storage. Salt cavern storage has proven with natural gas to be a viable solution for gas storage and seems to be a suitable option for hydrogen as well. In the literature review of chapter 2, the largest operating problems surrounding hydrogen are highlighted. Leakage

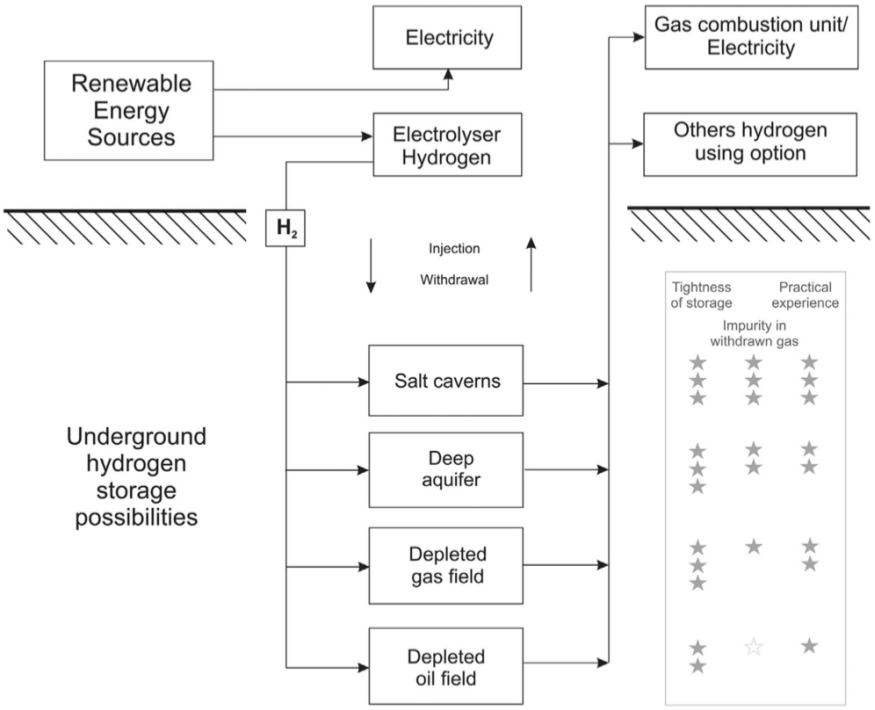

Figure 1.6: The concept of underground hydrogen storage in geological structures.[86]

risks, hydrogen embrittlement, risks of contamination, cost and volumetric density are factors which should be taken into account. The literature review showed that there is a lack of knowledge on what happens inside the cavern. A cavern operator should be fully comfortable knowing that the gas purity remains constant throughout the process. This research will therefore focus on the cavern's internal chemical processes, to determine if the hydrogen purity can be guaranteed.

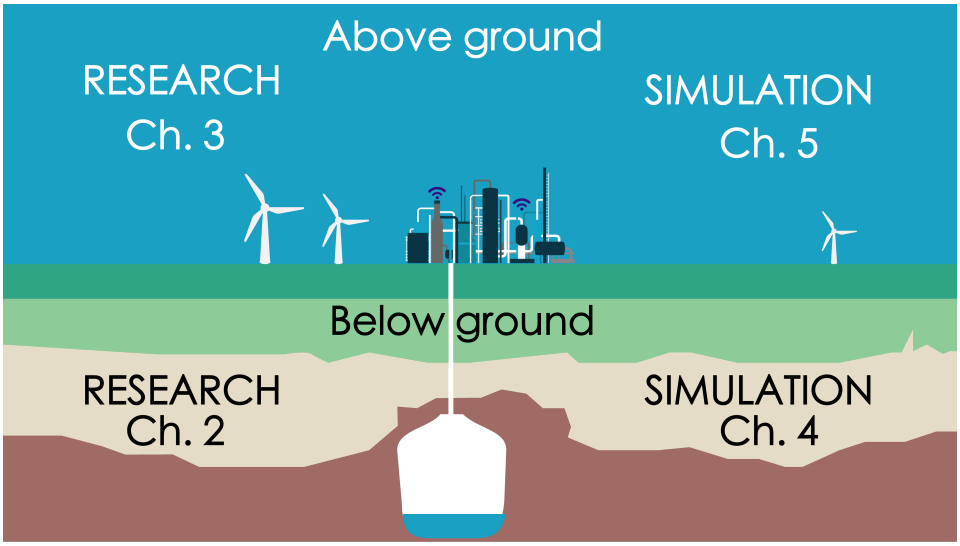

Figure 1.7: Overview of the paper layout.

1.3. Research objective

Combining the problem statement and problem background presented in this chapter, the main question of this thesis can be stated as follows:

What are key cavern conditions that influence the suitability of hydrogen storage in salt caverns and for what purpose can the storage plant be implemented?

The sub-research objectives are formulated as follows:

1. *What are potential process risks when storing hydrogen in salt caverns?*
2. *Are there substantial risks of contamination with subsurface hydrogen storage? What are the defining variables that contribute to said contamination?*
3. *How do these impurities build up when the salt cavern is used?*
4. *Is the equipment currently used in the gas storage facility in Epe useable for hydrogen gas storage? What changes should be made to the current storage process?*

The report is structured in such a way that sub-objectives are dedicated to specific chapters as explained in the following section (1.4) where the approach of this research is given.

1.4. Research approach

First of all, this report will need to answer the first sub-question and find out where the high risk areas will be when storing hydrogen in salt caverns. To do this a literature review is done, making a step by step journey through the below ground storage process in chapter 2. This way, high risk risk areas can be explained and this report finds out where literature alone proves to be unfulfilling when trying answer the sub-questions.
In chapter 3 the above ground process is analysed of an existing natural gas salt cavern storage plant. The goal in this chapter is to get a clear view of how the storage plant operates and to calculate constraints that are used in both the above and below ground process simulations. Investigation of cavern contamination can be divided into two equally important parts: First, a research should be done on the cause of contamination, the factors that define the level of contamination and what could be done to prevent contamination in the first place. This part, chapter 4, will be called the below ground process, what happens inside the cavern. The second part, chapter 5, concerns the above ground process and concerns what should be done to filter out the impurities in the gas flow coming out of the cavern. This is illustrated in figure 1.7
The cavern, cavern S43, that will be researched in this thesis is located in Epe Germany and is operated

by NUON Vattenfall. The data supplied by Vattenfall will determine the cavern and brine composition and dimensions. The cavern in Epe is selected, based on its average shape, size and depth.

1.4.1. Below ground process:

The goal is to build or find a modelling structure that can simulate gas mixture equations of state, transport of gas in aqueous solution, solid liquid equilibrium reactions and kinetic reactions. Lastly, it should do all this over time. To model what happens inside the cavern, this report uses the chemical modelling software PHREEQC. The model is verified by analysing its use in literature and by analysing different crucial reactions in the cavern, and comparing it to experimental data from literature. The saturation limit of NaCl in water and the solubility of CaSO4 are used for the verification. Following the results of the verification methods, there is an error in the solubility rate of minerals in brine with high ionic strength, which is is taken into account in the conclusions of the chemical analysis.

1.4.2. Above ground process

The above ground process is simulated through process modelling software. Since PHREEQC has given an estimation of what happens inside the cavern, the output concentrations of the gas can be calculated. The concentration and accompanying gas stream parameters are taken as inputs to the processing software. The simulation method is verified by comparing empirical data of a reference gas sweetening plant operated by Lurgi [14], to model output with the same plant inputs. Therefore, verifying the accuracy of H2S absorbing as calculated by Aspen Hysys. The process is partially designed via sizing methods available in literature, and partially by running simulations in Aspen Hysys. The simulation of the process is used as an rough numerical estimate of a real process, which function is only to determine if its possible to purify the gas streams to the ISO limits, and to analyse if the energy and cost requirements of such a process are reasonable.

1.5. Scope of the research

In order to fulfil the objective of the research and ensure the quality, validity and reliability of the findings within the limited time available. The scope of the research is presented, confined by the objectives as formulated in section 1.3. This report will limit itself to the microbial production of H_2S inside hydrogen filled salt caverns. It is hereby assumed that there is no CO_2 present in the cavern, which will exclude the possibility of methanogenesis. The hydrogen that enters the cavern is assumed to be *pure* and no other gas traces are found in the cavern. The gas inside the cavern is assumed to be *homogeneously* mixed, the same goes for the brine.

The cavern (S43) that will be researched in this thesis is located in Epe Germany and is operated by NUON Vattenfall. The cavern wall is assumed to be *impermeable* for hydrogen gas. The cavern in question is assumed to be contaminated by *Sulfate Reducing Bacteria*. The contamination level and bacterial growth rate are determined from literature.

2

Analysis of hydrogen storage in salt caverns

This chapter will address the different aspects of the hydrogen storing process that might provide necessary information when designing a salt cavern hydrogen storage plant. The goal of this chapter is to accumulate a viable supply of information from literature with which calculations and conclusions can be made on a later stage and with which the first sub-question can be answered:

What are the potential risks when storing hydrogen in salt caverns?

This goal will be obtained by first listing the properties of gaseous hydrogen that are significant in section 2.1. Starting of with the methods of production, followed by the thermal and chemical properties, concluded by the different safety aspects of hydrogen. This way a sub-conclusion can be given as to where the greatest risks will emerge in the process of sub surface gas storage in a salt caverns.
The same idea is applied to the salt caverns in which the gas is trapped in section 2.3. First a small look into the creation of these caverns is given. After which the possible location, structure and risks of failure are analysed. Also, like with hydrogen, the significant properties of the salt caverns are examined. Lastly, in section 2.3.4, this chapter will give a short risk analysis summarising the information found in literature.

2.1. Properties of hydrogen

Hydrogen is a colourless, odourless, nonmetallic, tasteless, highly flammable diatomic gas with the molecular formula H_2. Hydrogen, with just one proton and one electron, an atomic weight of 1.00794, is the simplest and lightest element in the universe. With its simplicity it is also the most abundant of the chemical elements, constituting roughly 75% of the universe's elemental mass. It enables the sun to warm the earth by converting hundreds of millions of tons to helium every second. On earth, however, hydrogen is primarily available attached to one oxygen atom, as water. Gaseous hydrogen is not as abundantly available here on Earth since it forms covalent compounds with most available non-metallics. It provides an important role in acid-bases, reduction-oxidation (REDOX) chemistry, as the the reactions commonly involve the exchange of protons (H^+) between soluble molecules. Acidic solutions are defined by a low pH, which in turn is defined as the concentration of H^+ available in the solution. With higher concentrations of H^+ comes a lower pH, therefore an acidic solution. Through out this chapter hydrogen will be often compared to methane in order to get create a reference point of view. Throughout calculations in this report it is assumed that the hydrogen is produced via electrolysers. Which is referred to as green hydrogen, in green hydrogen impurities are rare, but can consist of N_2, O_2 and H_2O. Based off article [57]. When we consider grey hydrogen, produced using methane reforming, impurities are more frequent and can consist of CH_4, Ar, CO, CO_2 and N_2. More information on the different production methods can be found in the appendix A.1.

2.2. Hydrogen Hazards

By their nature, all fuels are in some degree dangerous. To determine the risk level that accompanies a type of fuel, depends on the characteristics of the fuel system and on the properties of the fuel. A number of hydrogen properties make it safer to use then other fuel types and a number of properties require additional

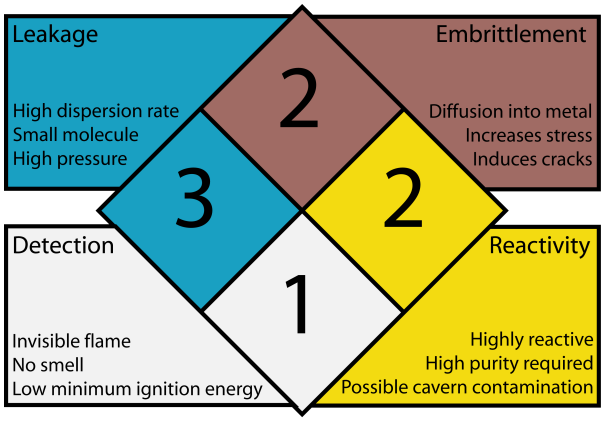

Figure 2.1: Hazzards of the use of high pressure hydrogen gas.

engineering controls to ensure safe use. Hydrogen safety can be divided and ranked into four different subsections: The leakage risks, the diffusion related embrittlement risks, problems with detection and possible contamination. This is illustrated in figure 2.1. The leakage risk is rated as the single biggest threat when processing high pressure hydrogen gas, the reason for this is explained in the following section.

2.2.1. Hydrogen embrittlement

Diffusion of hydrogen in metals has been the subject of great interest: [69],[13],[60],[76]. However is still not fully understood, because of the variety and complexity of mechanisms that can lead to embrittlement. Hydrogen embrittlement is a process where a metal becomes brittle, or fractures, due to the exposure or diffusion of hydrogen atoms, or ions, into the metal. In the storage process the primary cause of embrittlement are followed by the diffusion of hydrogen in the metal which followed by either absorption or adsorption of hydrogen into interstitial sites in metal lattices. The hydrogen can then either react to impurities or isotopes of metal, forming hydrides, or gasses and creating an imbalance in the metal structure.[13] Another more common form of embrittlement is caused by the diffusion of hydrogen to the metal grain boundaries, where it forms bubbles. These bubbles exert pressure on the metal grains. The pressure can build up to a point where the metal has reduced ductility and strength, which in turn can lead to cracks. [66] This is further illustrated in figure 2.2.

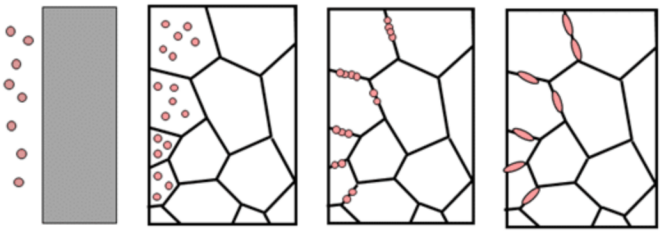

Figure 2.2: Embrittlement process
[66]

2.2.2. Hydrogen leakage

The high diffusion and dispersion rate of hydrogen can be seen as both its greatest safety asset, as well as the cause for its greatest concerns. As seen in table 2.2, the diffusivity of hydrogen in air is around three times higher then methane. Hydrogen embrittlement, as well as any other causes for cracks, holes and the smallest of openings will be the cause of hydrogen leakage. The small size of the molecule (125pm) in combination with a pressure driven force, will cause it to slip through materials previously thought were impermeable. In the storage process these risks will increase with pressure. All places with high pressure, from the compressor to the cavern, will be high risk areas. This will require extra attention to any seals, valves and piping equip-

ment used in the compressor stage as well as in the rest of the plant. The leak rate can be predicted when the leak rate of another gas is known using equation 2.1. Here M_x are the molecular weight of the two gasses. When comparing the leak rate of hydrogen relative to that of natural gas, a leakage ratio of 3.1 is calculated. These rough estimates do not take the viscosity into account [41]. When hydrogen leaks the high dispersion rate will prove a safety asset, as it will prevent build-up and therefore reduces explosive risks.

$$R_1 = R_2 \sqrt{(\frac{M_2}{M_1})} \tag{2.1}$$

2.2.3. Detection

Hydrogen and Methane are both odourless, colourless and tasteless. The smell of natural gas however is achieved by addition of an odorant as a safety measure. The odorant often used for natural gas is Butanethiol, also known as Butyl-Mercaptan. Mercaptan has the same chemical structure as alcohols except that the -OH groups are replaced with the Sulfur containing -SH groups. These Sulfur groups can contaminate fuel cells and are therefore incompatible with hydrogen gas. Properties of a suitable hydrogen odorant are highly specific as there is no known odorant light enough to "travel with" hydrogen at an equal dispersion rate.
Unlike Methane, a hydrogen gas flame is invisible in daytime conditions. Therefore, a hydrogen flame can not be easily detected by people during the day. Invisibility of hydrogen flames is due to the distinct spectra resulted by burning of hydrogen. Burning hydrogen emits thermal radiation in the Ultra Violet (UV) and Infra-Red (IR) spectra.[90] The invisibility of the flame of hydrogen-air combustion, is due to the absence of carbon particles causing the visible radiation in a standard flame. When in too close proximity to a hydrogen flame, there is little sensation of heat, making accidental contact with the flame a notable concern. UV overexposure is also a concern, as it can result in sun-burn like effects.
This, in combination with the high leakage and auto-ignition chance, greatly increases workers risk when handling hydrogen gas. Accurate hydrogen detection through sensors is critical in the application or storing process of hydrogen. A wide range of sensor technology is available for this purpose. The palladium-based hydrogen sensors are the most extensively researched and hold the most promise for the industry.[83]

(Auto)-ignition

Looking at table 2.2, an auto-ignition temperature for hydrogen is given as 858 K, since this temperature is not reached during the process, temperature will not be the source of ignition. When we look at figure 2.4, or in the table 2.2, we see that there is a high chance of electrostatic, or other types of spark fused, ignition. The low minimum ignition energy makes it far more sensitive to ignition than most other gaseous or vaporised flammable materials, and therefore the potential for electrostatic ignition is much greater. This is one of the reasons, the leakage risk of hydrogen gas is seen as such a big safety hazards. When the leaking hydrogen is ignited by a small spark it will cause an invisible hydrogen flame. As seen in table 2.2, the burning velocity of hydrogen in air can be around nine times larger then that of methane, which will result in a concentrated high velocity flame, perfect for rockets.

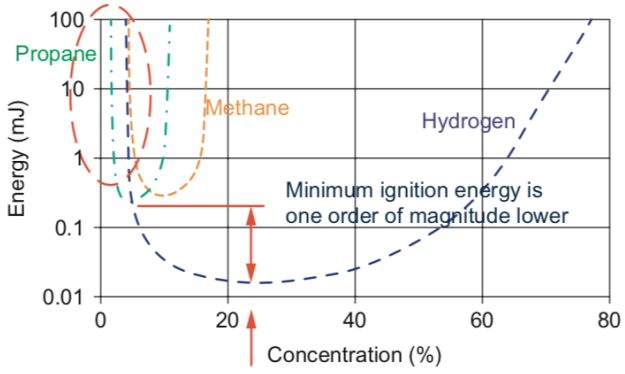

Figure 2.3: Comparison of ignition energy vs. concentration for hydrogen, methane, and propane.[20]

2.2.4. Contamination

Purity of hydrogen gas is an important aspect when concerning the hydrogen cycle. The importance of purity is primarily caused by the effects these contaminants have on Proton exchange membrane (PEM) fuel cells. PEM fuel cells are used as a replacement for internal combustion engines, producing zero emissions as they use hydrogen as the fuel and air as the oxidant. However, impurities in the air and hydrogen inflow can cause performance degradation and in time can even lead to permanent damage to the membrane electrode assemblies. Important impurities that have effect to the PEM fuel cell process include: Carbon Dioxide (CO_2), Carbon Monoxide (CO), Hydrogen Sulfide (H_2S), Ammonia (NH_3), Sulfur Carbons (S_n-C_m) and Carbon Hydrogen compounds (C_n-H_m). Considering PEM fuel cell technology for the automotive industry and its wide application due to its the advantage in low weight and volume compared with other fuel cells, this report will consider the formation of these impurities. In particular CO, CO_2 and H2S. Table 2.1 gives an overview of maximum allowable concentrations of contamination in hydrogen fuel according to limitations set for application in the automotive industry (grade D), as well as limitations set for applications industrial heating and power generation (grade B). These classifications are found in ISO-14687. This paper will use these limitations as a controlling factor for input variables as well as a limit set to calculated output variables.

IMPURITY	$Total(g)$	CH_4	H_2O	He	N_2/Ar	O_2	CO_2	CO	H_2S	$HCHO$	$HCOOH$
grade D (ppm)	300	100	5	300	300	5	2	0.2	0.004	0.2	0.2
grade B (ppm)	1000	-	-	-	400	100	-	-	10	-	-

Table 2.1: Maxmium allowable concentration according to ISO 14687- 2:2012, for grade D (Proton exchange membrane (PEM) fuel cell applications for road vehicles) and grade B (Indrustrial heating and power generation) in ppm(v).[48]

CO

Carbon Monoxide when available in hydrogen rich fuels can sharply degrade the fuel cell catalyst efficiency. This is caused by the characteristics of CO to bind to platinum sites, resulting in the reduction of active surface sites available for hydrogen adsorption and oxidation. Even the presence of small concentrations of CO present in the feed to the anode can block active Pt surfaces, this is because the bond between CO and Pt is much stronger than that between H_2 and Pt. [28]. The CO poisoning effects are strongly effected by cell current, concentration, temperature, exposure time and anode and catalyst types [22]. Concentration effects of CO contamination are displayed in figure 2.4. The maximum allowable concentration of Carbon Monoxide is 0.2 ppm(v).

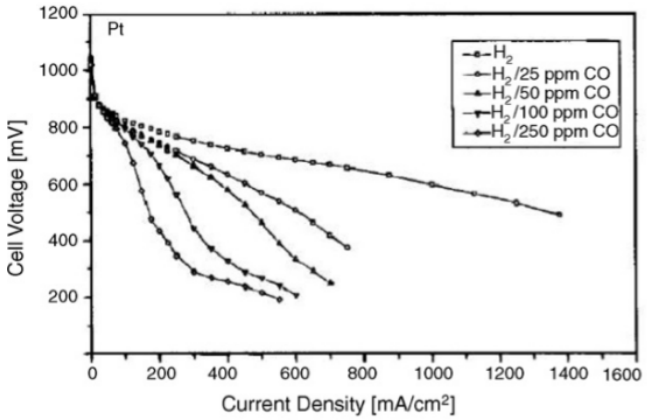

Figure 2.4: Effects of CO concentration and exposure time on cell performance for different anode catalysts. A = 4 cm^2; cathode catalyst: pure Pt; catalyst loadings: $1 mg cm^2$; Nafion 117; Tcell = 80 °C.[22]

CO_2

Effects of Carbon Dioxide contamination are often attributed to hydrogen fuel dilution, however, the availability of both hydrogen and carbon dioxide in combination with the availability of a suitable catalyst gives

rise to the reverse water gas shift reaction (RWGS), a simplification of the reaction is given in equation 2.2. This means that even a non-containing CO fuel can drastically degrade performance when sufficient CO_2 is available.

$$CO_2 + H_2 \rightarrow CO + H_2O \tag{2.2}$$

H2S

Hydrogen Sulfide allowable concentration is 0.004 ppm(v) (grade D) and 10 ppm (grade B). This means that even trace levels of H2S can cause severe performance degradation; It is reported that at a level of 1 ppm the fuel cell performance can be completely halted after only 20 hours [79]. The effect of H2S, as with CO, is primarily caused by the poisoning effect against the catalyst. Equation 2.3 describes H_2S adsorption and equation 2.4 describes HS^- adsorption. These equations use a platinum catalyst (Pt).

$$Pt + H_2S \leftrightharpoons Pt - H_2S_{ads} \tag{2.3}$$

Or:

$$Pt + SH^- \leftrightharpoons Pt - SH_{ads} \tag{2.4}$$

With the sulfur adsorbed species caused by H2S adsorption the effectiveness of the platinum electrode surface is reduced. After the adsorption and oxidation process, studies have found that even after cleaning, a percentage of the catalyst area remains inactive. A viable reason for the irreversible damage caused by H2S poisoning are subsurface sulfur build ups, or adsorbed sulfur contamination's that are difficult to remove.[80] Effects of sulfur poisoning are again effected by fuel cell current, temperature, electrode and anode type, concentration and exposure time. The effects of H2S concentration and current density are displayed in figure 2.5. The effects of CO and H2S poisoning are most frequently studied for PEM fuel cells [9],[93], [68], but the effects are also found on molten carbonate fuel cells and phosphoric acid electrolyte fuel cell.[74], [51] and [23] respectively.

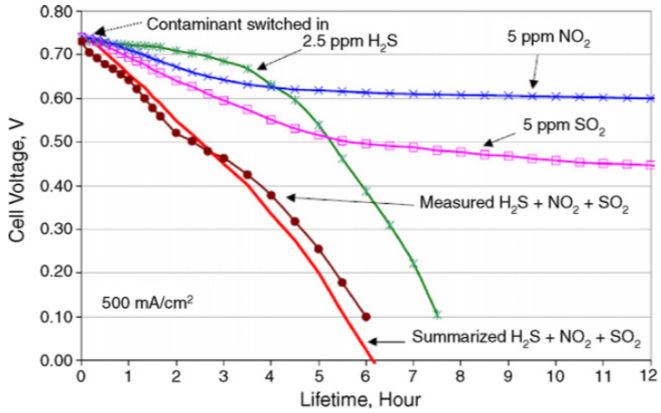

Figure 2.5: Individual and combined effects of 5 ppm NO2 and 5 ppm SO2 in air and 2.5ppm H2S in fuel on cell voltages and lifetime. Symbols represent experimental data, while solid lines show model simulation. Total Pt loadings at 1.0 mg cm2, Nafion 112 and 500 mA cm2. [22]

Properties [Unit]	**Hydrogen**	**Methane**	**L-Gas**
Chemical formula	H_2	CH_4	81% CH_4, 14% N_2 2.87% C_2H_6, 0.89% CO_2 0.38% C_3H_8, 0.15% C_4H_10 0.04% C_5H_12, 0.01% O_2
Chemical structure		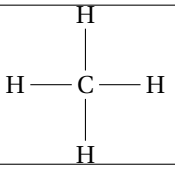	Mix
Molecular weight [g/mol]	2.016	16.043	18.63
Critical temperature [K]	33.2	190.65	187
Critical Pressure [bar]	13.15	45.4	44.6
Density of gas at NTP [Kg/m^3]	0.08376	0.65119	0.833
Normal boiling point (NBP) [K]	20	111	
Enthalpy of Vaporization at NBP [kJ/mole]	0.92	8.5	
Lower heating value (LHV) [MJ/kg]	119.96	50.02	38
Gibbs free energy [MJ/kg]	118.5	49.92	
Higher heating value (HHV) [MJ/kg]	141.80	50-55	33.32 MJ/m3
Limits of flammability in air [vol%]	4 - 75	5.3 - 15	4.7-16.6
Explosive limits in air [vol%]	18.3 - 59.0	6.3 - 13.5	
Minimum spontaneous ignition pressure [bar]	~41	~100	
Minimum ignition energy [J]	0.02	0.29	
Flame temperature in air [K]	2318	2148	
Auto-ignition temperature [K]	858	813	890
Burning velocity in NTP air [m/s]	2.6 - 3.2	0.37 - 0.45	
Diffusivity in air [cm^2/s]	0.63	0.2	

Table 2.2: Physical and Combustion Property Values for Hydrogen, L-Gas, and Methane.[54], [89]

2.3. Salt caverns

In order to analyse the risks that involved in sub-surface gas storage, this section will go deeper into the subject of salt caverns. It will analyse the caverns creation, the location and composition of salt layers that are capable of supporting gas storage. This report will focus on the Zechstein sea. The bore-data analysed is specific for the ground of the storage plant in Epe Germany.

2.3.1. Cavern creation

This section will describe the creation and first use of salt caverns for natural gas storage. It is divided into three phases:

1. *Leaching phase*
   The salt caverns are artificially constructed out of existing salt bed deposits. The construction process of a salt cavern is started by pumping water into the salt formation through an access-well. This process is called solution mining, the salt will slowly be dissolved, and the created brine can be extracted and used for salt production. The well construction process involves drilling a hole (d < 1m) into the ground with a depth depending on the storage product and the geological configurations, the depth of excavation may range between 300 and 2000m.[52] Several pipes are installed in a telescope formation [25] after which the pipes are cast in place by cement, making the arrangement gas-tight. The process is often fluctuated by two methods developing and shaping the cavern. First in the direct circulation method, the solvent is injected through the central pipe dissolving salt at the bottom of the cavern. Secondly, with the indirect circulation method, water is injected through the pipes outer annulus, entering the cavern from the top of the formation. Here the water will start dissolving the salt near the roof of the cavern, flowing downwards, where the brine will be extracted. The brine created by solution mining is used for the production of salt, for chemical purposes, or it can be deposited in the sea. Depending on the volume of the cavern, the first phase could range from one year to a few years. Detailed overview of the leaching phase structure is given in figure 2.6. In this figure an outer annulus is added to the construction where a protective blanket fluid is added to prevent brine from flowing upwards.

2. *Debrining phase*
   Once the salt cavern reaches its final volume, tests are carried out to determine the tightness of the cement casing, after which the debrining process starts. The brine is displaced by injecting gas into the cavern. The gas is injected through the outer pipe, while the brine is extracted through the inner leaching pipe. It is impossible to extract 100% of the brine as the pipes do not reach the bottom of the cavern.

3. *Filling phase*
   After the first filling, substituting brine with gas, an explosive charge is detonated splitting the pipeline near the mouth of the cavern. It is practically impossible to remove the pipe as injecting gas into the cavern has caused the piping from the top of the cavern to disfigure. The pipe deformations are created by the high outflow of the fluids, comparable to a loose garden hose that sprays water in an arch. For the controlled explosion, the purity of the working gas is significant as an ample availability of oxygen would amplify explosive range, possibly damaging the cavern head and wall. The pipes ending, now discarded from the storage well, will fall to the bottom of the reservoir and remain there indefinitely. It is now possible to withdraw the top remaining part of the pipe system, after which a pipe system can be inserted capable of injection and withdrawal of the gas, or liquid, for which the cavern functions as a storage medium.

2.3.2. Geographical location

Selection of geographic location of subsurface salt cavern for gas storage is done after a thorough geological analysis of the location using methods of deposit engineering. To understand where possibilities of salt cavern formation lie, this section will further investigate the origins and location of salt slabs. Analysis of these formations is important to determine the different substances and impurities that can be found in the cavern wall, essential for the ascertainment of potential reactions further on in the report.

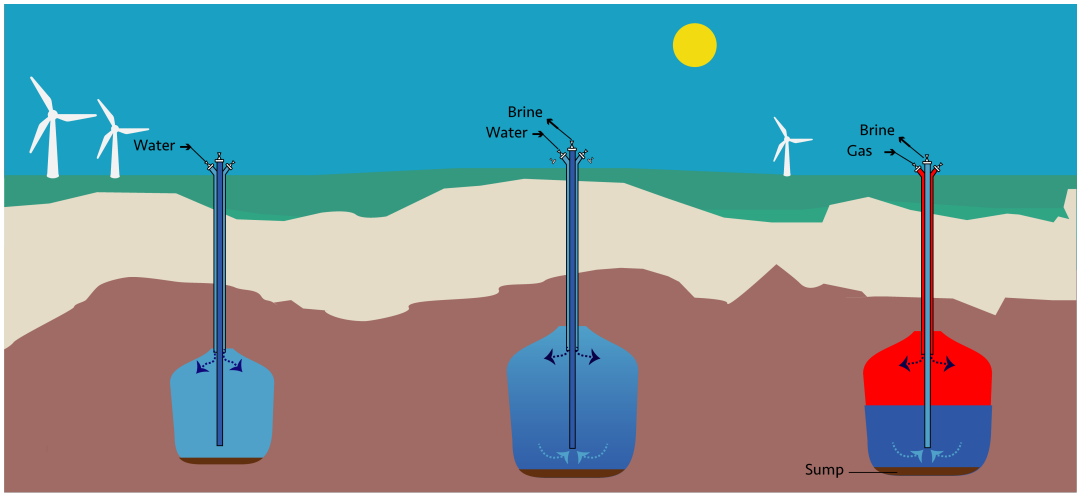

Figure 2.6: Simplification of solution mining of a salt cavern. Leaching phase (left), debrining phase (middle), filling phase (right).

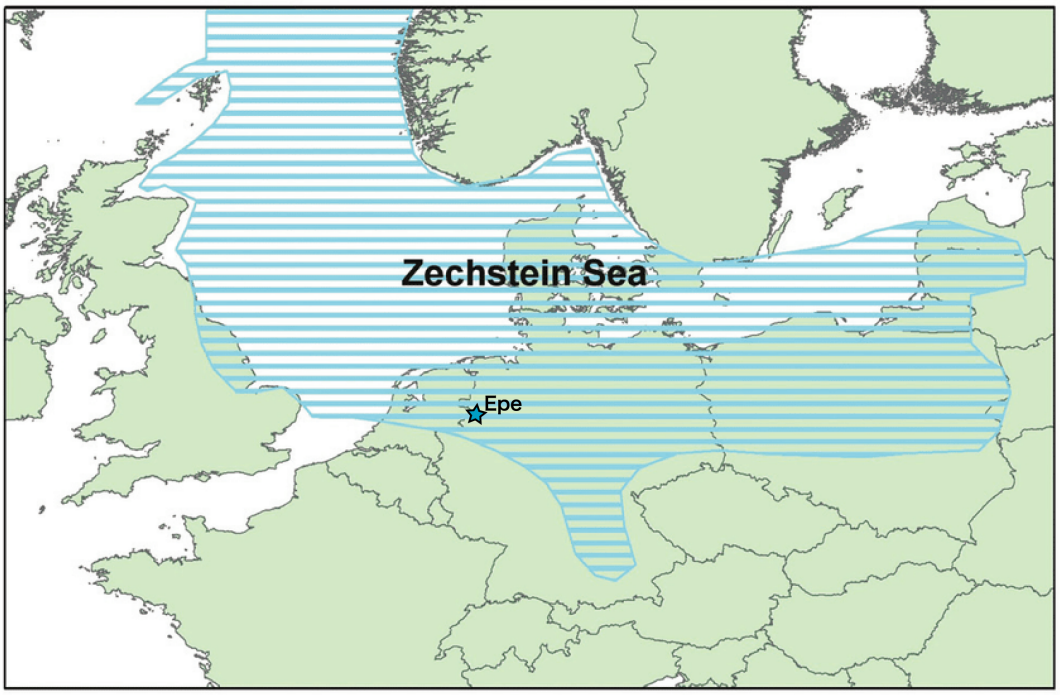

Figure 2.7: Topography of the Zechstein sea and the location of Epe Gasspeicher.

Zechstein sea

Salt formations are found on every continent around the world, these salt formations are commonly referred to as evaporites as they are originated from concentration and crystallisation by evaporation from an aqueous solution. In other words the evaporation of seas. This happens in a restricted environment where water input into this environment remains below the net rate of evaporation. With marine transgression a flooding on such an area is initiated. This is followed by a regression which results in lowering of the sea level and the precipitation of salt during an arid climate. To limit our scope, as mentioned in 1.5, this report will focus on the salt formations at Southern Permian Basin area, in particular the area where the Zechstein sea used to be. Specifications are given in figure 2.7.

The Zechstein of central Europe was deposited between 258 and 252.3 Ma [36], during the Lopingian (late Permian) Epoch. The Zechstein sea had a subtropic climate, which resulted in temperatures that allow the

Cavern	Depth	Volume	Date created	Cement-casing	Diameter	Min. dist. to cavern
S43	1241 - 1330m	371785 m^3	1984	1175m	83m	195m

Table 2.3: Cavern properties

formation of evaporites. The structure of this salt disposition is highly variable throughout its overlay. From almost undeformed salt layers in salt poor areas, to steep-flanked salt diapirs, pillows and walls (figure 2.9). These variations are closely linked to the tectonic evolution and original thickness of the layer. The base of the Zerchstein layer can vary from 700 to more then 5000 meter of depth.[30] As previously mentioned, the Zechstein salt layers were established by separate sedimentary cycles that reflect the type of deposit within the vast salt-basin. These cycle dependant Zechstein layers are generally divided chronologically into formation categories.

Salt layer composition
Since the salt plateau this paper will analyse is located in Germany, this paper will use the German categorisation of Zechstein formation layers. The layers range from Z1 to Z7, the first being the oldest and when existing the deepest [84]. The different cyclic layers differ by substance and structure, as their composition was defined by the revolutions of nature over several million years. The Zechstein layers compose of salts, anhydrites, carbonates and clay, as is illustrated in figure 2.8.
Picking the most suitable layer for gas storage depends on the thickness, depth, purity and composition of the saltlayer. Within the basin area, the distribution, thickness and continuation of the evaporitic rocks vary. This is highlighted by the availability of salt structures such as diapirs and pillows. These structures are caused by the movement of salt between its overlying strata and substrata. This is called halokinesis and is caused by buoyancy, differential loading, gravity spreading and thermal convective. [84] Especially buoyancy and the low density of salt compared to the surrounding tectonic plates have proven to be an important role of the deformations. The different type of salt structures are illustrated in figure 2.9 For an exact representation of the salt caverns in Epe, this paper will analyse the stratigraphic borehole research of cavern S43. The cavern is chosen to function as the model cavern throughout the report as it represents a stable spherical cavern shape, illustrated in appendix A.7 and in figure 2.10.

2.3.3. Cavern properties
The borehole research is found in appendix A.7. Cavern characteristics are displayed in table 2.3. When comparing the cavern depth with the borehole research, it can be concluded that the cavern is drilled in the Z1 Zechstein layer. The salt caverns operated in Epe, are constructed in a salt diapir.
Further analysis of the the layer at this depth concludes that cavern S43 consists of halite with small layers of anhydrite. When analysing other borehole reports from caverns in Epe the same conclusion can be made, therefore the two primary soil substances that will be analysed in this report are halite and anhydrite. Although the composition of the Z1 Zechstein layer is composed of around 99% pure halite[78], there are impurities that should be taken in to account. The most common insoluble impurities in the Z1 layer are Anhydrite ($CaSO_4$), Gypsum ($CaSO_4{\cdot}2H_2O$), Dolomite ($CaMg(CO_3)_2$), Calcite ($CaCO_3$), Pyrite (FeS_2), Quartz (SiO_2), also clay dispositions are possible. The most common soluble impurities include the following ions: Ca^{+2}, Fe^{+2}, Fe^{+3}, Mg^{+2}, K^+, Cl^-, CO_3^{-2}, and SO_4^{-2}; in addition, Ba^{+2}, Sr^{+2}, B^{+3} and Br may be present in minor amounts[37]. These impurities, however insignificant they may seem, can form obstacles for long therm hydrogen storage. Impurities in the cavern wall can, for instance, incite leaking or chemical reactions, which will have a negative effect on the stored quantity and quality of hydrogen.

- *Halite - Sodium Chloride (NaCl)*
  Halite is the main component in the Z1 Zechstein layer of the salt caverns in Epe. It has favourable properties to act as an underground leak-proof storage container thanks to its low permeability, plastic behaviour (creep), self-healing (damage recovery) properties, and high thermal conductivity. Halite does not react with hydrogen gas. [86]. Its high solubility (340 g/ L water at 20°C) creates the possibility for brine mining. Its impenetrability proven by nature as many of the worlds large natural carbon sources are organically captured in rock salt. However, the high dispersion rate that characterises hydrogen creates a potential concern that is being researched by the TU Delft Admire group.

- *Anhydrite - Calcium Sulfate ($CaSO_4$)*
  With the thin layers of Werra anhydrite found in the Z1 Zechtein layer of cavern S43, an analysis is

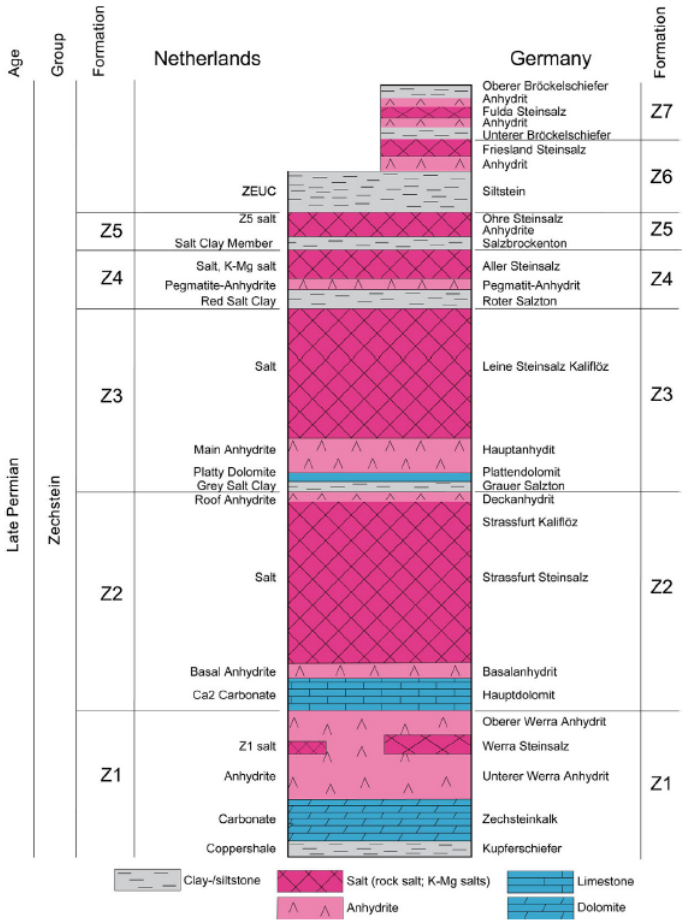

Figure 2.8: Comparison of the average Zechstein stratigraphy and lithology of the Netherlands (left) and Germany (right). Relative thicknesses of layers are indicated, but not to scale. Note also that the occurrence and thickness of units may vary with the facies (i.e., basin, diapir, pillow and platform). 3)[84]

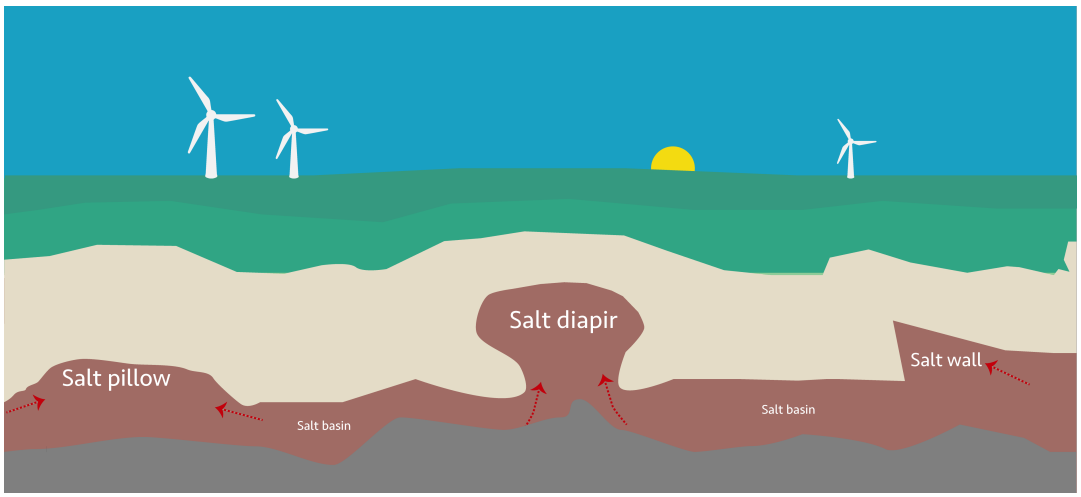

Figure 2.9: Main types of salt structure. (left) Salt pillow, showing salt move in a lateral sense and the covers are not pierced by salt; (middle) Salt diapir, showing that salts move in a vertical sense and salts pierce out the covers. Arrows show the direction of salt flow; (right) Salt wall, showing the salt slab being pushed over a tectonic plate.

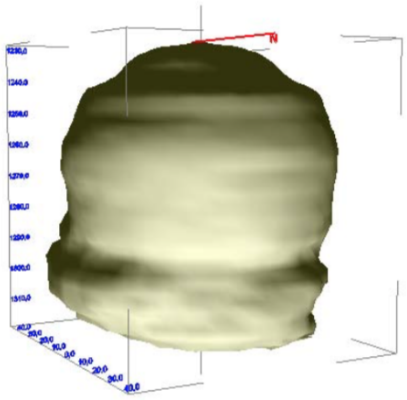

Figure 2.10: 3D representation of cavern S43

needed on the properties of this mineral. Calcium sulfate is highly hydroscopic. When in contact with water anhydrite reacts to the flexible inelastic mineral calcium sulfate dihydrate, also known as gypsum ($CaSO_4 \cdot 2H_2O$). anhydrite has a solubility that is around 140 times lower then that of Halite (2.5 g/ L water at 20°C), however there will be slight formation of SO_4^{2-} and Ca^{2+}. SO_4^{2-} can, in the presence of methane or hydrogen, create hydrogen sulfide via abiotic sulfate reduction [35]. Hydrogen sulfide is a toxic and corrosive gas that can lead to sulfide contamination in PEM fuel cells[79]. Further analysis on the formation of hydrogen sulfide is required and will be given in 4.2.3.

- *Calcite - Calcium Carbonate ($CaCO_3$)*
  Highlighted here as it is considered a microbial metabolic byproduct, research suggests that microbial sulfate reduction drives calcium carbonate precipitation [40]

- *Pyrite - FeS_2*
  Pyrite is the thermodynamically stable end product of iron compounds reacting with sulfide in reduced sediments, with the latter being produced mainly by microbial sulfate reduction [40].

Cavern leakage
As is further explained in appendix A.3, most cavern leakage incidents are consequences of breaches in the well casing, as a result of either salt creep, faulty welding or corrosion. However the sealability of the rock salt is an extremely important safety factor that should not be overlooked. Due to the self healing capacity of the rock salt and its low permeability, a pure salt mine is considered as an ideal selection for gas storage. However, abnormalities and halokinesis in the salt layer can result in an increase in the salt permeability, or can be the cause for breaches in the cavern wall [64][29]. A more extensive investigation into the effects and causes of cavern leakage can be found in appendix A.3.

2.3.4. Significant cavern storage plants

Practical experience in the development and operation of hydrogen caverns has been accumulated over 40 years in the (petro) chemical industry. At this moment there are four operational hydrogen salt caverns, of which three are in Texas, USA. Overview of published cavern properties is displayed in 2.4. The caverns in Teeside Uk act as a buffer in a shared distribution network for chemical producers and consumers. The caverns are relatively small and are situated in a 50 m thick salt layer. The working principle of the caverns in Teeside is not through compressing and decompressing of the stored gas, but by pumping brine into the cavern while keeping the caverns at a constant pressure of 45 bar. The three caverns in Texas follow the more conventional modern natural gas caverns method. The caverns are used to cover chemical operational shutdowns in producing or consuming installations and, consequently, ensure constant production operations. The caverns are attached to a hydrogen pipeline grid with a range of several hundred kilometres.[26]
Although these caverns have existed for some time, there is no further available data on the caverns or on the storage plants.

	Teeside (UK)	**Clemens Dome** (Texas)	**Moss Bluff** (Texas)	**Spindletop** (Texas)
Salt formation	Bedded Salt	Salt dome	Salt dome	Salt dome
Operator	Sabic Petrochem.	Chevron Phillips Chem. Comp.	Praxair	Air Liquide
Commissioned	1972	1986	2007	Information not available
Geometrical volume [m^3]	210 000	580 000	566 000	906 000
Mean cavern depth [m]	365	1 000	1 200	1 340
Pressure range [bar]	45	70-135	55-152	68-202
Net energy stored [GWh]	27	81	123	274
H_2 mass [ton]	810	2 400	3 690	8230
Net volume [m^3] (std)	9.12 x 10^6	27.3 x 10^6	41.5 x 10^6	92.6 x 10^6

Table 2.4: Metrics of Hydrogen caverns in the USA and the UK

2.4. Risk analysis

After a literature review on the potential risks when processing hydrogen, some conclusion can be made. It is expected that from an engineering standpoint, the leakage rate of hydrogen is going to be the biggest challenge: Combining the leakage risks with possible auto-ignition and an invisible flame poses great possible hazard in a gas storage facility, or any other hydrogen processing plant. Another possible challenge has to do with the diffusion rate of hydrogen in metals which can lead up to hydrogen embrittlement, which in turn can lead to equipment failure and more leaks. This is why a great amount of current and recent studies are focused on either the diffusion rate or the leakage rate of hydrogen when transported or stored under pressure. Since the effects have a great number of contributing variables such as: Temperature, pressure, material type, shape and volumetric flow. These studies are more often then not accompanied by extensive lab testing to confirm findings. Not a lot of research is done to find out what actually happens inside the cavern, while a lot of questions still remain unanswered. One of those questions concerns the demand for highly pure hydrogen. Is there a risk of contamination, either by aerobic or anaerobic reactions? This report will try to answer this question, in order to find out if hydrogen in = hydrogen out.

Key takeaways: Chapter 2

Biggest challenges when using salt caverns for long term hydrogen storage:

- Hydrogen leakage: The high leakage risks that accompany hydrogen are seen as biggest challenge for hydrogen processing. The small molecule size and high dispersion rate will cause the gas to slip through cracks as small as 130 pm. Hydrogen gas can diffuse through many materials considered airtight or impermeable to other gases.
- Hydrogen embrittlement: Constant exposure to hydrogen can lead metals to absorb hydrogen causing material fatigue and can lead to cracks.
- Detection: Hydrogen gas has a very low minimum ignition energy, making it sensitive for ignition risk. The combination with high leakage risks and the invisibility of a hydrogen flame for the human eye is a great hazard.
- Hydrogen contamination: Effects of hydrogen contamination are very relevant when using hydrogen for fuel cells. Limitations set to sulphur content has a maximum of 0.004 ppm. Water content has a maximum of 5 ppm.
- Salt caverns: While the cavern is located in a mostly pure halite (NaCl) salt layer, the cavern wall and brine could have natural impurities containing Ca^{+2}, Fe^{+2}, Fe^{+3}, Mg^{+2}, K^{+}, Cl^{-}, CO_3^{-2}, and SO_4^{-2}.
- Cavern leakage: Highest leakage risks is expected to be caused by breeches in the steel casing closest to the cavern, this in combination with porous cementation surrounding the casing can lead to costly cavern leaks.

3

Process conversion: From natural gas to hydrogen

To get an accurate view of how a subsurface hydrogen gas storage plant would look and where the critical areas will arise, this report reviews and compares the process to that of an existing natural gas storage plant. The plant is Vattenfall's Nuon Epe Gasspeicher GmbH, located in Germany near the border to the Netherlands. The goal of this chapter, like with chapter 2, is to find any high risk areas in the storage process, specifically when the process is changed from natural gas to hydrogen gas. Along side theory this chapter will give calculations to determine important variables specific to cavern S43 and the natural gas storage plant in Epe. These calculations are used in chapter 4 and 5 of the paper.

3.1. CNG storage process overview

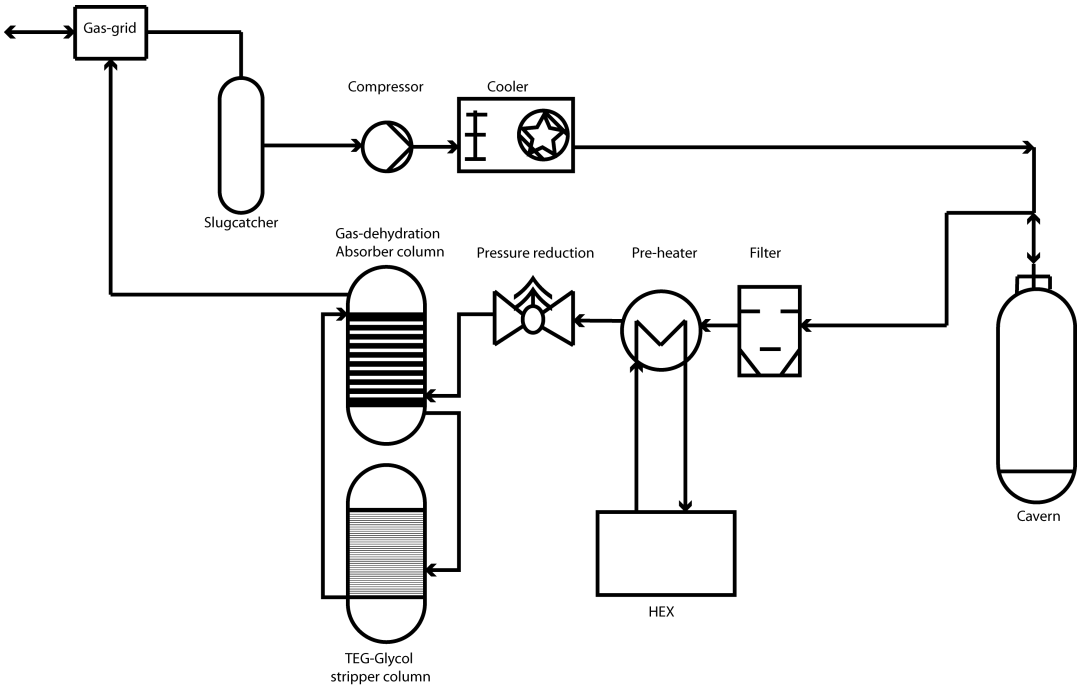

Figure 3.1: Natural gas storage process.

The storage plant in Epe is connected to two natural L-gas grids, the Gasunie Transport Services (GTS) and the Open Grid Europe (OGE). As the gas arrives from the gas networks, it flows through a slugcatcher to absorb any surges in the network, after which it will flow through measurement systems to determine flow

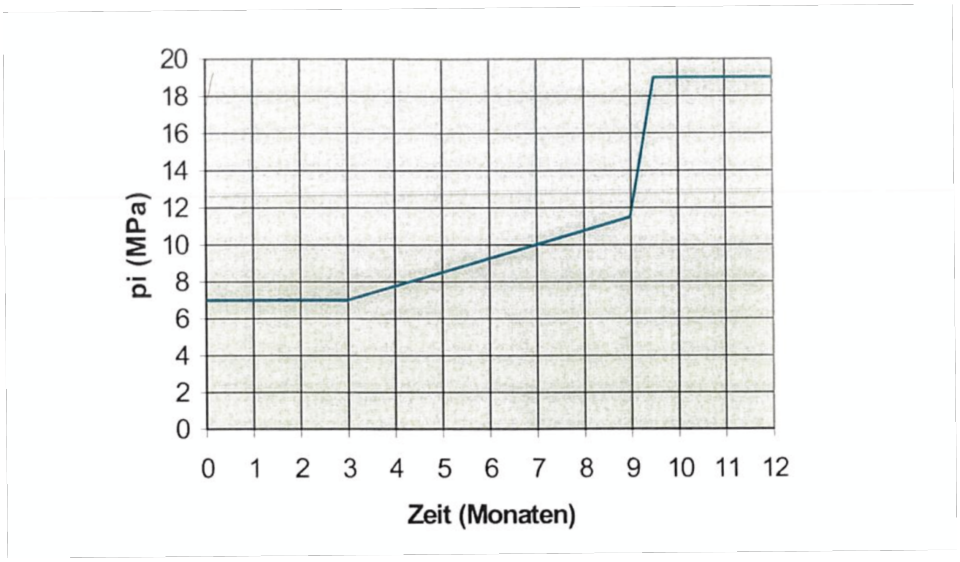

Figure 3.2: Maximum time (x-axis) to keep cavern at minimum cavern pressure (y-axis) for cavern S43. [62]

rate, pressure and temperature. A reciprocating compressor or, when taking on large volumes, a magnetic sealless centrifugal compressor is used to increase the pressure prior to injection. Air fan coolers then reduce the gas temperature, after which it is ready to be injected into one of the caverns.

When the gas is pumped out of the cavern, TEG-glycol (triethylene glycol) is injected as soon as it reaches the surface to prevent hydrate formation and agglomeration from the wellhead onward. The TEG-glycol is used in most natural gas processes for gas dehydration, the process works by physical absorption. The gas goes through a solid separator, after which the gas temperature is increased in a heat exchanger. The last step is further dehydration by a TEG-glycol installation, which makes it possible to separate the H2O from the TEG glycol and recycle the glycol back into the absorber towers. The natural gas is now at the right temperature, pressure and composition to be sold back into the Dutch or German grid. A simplified illustration explaining the process is given in figure 3.1.

3.2. Part by part function and constraints

In order to understand the process and the changes in the process when introducing hydrogen gas, three process steps are analysed that are considered high risk, or otherwise important areas. The cavern itself, the compressor and the dehydration step. Areas that are considered high risk are selected based on the gas pressure, as a consequence of the leakage risk. This section focuses on the differences between a process running on hydrogen gas, compared to a process running on natural gas.

3.2.1. Cavern constraints

Important cavern characteristics such as the pressure and temperature will remain the same regardless of the gas input. The cavern temperature is defined as a function of depth, since this is a function of the earths constant underground temperature. With a thermal gradient of around 30°C per km, an average cavern depth of 1285m, a constant temperature of 50 °C is assumed. The cavern pressure is also dependant on the cavern depth, with the maximum pressure calculated at the last cemented shoe depth (Z_{rs}) with equation 3.2.1. The cavern shoe is the lowest cement block which supports the cavern roof. Here γ is the average overlay weight (0.235 - 0.217) and ξ_F is a reduction factor (1.15 - 1.2) as calculated by K. Lux. [62]. For cavern S43 a maximum pressure of 23 MPa is calculated. The minimum pressure is regarded as a function of depth as well as time. This is illustrated in figure 3.2. Where the minimum cavern pressure for 1 month for cavern S43 is 7 MPa. While, when the storage duration is increased to for example 7 months, the minimum pressure is increased to 10 MPa. Another important cavern constraint used in this report is the maximum cavern outflow and inflow. This will limit stress caused by sudden pressure changes, as well as limit the constraints set on compressor flow rate. A value of 1 MPa/day is used by the cavern operator in Epe, which will also be the value used in this report.

$$P_{max} = \gamma \frac{Z_{RS}}{\xi_F} \tag{3.1}$$

3.3. Pressurised hydrogen gas

Not all compressors available are suitable for hydrogen gas compression, due to the small molecule size and low density, the most efficient way of increasing the pressure of hydrogen is by allowing electrolysers to work at higher pressures. But in the storage plant the gas will most likely be delivered by a gas grid. The most commonly used compressors for pressurising hydrogen are reciprocating processors that work by continuously decreasing the volume available for the gas and with that increasing the pressure. Efficiency of the compressor is highly effected by the leakage of the compressor valves, the piston rings and the rod packing. The leakage effect will be higher then when compressing natural gas due to the smaller molecule size.

3.3.1. Joule Thompson

A difference when analysing compressed hydrogen with compressed natural gas is the Joule Thompson effect for non-ideal gases. When a real gas at high pressure flows into a region of lower pressure without a significant change in kinetic energy, like what happens with cavern injection, you have what is called Joule-Thompson expansion. When we consider ideal isenthalpic, adiabatic expansion, the temperature change will be 0 as explained in equation 3.2. However, for a real gas, Joule and Thompson discovered that there was a thermal energy being released to overcome intermolecular effects of the gas, which they called the Joule Thompson effect. This is defined in equation 3.3, with μ_{JT} being the Joule Thompson constant (KPa^{-1}).

$$\Delta h = \int_{T_1}^{T_2} c_p dT = 0 \tag{3.2}$$

$$\Delta h = \int_{T_1}^{T_2} c_p dT + \int_{p_1}^{p_2} -c_p \mu_{JT} dp \tag{3.3}$$

The Joule Thompson coefficient is highly effected by the temperature of the system. The effect decreases for higher temperature, as is seen in figure 3.3. It is also dependant on the type of gas. For hydrogen and helium gas, the Joule Thompson coefficient is below 0 at standard conditions. For hydrogen this happens with a temperature above 200 K. This means that for hydrogen gas, expansion will cool the gas down, this is called the reverse Joule Thompson effect.[50] The Joule Thompson effect is an important factor for the design of gas storage facilities as it will influence the thermal processes necessary to maintain thermal restrictions.[87] The reverse Joule Thompson effect that accompanies hydrogen only goes in effect when the gas flows through a throttle, like with the cavern mouth. The Joule Thompson effect when expanding the gas from 230 bar to 70 bar at 50 °C: For natural gas a temperature increase of 19 °C. For hydrogen gas a temperature decrease of 7 °C. Standard compression will still result in a rise of gas temperature which can be accurately calculated using equations that model the behaviour of real gases.

3.3.2. Compressor

In order to find out more on the effect hydrogen gas would have on a reciprocating compressor, the sizing and parameters of the compressor used in Epe are taken as a reference case. This way, conclusions can be made as to what effects hydrogen gas has on the energy losses caused by the compression stage. Key compressor parameters used are found in table 3.1. Gas properties and compressor calculations are made using Aspen Hysys, while the friction losses are calculated using methods explained in literature [42]. The compressor in question is a 2-stage, 4-cylinder, double-acting, non-lubricated reciprocating compressor. The reference case takes a constant molar flow of 1000 kmole/hr, raising the pressure from 50 bar (P_{in}), the grid pressure, to 230 bar (P_{out}), the maximum cavern pressure. Since the compressor is dual staged, an estimate should be made to find the compressor ratio of the first stage. This is done using the sizing guidelines of [42]. For these calculations a polytropic efficiency of 92% is assumed, and 82% for natural gas [**?**]. The compressor ratio (R_c) of the first stage is calculated with equation 3.4, with Z being the gas compressibility. This gives a ratio of 2, resulting in a first stage discharge pressure of 100 bar. This ratio is also used in the natural gas calculations.

$$R_c = \sqrt{\frac{P_{out} Z_{in}}{P_{in} Z_{out}}} \tag{3.4}$$

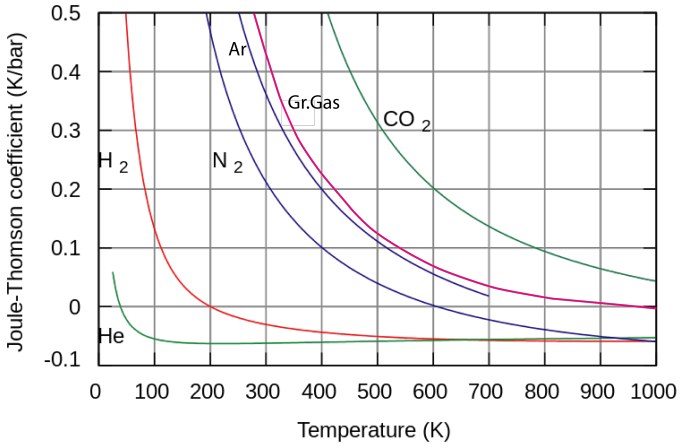

Figure 3.3: Joule Thompson coefficient as a function of temperature, Hydrogen in red, Groningen gas in pink.

Compressor characteristics			**Hydrogen**	**Natural gas**
P_{in} [bar]	50	Polytropic efficiency	92	82
P_{inter} [bar]	100	T_{inter}	93	84
P_{out} [bar]	230	T_{out}	205	171
T_{in} [°C] and T_{cool} [C]	20	Compressor power [MW]	7.8	7.7
Molar flow [kmol/hr]	5173	Friction losses [MW]	0.1	0.8
Bore diameter [m]	0.171	Cooling [MW]	-7.6	-10.6
Stroke [m]	0.165	Tot [MW]	*7.9*	*8.5*
Piston rod diameter [m]	0.0635	HHV [MJ/kmole]	282	776
Vol. eff. 1st stage [%]	72.85	Energy losses [% HHV]	*1.95%*	*0.76%*
Vol. eff. 2nd stage [%]	68.75			

Table 3.1: Compressor comparison of a dual stage - double acting - four cylinder reciprocating compressor active in the gas storage plant in Epe.

Friction losses

The properties of hydrogen have a beneficial effect to the friction losses in the compressor. The volumetric efficiency (VE) is not effected by the type of gas that flows through the compressor, as it is a compressor characteristic. The VE_x together with twice (double-acting) the compressor piston speed (R_{speed}), a resistance factor (R_p), the cylinder bore area (A_{bore}), the number of valves (N), the molecular weight of the gas (MW) and the cross section area of the valve bore A_{vlv}, will lead to the Valve Power Losses (VPL). The sum of the VLPs will result in the friction losses over all 4 cylinders.

$$\sum_{x=1-4} VPL_x = \frac{(MW)(P1_x)(VE_x)(R_p)(A^3_{bore})}{(Z_x)(T_x)(N)(A_{vlv-x})^2} \tag{3.5}$$

Compressor calculation results

The adiabatic work of the specified dual stage compressor, is calculated by Aspen Hysys and is about similar for both gases. There are large differences to output temperature of the gas, for hydrogen this will reach 205 °C, for natural gas this is 172 °C. Hydrogen is easier to cool, as the cooling required to get the gas back to room temperature (7;6MW) is lower then when processing natural gas (10.6MW). It is seen that the valve losses of the hydrogen compressor (0.1MW) are well below that of a methane compressor (0.8MW). The total power required for compression is higher for natural gas, but when you compare the energy losses as a function of the Higher Heating Value (HHV), the energy losses for hydrogen (3.8%) are around twice as high, compared to natural gas (1.7%). These calculations do not include any energy losses caused by leakage in the compressor.

3.3.3. Dehydration unit

As of right now the natural gas has to be dehydrated due to the water vapour concentration being too high. Water in combination with methane has the chance to form hydrates, which can clog the pipelines. The water

concentration in natural gas is estimated using the McKetta-Wehe curve, given in figure A.3. For the cavern characteristics of cavern S43 at a maximum pressure, water concentration is 2.5 kg/hr. For hydrogen there are different limits defined by the ISO. The limits set for hydrogen, given in table 2.1, are 5 ppm for fuel cell grade hydrogen. When consulting a similar curve, figure A.4 predicting the water concentration in hydrogen gas that is in contact with water at a specified temperature and pressure (50 °C, 230 bar), a concentration of 58 kg/hr is found. With a maximum cavern outflow rate (5127 kmol/hr), this would lead to a concentration of 654ppm which exceeds the maximum allowable concentration for fuel cells of 5 ppm. Dehydration will therefore be a necessary process step, like with natural gas. Magnified versions of these graphs are diplayed in the appendix A.4.

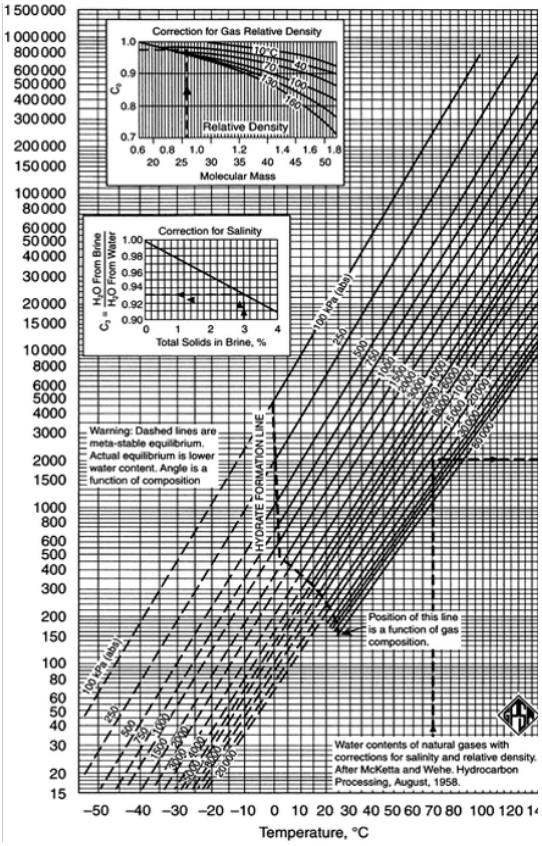

Figure 3.4: Water content of natural gas as a function of pressure and temperature (Mc Ketta-Wehe chart) [38]

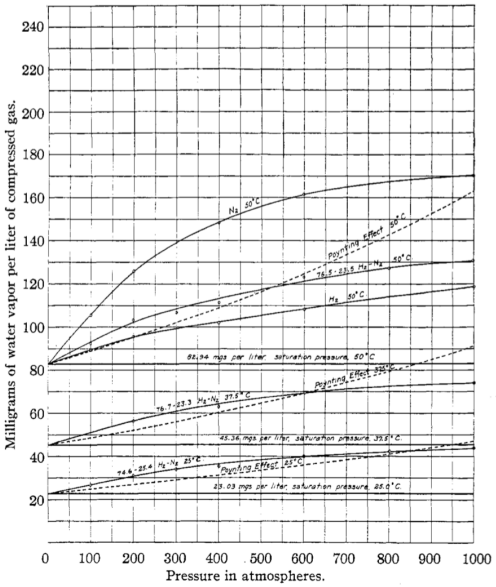

Figure 3.5: Water-vapor content of compressed hydrogen gas in contact with liquid water, 25.0°, 37.5°, 50.0°. [8]

Key takeaways: Chapter 3

Chapter 3 discusses the natural gas storage in the Vattenfall storage plant in Epe. After which it will focus on the changes in some of the process sectors when replacing the natural gas for hydrogen.

- Cavern constraints: A maximum pressure of 230 bar.
  A minimum pressure of 70 bar.
  A maximum pressure flux of 10 bar per day.
  And an estimated cavern temperature of 50 °C.
- Joule Thompson effect would lead to a temperature rise of 19 °C at the maximum (230bar - 70bar) constraints for the expansion of natural gas.
  A temperature reduction of 7 °C for the expansion of hydrogen gas.
- Total compression energy requirements (including cooling) are higher (8.5MW) for natural gas then for hydrogen gas (7.9MW). However when comparing it to the HHV the energy losses are higher for hydrogen gas (1.95%) compared to natural gas (0.76%)
- Water concentration in natural gas at maximum cavern constraints is 2.5 kg/hr. For hydrogen this rises to 43.5 kg/hr. Which would mean a concentration of 654 ppm.
  Dehydration step is necessary for fuel cell applications

4

Chemical modelling of hydrogen storage

4.1. Introduction

One of the primary goals of fuel storage is achieving the highest possible round trip efficiency. This is done by minimising mass and energy losses. But another storage aspect is equally important: maintaining the demanded purity.
When reviewing the process of hydrogen storage from input to output there is a risk of contamination throughout the process. These impurities are caused by different aspects in the storage process. This can be caused by gas input impurities, but also contact with equipment and chemical reactions in the cavern or other parts of the process can be viable contributors. Subsurface deposits carry microbes. They can either be autochthonic or anthropogenic. The first kind was embedded in the reservoir millions of years ago when the sediments composing the reservoir were precipitated. The second kind (anthropogenic) was brought into the reservoir by unnatural means. This can either be during drilling, or during work-over operations in the borehole. This chapter will analyse the chemical process caused by these microbes, that will contribute to the loss of hydrogen, the loss of hydrogen purity, or a combination of the two.

4.2. Chemical model

After the previous explanation of the importance of hydrogen purity, this chapter will focus on the use of a suitable method to determine the amounts of impurities that will be found in the hydrogen gas after subsurface storage. With the availability of actual data from Nuon Gasspeicher Epe, this report attempts to make a model that is closest to a realistic scenario. However, since the model is still a simplification of actuality the primary use of the model is to be used as a reference state, through which defining factors and variables can be highlighted and is therefore built to assist the theory explained in this report, after which the theory can be applied to other storage caverns. First the program used for the chemical modelling, PHREEQC, is introduced. To avoid the use of the model as a input-ouput 'blackbox', this report will analyse calculation steps used by PHREEQC and its databases: phreeqc.dat and pitzer.dat. In particular the solubility, the equation of state, diffusion and both the equilibrium and kinetic reaction types will be examined. To get close to the goal of making a realistic reference state, this report will use two models. One that simulates the equilibrium between the brine and sump over a period of 9 years, which results in the composition of the brine and sump to be accurate. This is further explained in chapter 4.3.1 and 4.3.2. The second model simulates the storage process of hydrogen, using the results of the first model in its setup. Concluding in this chapter are results generated from both models, with the defining variables highlighted and explained.

4.2.1. PHREEQC

PHREEQC works in combination with a selected geo-chemical database. The database file is basically a preset to the input file, each database has its own specialisation and functions and may therefore use different sets of elements, different notation for the element names, or different default conversion formulas. After analysing comparative studies [46], the most accurate database to use would be pitzer.dat, which incorporates the Pitzer equation to calculate the activity coefficient. However the Pitzer database does not include the bulk of the sulfate-sulfide related chemical equations. Therefore, phreeqc.dat is used. Phreeqc.dat is an

ion-association database that accounts for ion-ion interactions with ion pairs and complexes. In high ionic strength it is known to lose some accuracy on the calculation of solid-liquid equilibrium reactions. This is analysed in article, [46], and is also tested in the next section 4.2.1, where the solubility of aqueous anhydrite is compared with experimental data.

Validation of chemical model
PHREEQC [70] is a chemical modelling program created by the U.S. Geological Survey written in the C++ programming language, capable of describing equilibrium and kinetic reactions as well as aqueous 1D transport processes including diffusion, advection and dispersion. It is based on the equilibrium chemistry of aqueous solutions with other components, such as minerals, gases, solid solutions, and sorbing surfaces. Since the program is capable of modelling 1D gas diffusion, kinetic reactions and equilibrium reactions over time, it is suitable for simulating batch reactions in salt-caverns. An analysis of the modelling structure used in PHREEQC is found in the appendix A.5. The analysis is used to make conclusions to the results from the PHREEQC model.

PHREEQC is widely used in scientific studies to model aqueous transport in porous media, or other geochemical applications like salt-caverns. In a literature review the focus was set on subsurface gas storage. A wide range of studies were found ranging from corrosion effects in geothermal wells. [18], to the potential risks of underground hydrogen storage in depleted gas fields [44]. The program is used for solubility calculations in porous media in article [81] and in [45]. Lastly, a studies was found in which PHREEQC was used to model H2S production in salt caverns: article [43], the theory behind this study was used to setup the PHREEQC model used in this thesis.
To validate that PHREEQC (using phreeqc.dat) produces correct results, even under high NaCl concentrations and high ionic strength, three studies are done. These studies verify the suitability of PHREEQC to key aspects of the below ground process.

- The first verifies the NaCl solubility [mol/kgw] in pure water at different temperatures from literature [94] to calculated values in PHREEQC This is displayed in table 4.1.

- The second compares the solubility of $CaSO_4 \cdot 2H2O$ in brine with variable ionic strength at 50ºC to experimental data. Displayed in table 4.1.

- The third compares the diffusion rate of hydrogen gas in pure water with a pH of 7 at atmospheric pressure as calculated by PHREEQC to experimental data. As compared in table 4.2.

Solubility NaCl	0 ºC	20 ºC	40 ºC	60 ºC
	[mol/kgw]	[mol/kgw]	[mol/kgw]	[mol/kgw]
Zimmerman et al (1986)	6.09	6.13	6.23	6.34
PHREEQC.dat	6.00	6.10	6.24	6.39

Table 4.1: NaCl solubility [mol/kgw] in pure water at different temperatures from literature (experimental data) and modelled data. The database phreeqc.dat is used in the PHREEQC model. [43], [94]

		Kolev	**PHREEQC**
Solubility H2 in water	$10^5 \frac{mol}{mol}$	4.68	4.02

Table 4.2: Comparing solubility of Phreeqc calculated saturation limit at 50°C, 1 atm with experimental data.[55]

A conclusion can be made by comparing the data from these tests. Both the diffusion and equilibrium solubility of halite are comparable to experimental data with and average error of 0.48% for the halite saturation and a minimum error of 5% for diffusion coefficient of hydrogen in water depending on the experimental data. When analysing the $CaSO_4$ in the brine however there is a noticeable error margin when increasing the

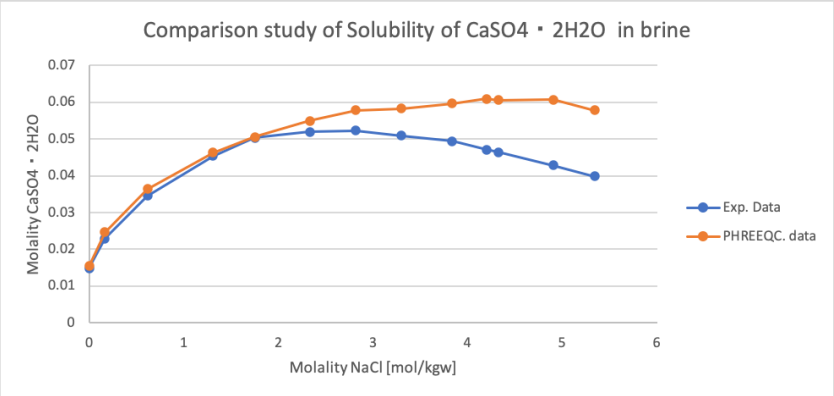

Figure 4.1: Solubility of $CaSO4 \cdot 2H2O$ in NaCl rich brine, comparison of PHREEQC.dat modelling to experimental data. [10]

Ionic strength of the brine. This is also explained in comparative studies to database accuracy in [46]. Since the brine in the cavern will reach saturated concentrations of halite, this means that the anhydrite dissolution will be calculated higher than what would realistic, which is taken into account in conclusions made to the test cases.

4.2.2. Solid-liquid equilibrium reactions

Table 4.3 defines the solid-liquid equilibrium reactions that are taken into account, as inputs or as possible secondary phases, in both chemical models. It also defines the equilibrium constants that are defined in phreeqc.dat. The equilibrium constants are defined for 25 °C at 1 atm, however these can be adjusted for temperature and pressure. The database phreeqc.dat gives the standard equilibrium constants. For most substances it will also give the standard enthalpy of reaction, making it possible to adjust the equilibrium constant for temperature using the van 't Hoff equation 4.1. Here K_1 is the equilibrium constant at the temperature T_1, which is 25 °C, while K_2 is the equilibrium constant at the temperature defined in the input model, T_2.

$$ln\frac{K_2}{K_1} = \frac{-\Delta V_r}{R}\left(\frac{1}{T_2} - \frac{1}{T_1}\right) \tag{4.1}$$

For the most common or defining reactions equation 4.2 is used to get an accurate equilibrium constant dependant on temperature. Where $A_{1...5}$ are analytical constants defined in the database.

$$log_{10}(K_p) = A_1 + \frac{A_2}{T} + A_4 log_{10} T + \frac{A_5}{T^2} \tag{4.2}$$

Equilibrium phase	Equilibrium reaction	log K
Halite	$NaCl \rightleftharpoons Cl^- + Na^+$	1.570
Anhydrite	$CaSO_4 \rightleftharpoons Ca^{2+} + SO_4^{2-}$	-4.39
Siderite	$FeCO_3 \rightleftharpoons Fe^{2+} + CO_3^{2-}$	-10.89
Goethite	$FeO(OH) + 3H^+ \rightleftharpoons Fe^{+3} + 2H_2O$	-1.0
Pyrite	$FeS_2 + 2H^+ + 2e^- \rightleftharpoons Fe^{+2} + 2HS^-$	-18.479
Mackinawite	$FeS + H^+ \rightleftharpoons Fe^{2+} + HS^-$	-4.648
Sulfur	$S + 2H^+ + 2e^- \rightleftharpoons H_2S$	4.882
Gypsum	$CaSO_4 : 2H_2O \rightleftharpoons Ca^{2+} + SO_4^{2-} + 2H_2O$	-4.58
Calcite	$CaCO_3 \rightleftharpoons CO_3^{2-} + Ca^{2+}$	-8.48
H_2S	$H_2S \rightleftharpoons HS^- + H^+$	-6.994
HS^-	$H_2S \rightleftharpoons S^{-2} + H^+$	-12.918

Table 4.3: Important equilibrium -phases, -equations and -constants (log K, at 25°C and 1atm) taken in to account. Data from phreeqc.dat

4.2.3. Kinetic reactions

This section will delve deeper in to the origins of the sulfate reducing bacteria, as well as the methods to defining the reduction rate that is used in the mode.

Sulfate Reducing Bacteria

The primary contamination risk as described in 2.1 is H_2S, which can be created via sulfate reducing bacteria. It can be assumed that there is no methanogenis (production of CH4 from CO2 and H2) process in the cavern, due to the lack of CO2 in the relatively pure H2 inflow. The sulfate reducing bacteria (SRB), or Desulfovibrio Vulgaris, use sulfate as the main electron acceptor during anaerobic metabolism. They live on the reduction of sulfate (S[+VI]) to sulfide (S[-II]), described in figure 4.2. Before sulfate can be used as an electron acceptor, it must be activated. This is done by the enzyme ATP-sulfurylase, which uses ATP and sulfate to create adenosine 5'-phosphosulfate (APS). APS is subsequently reduced to sulfite (SO_3^2_ and AMP (Adenosine monophosphate). A simplification of the complete reaction is given in equation 4.4 and in the overview of figure4.3.

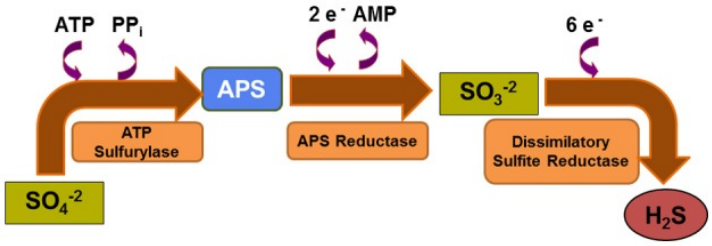

Figure 4.2: Overview of the three key enzymatic steps of the dissimilatory sulfate reduction pathway. Enzymes: ATP stands for Adenosine triphosphate; APS is used to adenosine-5'-phosphosulfate; and AMP is Adenosine monophosphate. [19]

The sulfate used for these bacteria catalyzed reactions are available due to the anhydrite ($CaSO_4$) dissolution, available in the sump and cavern wall. Bacterial sulfate reduction is an important process in the mineralization in marine and hypersaline systems. In the brinal environment, reduction occurs mainly in the anoxic solution of the brine, but also in the anoxic sump sediment.
In the model the electron donor is hydrogen, equation 4.3, while the acceptor is sulfate. Together this gives equation 4.4.

$$H_{2_{aq}} \rightleftharpoons 2H^+ + 2e^- \tag{4.3}$$

$$4H_{2_{(aq)}} + SO_4^{2-} + 2H^+ \rightarrow H_2S + 4H_2O \tag{4.4}$$

Restrictions to bacterial growth

The presence of sulfate reducing bacteria is highly influenced by a variety of factors. It is dependant on temperature, activity of the brine water, alkalinity and salinity (% of NaCl) of the ecosystem in which they grow. Also, availability of both the acceptors and donors will determine the bacterial growth factor. The temperate optimum ranges from 30 to 50 °Celsius, but can reach up to 120 °C for thermophyle species.[27] A few SRB can tolerate high salt concentrations and live, though with diminished activity, near salt saturation far beyond the optimum. Halophilic SRB require salt for their growth and can be classified into three groups on the basis of their response to NaCl: slight- (optimal growth at 2–5% NaCl), moderate- (optimal growth at 5–20% NaCl) and extreme-halophiles (optimal growth at 20–30% NaCl). [24]. Activity thus depends on the purity of the salt in which the cavern is situated. When the cavern is situated in a salt layer with lower halite purity, or situated within several salt layers, the chance for bacteria is increased, this is caused by the fractional decrease of NaCl.

Prediction of the reduction rate

In the model the kinetic rate of reduction is taken as a constant taken from literature [73], but will also be taken as a variable to determine the actual effect of the reduction rate.
The best way to get an accurate prediction would be to preform a microbiological analysis of a ground sample to measure the number of reducing bacteria present and multiply this to a bacterial reduction rate per cell constant as is done in equation 4.7. Here N_{cells} is the number of cells per Kg, this value can be taken from

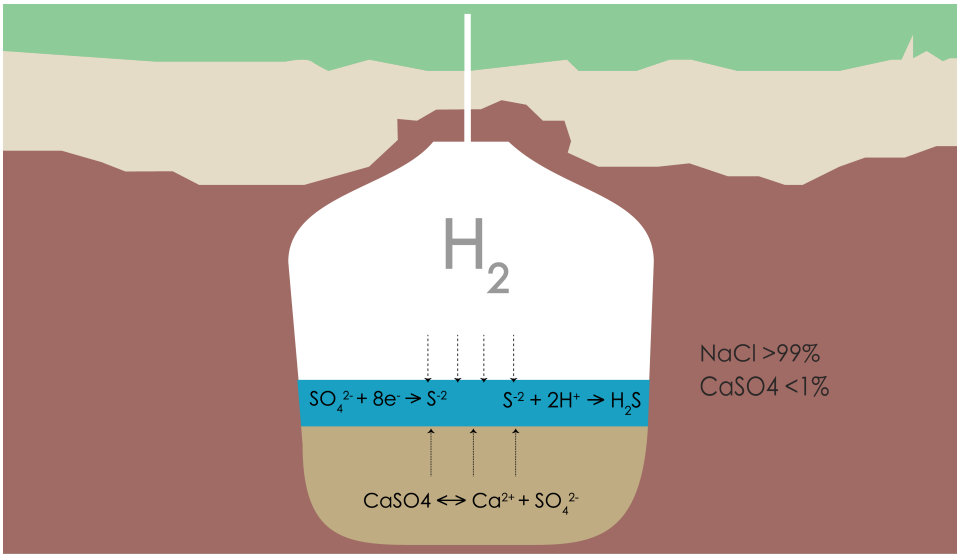

Figure 4.3: Simplification of reactions important for the production of H2S

ground sample testing, dR is the reduction rate per cell, which is around 40 fmol/cell/day. [82]. This method can also be used to predict the maximum kinetic rate, with the minimum amount of detectable cells. The minimum detectable rate in this case, is estimated around 3.1E-11 $\frac{mol}{kgw \cdot s}$.

The kinetic rate is adjusted for amount of available sulfate and hydrogen using equation 4.8, here k is the kinematic rate (in $\frac{mol}{kgw \cdot s}$), kgw is the mass of available water. This follows the estimate that the sulfate rate is considered linear until the concentration of sulfate reaches around 0.001 M. After consulting the research done by the TNO [88], the minimum amount of hydrogen necessary for sulfate reduction is close to 0.001 M.

To get an accurate estimate for the kinetic rate constant used in the reference state, this report consults tests done in environments with similar salinity, in particular the sediment of hyper saline soda lakes. Looking at the results done for seasonal testing for dissimilatory sulfate reduction in hyper saline coastal pans [73], the bacterial reduction rate (BRR) increases with salinity. This is partially due to the bacteria's halophilic properties. The BRR for a solution with the salinity of the brine substance when taking the linear regression line given in figure 4.4 (a), would give a BRR of 1E-08 ($molkgw^{-1}s^{-1}$). However, high salinity does not immediately implicates a rise in NaCl concentration. Also, this would not take in to account the concentration of sulfate in the solution, which is assumed to be a more important factor in these calculation. Therefore, taking this in to account figure 4.4 (b), following the linear regression line, a BRR of 9E-10 ($molkgw^{-1}s^{-1}$) is calculated (with a sulfate molarity of 0.0275, equal to that of the cavern brine).

$$H_2S \rightleftharpoons HS^- + H^+ \tag{4.5}$$

$$H_2S \rightleftharpoons S^{-2} + 2H^+ \tag{4.6}$$

$$Rate = N_{cells} * dR \tag{4.7}$$

$$Rate = k * kgw * \frac{SO_4^{2-}}{0.001 + SO_4^{2-}} * \frac{H_2}{0.001 + H_2} \tag{4.8}$$

4.2.4. Cavern setup

With the empirical data of a range of salt caverns in use by Vattenfall's Nuon Gasspeicher Epe, this study has access to wide range of defining parameters. The test drilling data report, illustrated in the appendix A.6. give

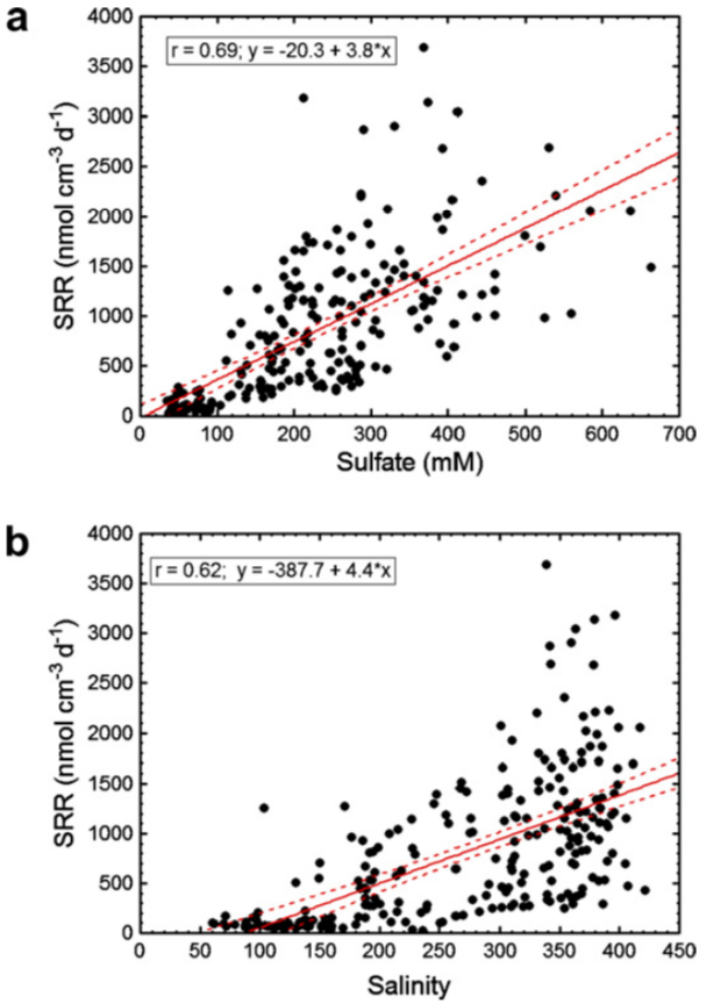

Figure 4.4: Sulfate reduction rates measured for all seasons and sites were combined together and plotted against (a) porewater sulfate concentration and (b) porewater salinity. A linear regression line was applied to the data. Dashed lines depict the 95% confidence envelope. [73]

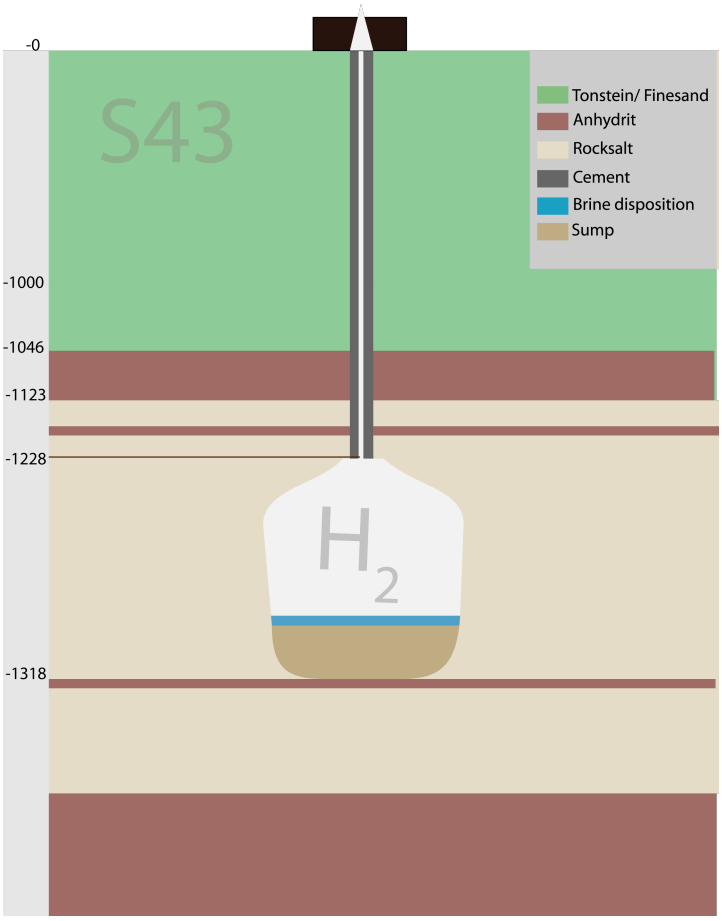

Figure 4.5: Representation of cavern S43 shape, size and salt and brine composition.

a representation of the salt composition of the cavern wall, roof and bottom. Further analysis of the data obtained from the drilling data, appendix A.8, obtained with the construction of the caverns for their primary function, salt leaching, give further information on impure salt layers and impurities in the halite salt.
A conclusion can be made after analysis of the reports: reactions between hydrogen gas and cavern wall will be minimal. The cavern wall consists primarily out of highly pure halite which is nonreactive to hydrogen.

However, after completion of the salt cavern, which is a result of years of salt dissolution and extraction. Two extra mediums are created that are critical in the chemical process.
A brine deposit remains that is impossible to extract. This brine disposition is saturated with the salts that are dissolved in the debrining process. This brine is in saturation equilibrium with the gas above and in phase equilibrium with its surrounding minerals of the rock salt formation.
Below the brine a sump is precipitated, composed of insoluble residues. This layer can reach to one third of the total cavern height.[43] The sump is composed of minerals with an estimated porosity of 30 % and a residual pore filling solution that is not discharged after leaching. Due to the fact that the residual minerals precipitated, it is expected that the halite concentration in the sump minerals will be less then the halite concentration in the salt layer itself, which is due to the differences in solubility of available minerals. This gives room to a higher concentration of less soluble but more reactive minerals, such as anhydrite.
Further explanation of the different compositions of the brine and sump layers are explained in chapter 4.3.1 and 4.3.2. As mentioned before, the model attempts to create a reference state composed of parameters closest to reality. Therefore, a specific cavern is chosen. The cavern S43 in Epe is picked for the amount of available data and the close to average shape, size and salt composition. A simplified overview of the cavern setup is given in figure 4.8.

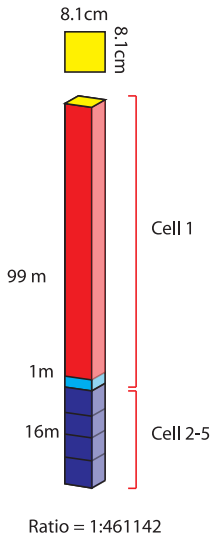

Figure 4.6: Overview of model setup.

4.3. Model setup

The constructed model is is divided over three parts:

- The gas phase on top.
- The brine interface.
- The sump disposition.

The brine is in solubility equilibrium with the gas and with the surrounding brine of the sump. The focal point of calculations is found in the gas-brine interface and in the first meters of the sump. Therefore the model is divided in to 5 cells or solutions.
The first cell containing the brine solution and the gas phase specified to a fixed volume at the input pressure and temperature.
The remaining four cells are the sump disposition which consist of the pore filling residual and the mineral equilibrium phases.
The model applies diffusive transport over 24 time steps, with a species component specific diffusive rate. There is one-dimensional transport over the total height of the cavern. The first cell is 100 meter, cell 2-5 are 4 meter each. The cavern height and volume specified represent the actual values found in the data from cavern S43.
PHREEQC does not work well with large quantities of water, therefore this model works with a ratio controlled by the mass of brine water. This is set to 1kg, and all input values are adjusted to this ratio (R=461172).
The simplification can be assumed accurate, as the transport in the model is one dimensional. An illustration to summarise the setup is presented in figure 4.6.

4.3.1. Brine composition

The brine composition follows the measurements done by Salzgewinnungsgesellschaft Westfalen (SGW). The data provided concerns the chemical composition of one of their brine production streams. This include concentration of different solubles and the pH of the solution. To be certain the brine and sump are in equilibrium, a model is made which allows equilibrium reactions for a period of 9 years. The result of the brine composition is given in table 4.4. Aside from the chemical structure, the dimensions of the brine disposition will be a leading factor in calculations. To make an accurate prediction this report uses Sonar Control (SOCON) renderings of the S43 cavern. These laser and ultra sound surveys are carried out to establish the differences in geometry of the cavern over time and can determine the exact amount of brine in the cavern.

A 3D rendering of a SOCON survey done in 2018 is displayed in figure 4.7. Total volume of the cavern is measured to be 310 029.9 m^3 from 1226.0 m to 1310.1 m, while the gas volume is measured to be 307 289.7 m^3 from 1226.0 to 1313.7 m. This will amount to a brine volume of 2740.2 m^3 with an average depth of 1.8 m.

Brine composition	
Density	1.2
pH	6.9
X	*Molarity*
Na	5.33E+0
Cl	5.33E+0
S(6)	2.75E-2
K	3.32E-4
Mg	3.29E-4
Ca	2.89E-2
Fe	1.16E-4
C	1.83E-5

Table 4.4: Calculated brine composition

Sump composition	
Density	1.2
pH	6.9
X	*Molarity*
Na	5.33E+0
Cl	5.33E+0
S(6)	5.13E-2
K	3.32E-4
Mg	3.29E-4
Ca	5.53E-2
Fe	2.60E-3
C	2.70E-2

Table 4.5: Calculated brine composition in the sump

Sump (s) Composition			
Mineral	*X*	*Mol*	*g/mol*
Halite	$NaCl$	1.794E9	58.4
Anhydrite	$CaSO_4$	4.85E6	136
Goethite	$Fe(O)OH$	2.29E7	88.8
Siderit	$FeCO_3$	1.47E6	116

Table 4.6: Sump minerals

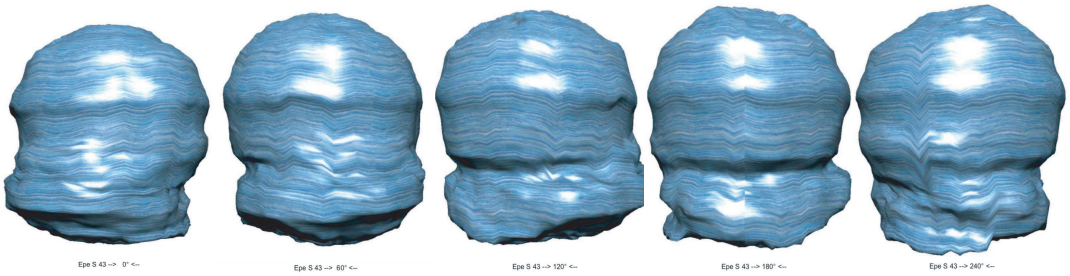

Figure 4.7: 3D rendering of cavern S43

4.3.2. Sump composition

The sump composition is somewhat more difficult to predict as their are no samples from the actual sump disposition. However, there is a ground sample chemical analysis from the caverns approximate location and depth, this will give an indication of the purity of the salt layer and it's original composition.
As the cavern debrining process takes place, the highly soluble (357 g/L 25 °C) halite will dissolve, while the less soluble anhydrite and other in-solubles have the possibility to be released and will therefore precipitate to the bottom of the incomplete cavern.
When the water reaches near saturation it will be extracted and replaced with fresh water. Since this is a batch process with a finite amount of water, the anhydrite will have insufficient time to be fully dissolved, creating a dissipated layer.
However, since the chemical modelling of this process involves predicting the water to salt ratio of the extraction process which is unknown; this report will use the ground composition analysis as a measure for the

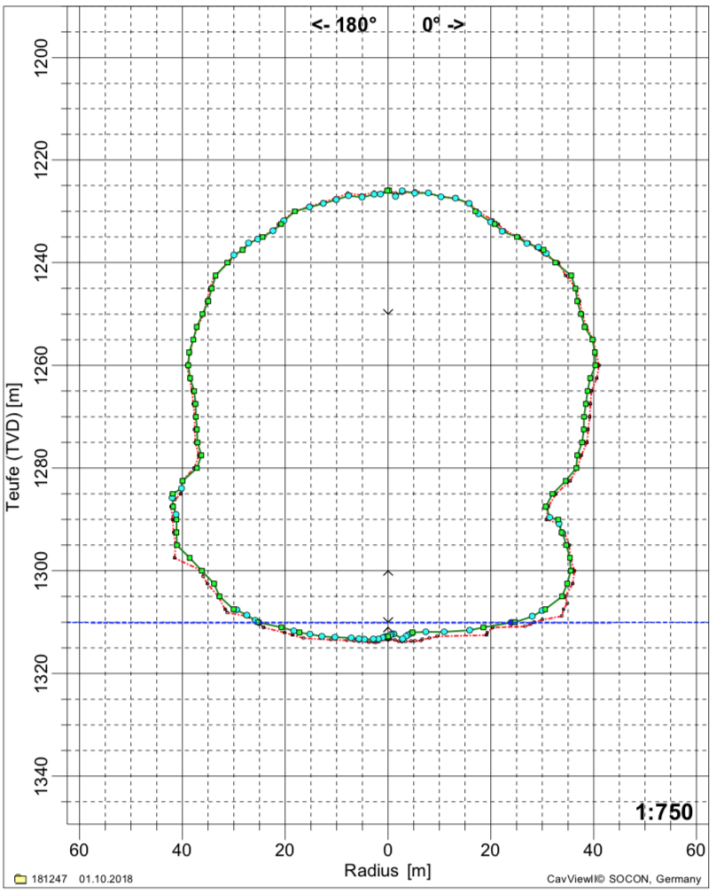

Figure 4.8: Cavern dimensions: Cavern wall in green, brine interface in blue.

sump composition. Therefore stating that the sump composition is equal to the surrounding salt composition.
The ground sample analysis done by Open Grid Europe (OGE), Apendix A.8, on cavern S43 gives the molecular mass percentages present. Furthermore OGE predicts the presence of halite, anhydrite, siderite and goethite. Taking the molecular masses of these minerals the mineral composition of the ground sample can be calculated displayed in table 4.6.

To determine the dimensions of the sump a geometric survey is taken from 1998, right after cavern completion. This gives a cavern volume of 371 785 m^3. The difference from the current volume is 61756 m^3, which is taken as the solid sump volume. The sump is believed to be loosely settled and to have a porosity of 30%. which is filled with another brine fluid. The composition of both the brine and the minerals are calculated using a PHREEQC based model, allowing solid-liquid equilibrium reactions and diffusive transport of aqueous species over 9 years, this is done to make sure the system is in equilibrium before the hydrogen gas is added.

4.4. Results

After understanding how PHREEQC works, it is clear what parameters are necessary for the model to run accurately. The calculations in chapter 3 were done to define the maximum pressure, minimum pressure, maximum pressure differential and water vapour concentration. The beginning of this chapter determines the brine composition, sump composition, overall cavern geometry and kinetic rate constant. With these parameters data can be generated using PHREEQC, which in turn can be analysed using Matlab. First the diffusion rate of hydrogen into the brine will be analysed, this is done to determine if there will be sulfate reduction in the sump. After that a reference case is analysed inline with cavern S43 in Epe storing gas at a maximum pressure of 230 bar. Important cavern conditions will be taken as variables to determine the effects they have on H_2S production. Lastly, this chapter will go deeper into the effects the use of the cavern has on H_2S build up and eventual output concentration.

4.4.1. Diffusion

With the simulation run by PHREEQC, the solubility of hydrogen in the brine is determined to be 0.012M. This is the maximum concentration of hydrogen gas in the brine. With a diffusion coefficient of hydrogen ($6.1\frac{m^2}{s^{-1}}$ in water, from literature [91]. It is possible to determine the concentration of hydrogen at 1m depth of brine over time. The concentration follows Fick's second law for 1D diffusion with a constant source concentration and diffusion length. This is explained in equation 4.9. The concentration at x meters, can be determined using equation 4.10. The results of this determination are displayed in figure 4.9. Here the concentration at 1 m brine depth is displayed as a function of time in days. After analysis it can be determined that the hydrogen will reach the required concentration of 0.001 M at 1 meter depth in approximately 320 days. Note that for these calculations the diffusion coefficient of hydrogen is used for pure water at 50°C at atmospheric pressure. The true diffusion coefficient will be effected by both the ionic strength as well as the cavern pressure. Because the hydrogen reaches the sump in less then a year, it will be possible to have bacterial sulfate reduction in the sump. Following article [49]: "...the sulfate-reducing activity is correlated to sediment depth and age following a power law function, and sulfate reduction rates thus decrease by orders of magnitude across sediment depth." The sulfate reduction rate in the sump is not taken into account in this research, but could imply that there will be a higher H_2S production rate then is estimated in this report.

$$\frac{\delta C}{\delta t} = D\frac{\delta^2 C}{\delta x^2} \tag{4.9}$$

$$C(x,t) = C_{sat}\texttt{erfc}(\frac{x}{2\sqrt{Dt}}) \tag{4.10}$$

Aqueous diffusion of sulfate into brine

It is possible for the sulfate from dissoluted anhydrite in the sump to diffuse in to the brine layer. This would results in a large (750000+ mol) supply of sulfate available for reduction.

4.4.2. Reference state results

This model will focus on the reduction in the brine layer. Figure 4.10 presents the H2S production of the reference state over 5 years. This result follows the calculated compositions of the brine and sump based on the actual data, and the kinetic rate factor as taken from literature.

In figure 4.10 a noticeable decline in H2S production is observable. In the first 1.75 years, an average production rate of 11.2 mol per day is calculated. This will be the case until the sulfate concentration in the brine approaches 0.001 M. The sulfate in the brine will be depleted. During this time there is an inflow of aqueous sulfate from the sump layers, partly due to the available S(VI) ions in the sump solution, as well as due to anhydrite dissolution. The sulfate inflow from the sump is at a rate that is lower than the sulfate reduction rate. This is seen in the graph at around t=1.75 years. After the sulfate is exhausted in the brine, the limiting factor of the sulfate reduction will therefore be the transport rate of S(VI) to the brine, which in turn is highly dependant on the anhydrite dissolution rate in the sump. Taking in to account the conversion rate of S(VI) to H2S, this results in an average H2S production rate of 5.4 mol per day. The dependency of the sulfate reduction rate on the anhydrite dissolution rate is also perceived in studies on H2S production caused by thermal sulfate reduction [12].

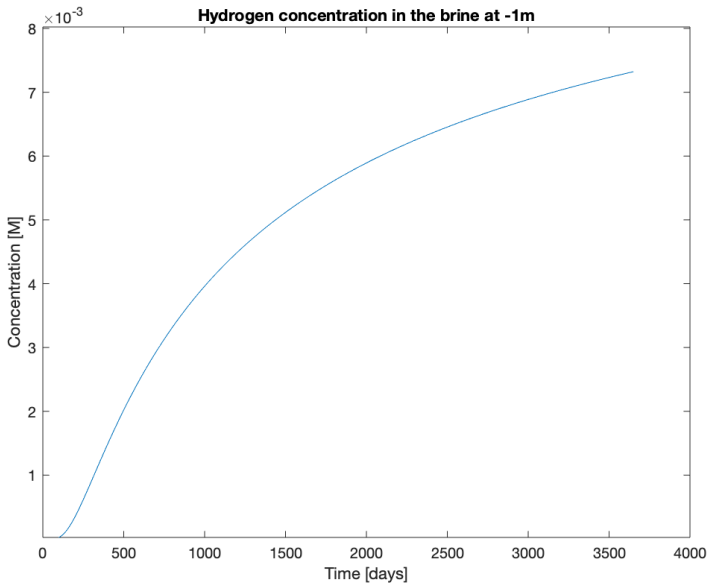

Figure 4.9: Hydrogen concentration at 1 meter over 10 years.

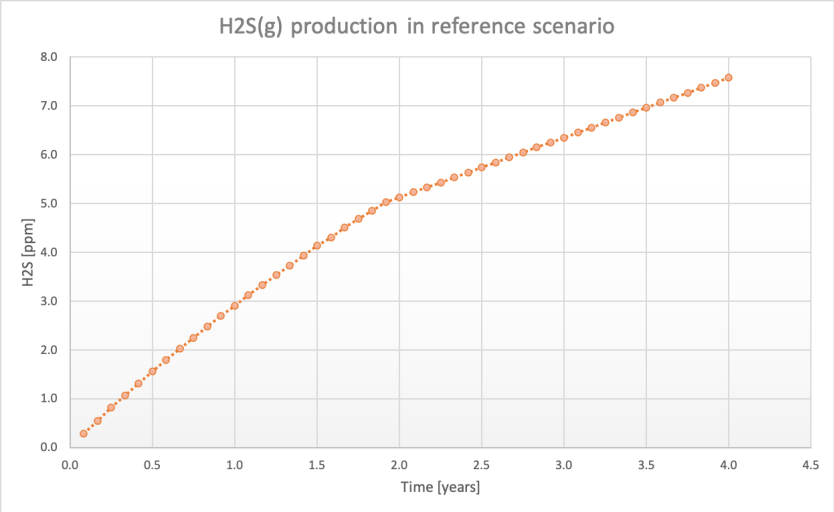

Figure 4.10: H2S production in reference state. Max concentratin for fuel cells is 0.004 ppm, max concentration for heat and power is 10 ppm.

4.4.3. Effects on H2S production

After analysing the reference state it is important to adjust variables in the model to review the effects they have on the production of H2S. After this, a conclusion can be made on the factors that have the most effect on contamination, as well as a method to prevent H2S from being produced. The report will review effects caused by pH, temperature, pressure, kinetic rate constant, availability of sulfate and availability of aqueous iron.

pH

The pH of the solution is an important factor as it has effect on how much of the S(-2) will be reacted to HS^-, to H_2S, or how much will remain unreacted. The pH of the brine solution is expected to increase as part of the H_2S in the solution will be released as a gas. Since H^+ is a reactant, the overall H^+ will decrease. It is possible to manually adjust the pH of the solution in PHREEQC. This is done by adding either NaOH or HCl to the system, keeping the pH at the demanded level. The Na+ and Cl- added will be insignificant compared

to the available NaCl concentration. The production of H2S(g) as a function of the pH, is seen in figure 4.11. When the pH is low, the equilibrium will shift towards H_2S(aq), while when the pH is high it will shift to S(-2) and HS^-. Higher pH will prevent the production of H_2S(g).

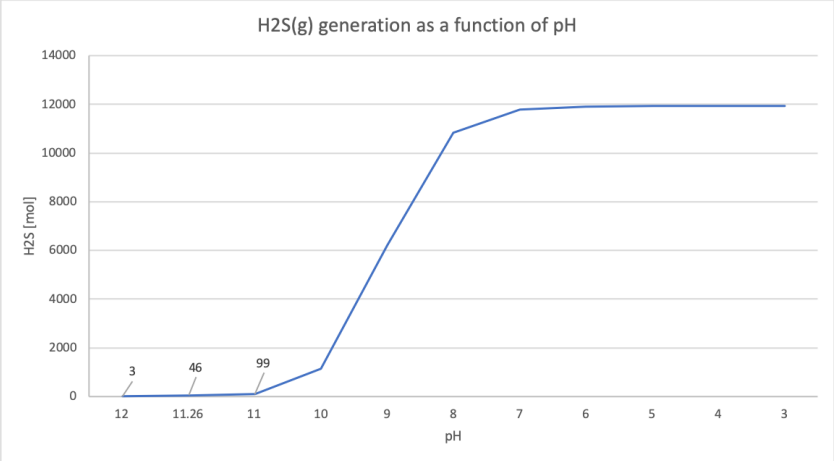

Figure 4.11: H2S production as a function of pH, when pH is controlled by adding NaOH. At t = 1 years.

Temperature

Temperature, as displayed in figure 4.12, has effect on the production of H2S. Increasing the temperature increases reaction rates due to the large increase in the number of high energy collisions, which activate the reaction. This should be taken in to account when choosing cavern depth. For an existing cavern it is impossible to adjust the temperature as this is defined by the geothermal temperature rather then then anything else. The temperature in cavern S43 is calculated to be 50 °C at an average depth of 1100 m.

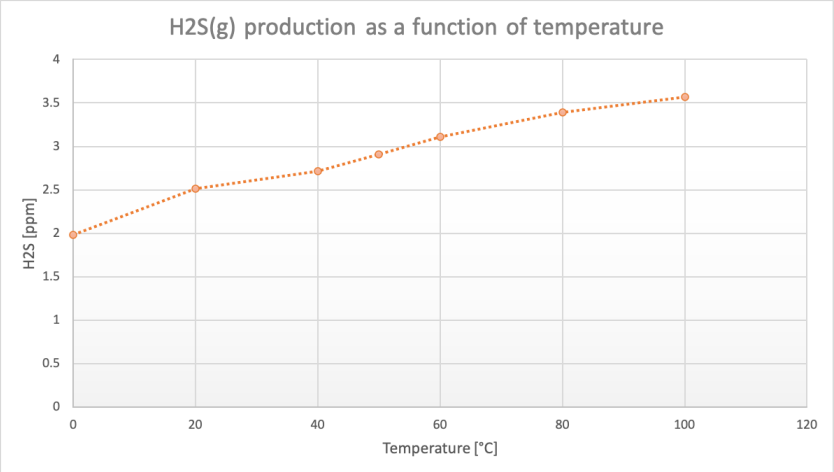

Figure 4.12: H2S production as a function of temperature, at t=1 year.

Pressure

Pressure fluctuation effects are described with dynamic modelling, but stationary pressure effects have influence on the production of H2S, as well as on the diffusion rate of the hydrogen gas and aqueous species. The effects on the H2S production are displayed in figure 4.13. When taking into account that the minimum pressure, due to the availability of the cushion gas, is 70 bar for cavern S43. The maximum change in H2S production due to pressure (from 230 bar to 70 bar) is measured to be around 7%.

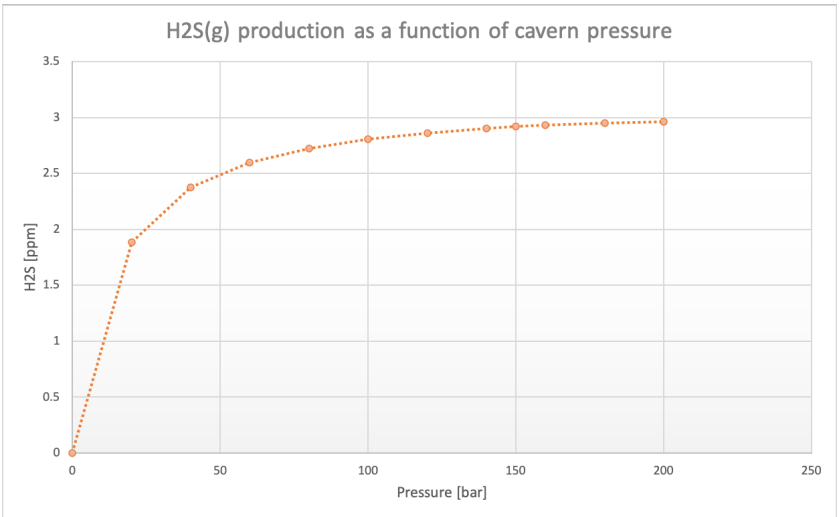

Figure 4.13: H2S production as a function of pressure, at t= 1 year.

Sulfate availability

An important factor, already explained in the explanation of the sulfate reduction rate in 4.2.3, is the concentration of available sulfate for reduction. The sulfate is a controlling factor as it is used as an electron acceptor in the reduction reaction and supplies the S(-2) necessary for the production of H2S. Figure 4.14 illustrates the effects when adjusting the sulfate concentration. The effects of the sulfate concentration are important to take into account when analysing possible location for salt caverns. Salt disposition with high concentration of anhydrite will have an increased H2S contamination risk. The concentration of sulfate will be reduced over time due to the reduction reaction, but will also be added due to diffusion of aqueous sulfate from the sump layers. This is explained in the chapter on the reference state 4.4.2. The sulfate concentration therefore has an effect on the rate of H2S production, as well as on how long it takes before the sulfate is reacted away and thus on the total amount of H2S that can be produced before the production rate will decrease.

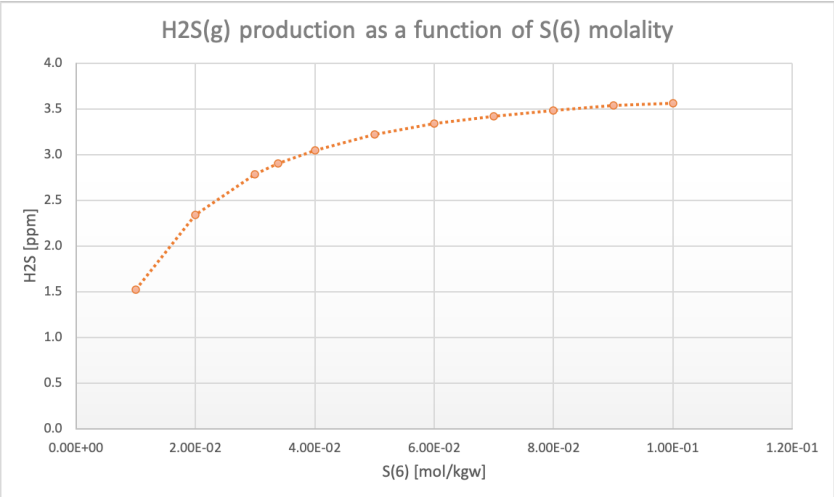

Figure 4.14: H2S production as a function of sulfate molality, at t=1 year.

Kinetic rate factor

The kinetic rate factor (k), defines the rate at which the sulfate is reduced by sulfate reducing bacteria. In this model for the reference state a value is taken from literature, but to get a good understanding of the effects of the kinetic rate, it is also taken as a variable. This is illustrated in figures 4.15 and 4.16. The minimal detectable kinetic rate, as explained in 4.2.3, highlighted by the label MIN in figure 4.16, is estimated to produce a H_2S

concentration of around 0.125 ppm after 1 year. This would still exceed the ISO limit. The kinetic rate is linear until just before the kinetic rate constant reaches 2E-09. The nonlinearity is caused by the time it takes for the system to deplete the sulfate available in the brine. When the sulfate in the brine is depleted in less then 12 months, the rate is controlled by the sulfate diffusion rate (5.4mol per day) from the time of sulfate depletion until t = 1 year. For the highest calculated rate (1E-08 $mol\ kgw^{-1}s^{-1}$), the sulfate in the brine is completely reacted away after 1 month.

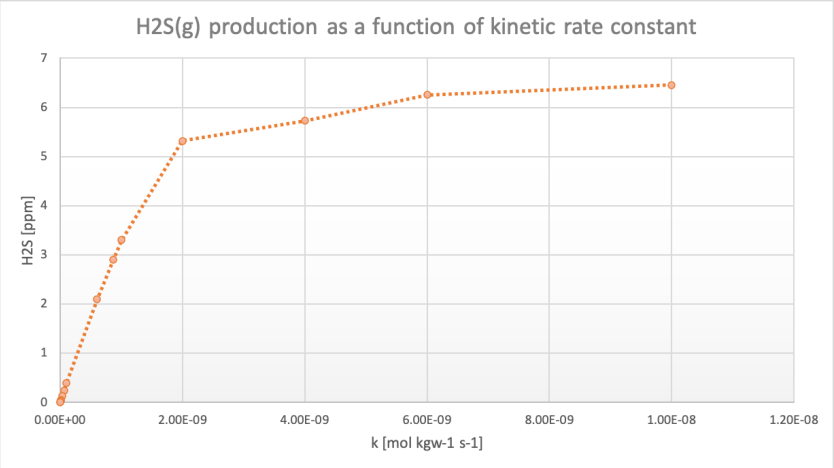

Figure 4.15: H2S production as a function of kinetic rate, at t=1 year.

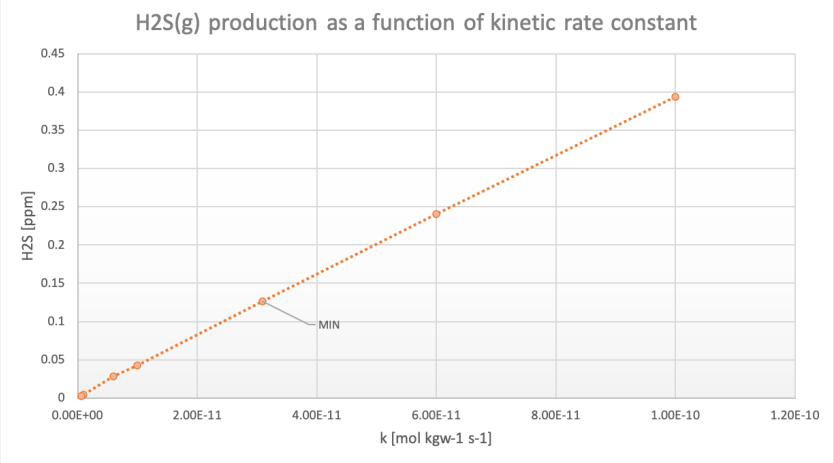

Figure 4.16: H2S production as a function of kinetic rate (zoomed in), at t=1 year.

Effect of solution composition

An important study to make, is the effect the concentration of different aqueous species in the brine have on the production of H2S. The availability of different soluted minerals can create equilibrium reaction that either take away S(+6), or S(-2), preventing it to react to H2S. An example of this is Fe(+2), or Fe(+3) in the solution. This creates the equilibrium reaction between Fe(+2) and Fe(+3) and S(-2) creating pyrite (FeS_2) and Mackinawite (FeS). The initial concentration of Goethite (FeO(OH)) and Siderite in the sump composition effects the eventual concentration Fe(+2) and Fe(+3) in the solution. In turn effecting the amount of (S-2) that is reacted away. The effect this has on the production of H2S is displayed in figure 4.17 The same is theoretically possible with a a high enough concentrations of Zn(+2), creating Sphalerite (ZnS). Addition of Iron salts or Zinc salts, is a possible method to reduce H2S production. However, as is seen in figure 4.17, the effect is limited.

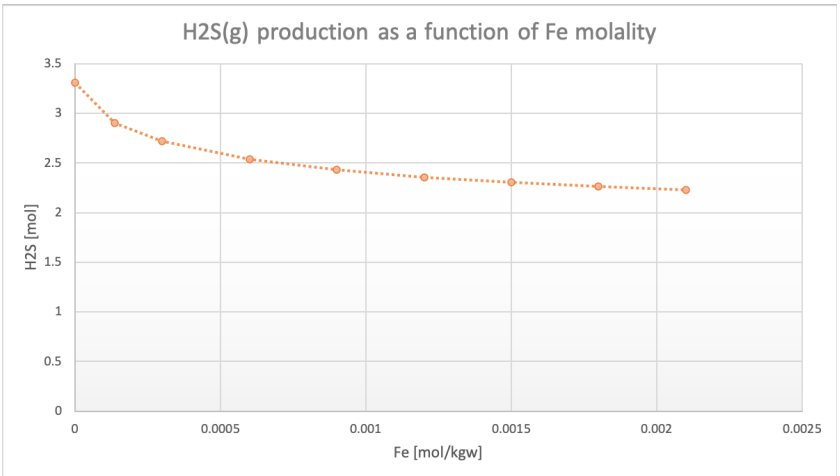

Figure 4.17: H2S production as a function of Fe concentration, at t= 1 year.

4.5. Dynamic modelling

These result take two important aspects into account, the output gas is assumed to be homogeneously mixed, and the cavern is used as a batch reactor simulated over time. In actuality hydrogen gas production from the storage facility will alter H_2S build up in the cavern since part of the H_2S will be purged in the production stream. A model is constructed using Matlab to define the estimated H_2S build up in the cavern, while taking the results from the reference model used in PHREEQC into account. The height of the H2S concentration in the output hydrogen gas from the storage cavern is highly dependant on the production- or use-curve of the cavern. When the cavern is used in high frequency and with high pressure fluctuations, the H2S concentration in the output will be low. If, however, the H2S has time to build up and the pressure fluctuations are lower, the concentration will rise. To illustrate this, a number of cases are constructed, each having distinctive properties that will highlight important variables, as well as give a maximum and minimum H2S concentration in the output gas.

Case 1: Max-use

First case is the maximum use case, in this case the cavern is filled until the maximum pressure is reached with a maximum filling rate of 1 MPa/day. When maximum pressure of 23 MPa is reached, the cavern will be emptied with 1 MPa/day until the minimum/ cushion pressure of 7 MPa is reached. This process will repeat over a time of 5 years.

This is displayed in figure 4.18 and 4.19. In figure 4.18, the total molar amount of H_2S is given as a function of time. The total amount will reach a maximum and minimum equilibrium of around 550 mol to 310 mol H_2S, until the sulfate in the brine is depleted. Then a decline is noticeable, reducing the molar amount to approximately 200 mol to 120 mol H_2S. The lower molar amount is attributed to an empty cavern (70 bar), while the higher molar amount will be in line with a full cavern (230 bar). Figure 4.19 gives the eventual concentration of H_2S in the output gas, during one output cycle in the first year. A maxumum concentration of 0.035 ppm is calculated when the cavern nears the minimum pressure.

Case 2: Production-curve

The maximum use scenario requires a steady hydrogen demand and supply. This makes it possible to vent the H_2S concentration in the cavern and by doing so prevent build-up. This is often not the case in the . To simulate a more realistic scenario, a production-curve is used as calculated by Nick Kimman in [53]. This curve estimates the demand of hydrogen when the cavern is used to supply for a CCGT hydrogen gas-turbine. The gas-turbine produces for premium power spot prices. The fluctuations in prices are highly effected by the season. There will be a higher demand for hydrogen in the winter, creating long stretches during the summer where the cavern is inactive. The total mass of hydrogen in the cavern is modelled over two years in figure 4.22 and over 10 years in figure 4.25. The supply of hydrogen to the cavern in this case will be supplied by electrolysers, giving a constant supply of hydrogen of 20kg/min. The total amount of H_2S, will have less opportunity to be purged and will continue to build up over the years. This is seen for 2 years in figure 4.22

and for 10 years in figure 4.23. After the time it takes for the sulfate in the brine to be depleted, there will be less H_2S production. But when looking at the build up over 10 years, it will take longer to reach a steady state. Increasing the concentration of H_2S every year. A much higher overall concentration of H_2S is calculated in the outflow is seen in figure 4.24. Reaching values of 24 ppm at year 10.

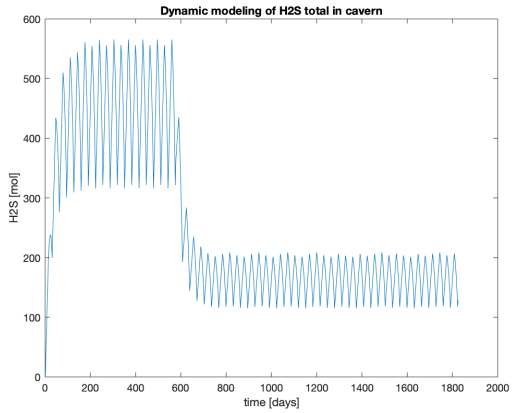

Figure 4.18: Max use case: Total mol H_2S in cavern over 5 years.

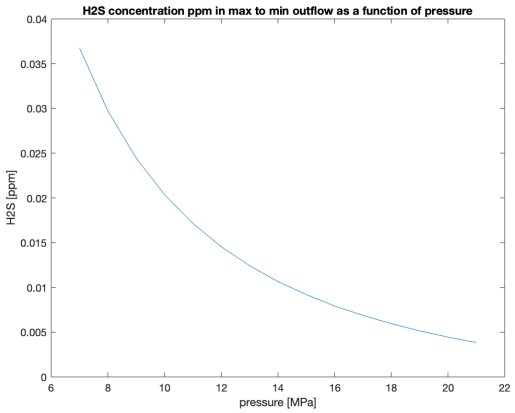

Figure 4.19: Max use case: Concentration H_2S in gas output in the first year

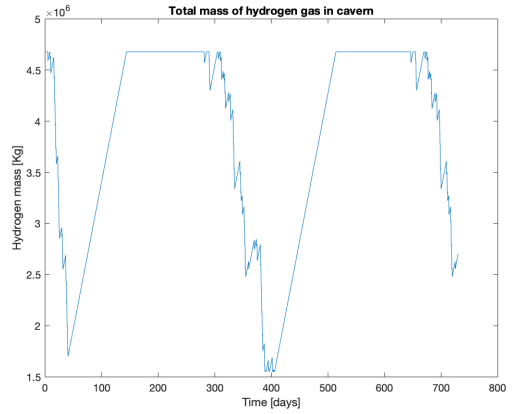

Figure 4.20: Demand case: Total mass hydrogen in cavern over 2 years.

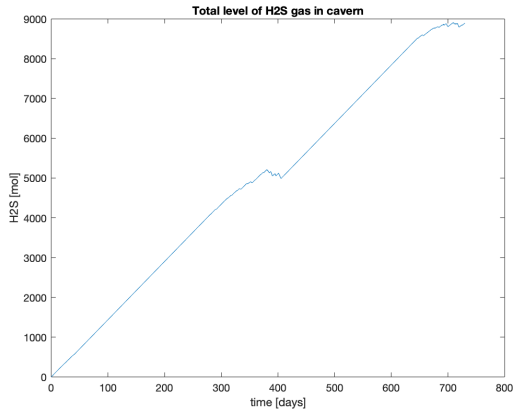

Figure 4.21: Demand case: Total mol H_2S in cavern over 2 years.

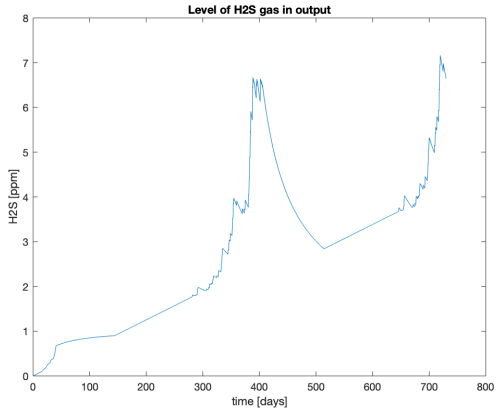

Figure 4.22: Demand case: Total mass hydrogen in cavern over 2 years.

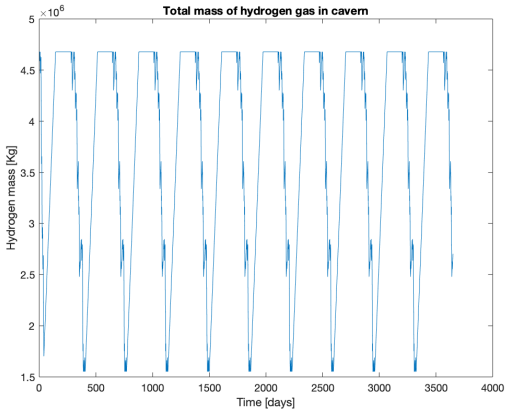

Figure 4.23: Dynamic modeling c, Pmin = 150, Pmax = 220, n = every 2 days, over 30 days

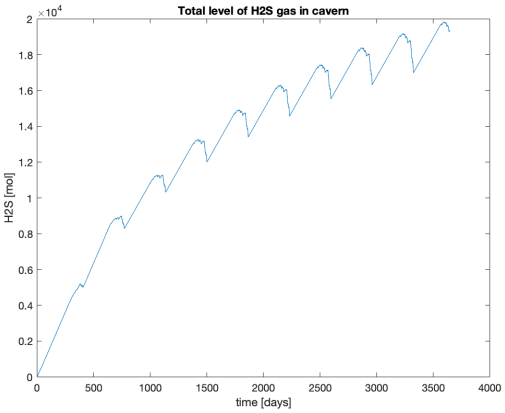

Figure 4.24: Demand case: Total mol H_2S in cavern over 10 years.

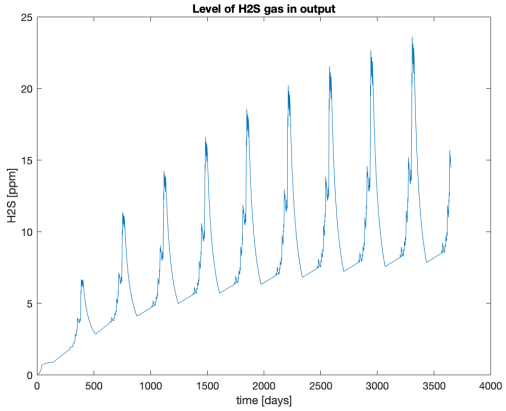

Figure 4.25: Demand case: Concentration H_2S in gas outflow over 10 years.

4.6. Conclusion

The H_2S production inside the cavern is simulated with existing cavern characteristics and with different use-cases. By using these simulations, it can be determined how a cavern can be used or constructed in order to minimise H_2S production.

Cavern selection

Following the batch-type simulations it is determined that a low temperature and low pressure will prevent H_2S production. This can be achieved by reducing cavern depth. Low S(6+) and high Fe(2+), or Fe(3+) concentrations will prevent build up. It it is therefore advisable to create the cavern in an anhydrite poor and pyrite/ mackinawite/ goethite rich salt layer. Or a high salt layer with high halite purity in general.
It is highly advisable to test both the cavern brine as well as the cavern salt for microbial activity. This can be an early and clear indicator for the suitability of hydrogen storage for fuel cell application in the cavern. However, according to results in chapter 4.2.3, there is still a large enough risk of H_2S production when the bacterial reduction rate is calculated for the minimal detectable bacteria activity.

Prevention of H_2S production.

In order to reduce the sulfate reduction rate, it is theoretically possible to increase the brine pH, or to increase the iron-ion concentration in the brine. This can help by preventing the created S(-2) to form equilibrium reactions to H_2S. Instead by increasing the pH it will form HS^-. Or when adding iron-ions, FeS and FeS2 will

be created.

Dynamic modelling results.
After analysis of the dynamic modelling, it is clear how detrimental the use of the cavern is to H_2S build up. When comparing the maximum use-case to a predicted use-case, the concentration in the outflow gas rise by a factor of 500 in 5 years. For this reason, even the smallest colony of sulfate reducing bacteria can have increasingly negative effects on hydrogen purity. When looking at the maximum use-case there is a reduction in the concentration after the sulfate concentration in the brine has been depleted. The newly established reduction rate is a function of the anhdyrite dissolution rate in the sump, as well as the transport rate of the newly available sulfate from the sump to the brine layer.

Key takeaways: Chapter 4

In this chapter the chemical model is discussed. The bacterial reduction rate is determined. The cavern's mineral composition, brine composition and the cavern dimensions are discussed.

- The diffusion of hydrogen in the brine is simulated over 6 years and it is estimated that the hydrogen will reach the minimum concentration for sulfate reduction in the sump after 11 years.
- When simulating the reference case, after 2.75 years there is a reduction in H2S production. This is due to the depletion of sulfate in the brine. Sulfate is now transported from the sump, which limits the kinetic rate.
- Parameters that positively influence H2S production are: high bacterial reduction rate, high pH, high sulfate concentration, high temperature, high pressure and low Fe concentration.
- Both pH and Fe concentration are parameters that can be adjusted, by injecting either NaOH or Fe rich solutions to the brine. This could lead to a reduction of H2S production

The results from the chemical model are implemented in a dynamic model in order to see the effect the use-curve of the cavern has on the H2S output concentration Two cases are made: Case 1 implies a maximum use curve to the cavern. For case 2 the use curve is constructed after a theoretical demand curve of a hydrogen gas power turbine. Conclusions after analysis of both cases:

- For both cases the H2S concentrations exceed ISO limits of 0.004 ppm H2S, for case 1 the maximum is at 0.04 ppm and for case 2 the maximum rises every year. With the first year reaching 6.6 ppm and within 10 years reaching 24 ppm.
- The reduction of the H2S production after 1.75 years is clearly seen in the maximum use case, and is also measurable in case 2.

5

Above ground storage process

In the previous chapters, this report has established the factors that influence the production and build-up of H2S in salt caverns. By knowing the variables that contribute to the contamination rate, it is possible to reduce it significantly. However, the concentration limit set by the ISO norms of 0.004 ppm for H2S and 5 ppm for H2O are challenging to achieve. This chapter will provide insight into the possibilities of a post storage Purification processes, to find out if it is possible to purify the H2S with the S43 cavern conditions as specified in this report, at reasonable (extra) energy cost. The removal of H2S is known as gas sweetening and is a common process within oil refineries or chemical processing plants. A simplified overview of the gas-sweetening process is given in figure 5.1.

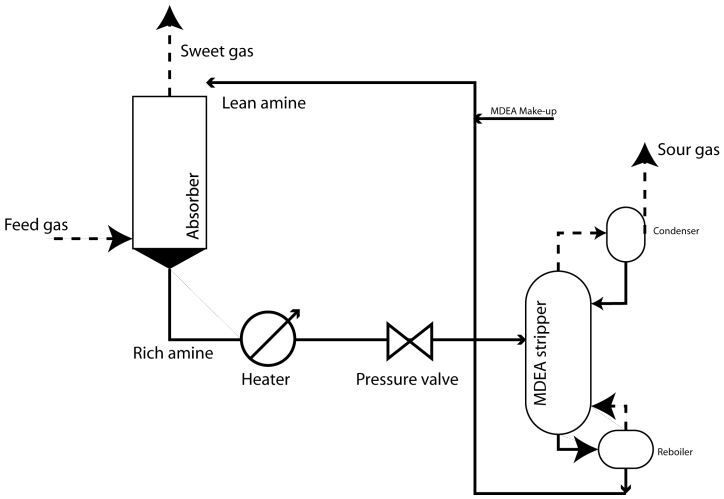

Figure 5.1: MDEA gas sweetening process overview.

Amine	MEA	DEA	DGA	MDEA
Solution strength, w%	15-20	25-35	50-70	20-50
Acid gas loading, mole/ mole	0-0.35	0-0.35	0-0.35	0-0.4
Ability to selectively absorbe H_2S	No	Under limited conditions	No	Under most conditions

Table 5.1: Typical operating conditions and data for amines [72]

5.1. Gas-sweetening

The process that will be analysed in this chapter uses amines in a chemical absorption process[34]. In a general version of this process, the H2S rich gas is controlled for pressure, after which it enters the bottom of a

chemical absorption tower. The amine solution enters the top of the absorption tower, where it will come in contact with the sour gas as it flows counter-current down the tower. After the H2S rich liquid flows out of the tower, it flows to a desorption tower, where the H2S rich liquid is scrubbed, filtering out the H2S. The amine is now regenerated, and it can be recycled back into the process.

The first step is to differentiate between amine-solution, as they have different properties that alter the effectiveness of the process. Four different amine solutions are compared in table 5.1. The choice is made to use MDEA (Methyl diethanolamine) as the absorbent. MDEA has high H2S selectivity, and although it is considered corrosive, it can still be used in a solution with up to 50 w% MDEA. It is considered most efficient for removing H2S at low concentrations [15]. The MDEA reacts directly with the H_2S, creating a salt, which can then be dissolved in the water of the MDEA solution.

$$MDEA + H_2S \leftrightarrow MDEA^+ + HS^- \tag{5.1}$$

5.2. Gas-dehydration

In order to simulate a method that could potentially purify dehydrate the H_2O rich hydrogen gas. This report will look into TEG-glycol dehydration. This dehydration method is selected as it is used in the storage plant in Epe for natural gas dehydration. With a potential plant refit in mind, this report investigates the effectiveness of TEG-glycol for hydrogen gas dehydration. TEG-glycol works with physical absorption, the wet gas is brought into contact with dry glycol in an absorber. The wet, rich, glycol then flows from the absorber to a regeneration system in which the entrained gas is purifiedd and fractionated in a column and reboiler.

5.3. Process modelling

This report uses Aspen Hysys for the process simulation. Literature studies are done before hand to determine the accuracy compared to other available processing software like Aspen plus, Aspen RadFrac, ProTreat, ProMax, Aspen RateSep, CHEMASIM and CO2SIM in [61] and [32]. Following this review, Aspen Hysys performed with similar accuracy at rate-based simulation and better at achieving an accurate amine removal grade. In Aspen Hysys the fluid package used is the 'acid gas' package which is based on the Electrolyte Non-Random Two-Liquid (Electrolyte NRTL) model with the required aqueous-phase equilibrium and kinetics reactions needed for rigorous computations of the process. The Peng-Robinson Equation of State is used for vapour phase properties.

Verification of process model

In order to verify the accuracy of the Purification of H2S from the hydrogen outflow, the process model in Aspen Hysys is verified to the output data from an existing plant.[14] The characteristics of the streams, absorber column and stripper column are set equal to what is used in existing plant operated by Lurgi in Germany in order to verify the calculations done by Aspen Hysys. Table 5.2 compares the Lurgi plant output data to the calculated data from our Aspen Hysys model, as well as to two comparative studies to the Lurgi plant both documented in article [14], one modelled in Aspen Plus using equilibrium equations and one modelled in TSWEET. When analysing the data, Aspen Hysys is noticeably more accurate in predicting the H2S absorption and desorption, while being less accurate in modelling CO2 transport. Since the system primarily focuses on H2S production in the salt cavern, Aspen Hysys is deemed an accurate method to simulate this process.

	Plant data	*Average deviation*		
Absorber	**Lurgi**	**HYSYS**	**ASPEN PLUS**	**TSWEET**
H2S out [ppm]	46-50	6.5	21	40
CO2 out [mol%]	2.7	2.44	0.22	0.28
Desorber				
Lean amine H2S loading	0.0056	0.00135	0.012	0.005
Lean amine CO2 Loading [mol/mol]	2.90E-05	1.37E-05	1.20E-04	1.40E-04

Table 5.2: Comparison of process model accuracy with Lurgi natural gas sweetening plant.

	Set input			**Set limits**	
	Gas in comp.	635 ppm H2O 24 ppm H2S		Gas out comp.	5 ppm H2O 0.004 ppm H2S
	Gas in P [bar]	230		Gas plant out P [bar]	40-80
	Gas in T [°C]	50		Gas plant out T [°C]	0. –35
	Gas in flowrate [kmole/hr]	5200		Absorber tower (MDEA) P [bar]	1 – 70
	Packing type	Mellapak 250X		Absorber tower (MDEA) T [°C]	25-70
	Gas sweetening absorbent	MDEA		MDEA T limit [°C]	205
	Gas dehydration absorbent	TEG		TEG T limit [°C]	187
				Min. liq. loading Mellapak	0.2[m^3/m^2hr]
	Sizing estimations			**Important free variables**	
Gas sweetening				**Gas sweetening**	
Absorber	Estimate MDEA inflow rate [kmole/hr]	50		***Absorber***	MDEA loading [mole/mole amine]
	Tower pressure [bar]	45			H2S concentration [ppm[
	Tower temperature [°C]	25			Gas and liquid outflow [kmole/hr]
Stripper	Gas inflow stage temperature [°C]	130		***Stripper***	Reflux ratio
	Tower dimensions (DXH) [m]	1.7X12			Condenser temperature [°C]
	Reboiler temperature [°C]	195			Tower temperature distribution [°C]
Gas dehydration					Gas and liquid out flow [kmole/hr]
Absorber	Estimate TEG inflow rate [kmole/hr]	10			Gas and liquid composition
	Tower pressure [bar]	45		**Gas dehydration**	
	Tower temperature [°C]	25		***Absorber***	TEG loading [mole/mole TEG]
Stripper	Tower dimensions (DXH) [m]	1.5X9			H2O concentration [ppm]
	Reboiler temperature [°C]	187			Gas and liquid outflow [kmole/hr]
	Condenser temperature [°C]	98		***Stripper***	Reflux ratio
	Calculated variables by graphical determination				Gas and liquid out flow [kmole/hr]
	Graphical determination				Gas and liquid composition
Gas sweetening	Tower height [m]	4			Tower temperature distribution [°C]
	Tower stages []	8			Gas feed temperature [°C]
	(Check) MDEA inflow rate [kmole/hr]	50			
Gas dehydration					
	(Check) TEG inflow rate [kmole/hr]	10			

Table 5.3: Parameters used in the design process, divided over four subgroups. The set input parameters, the limits, the calculated estimates and lastly important free variables

5.4. Design process

This chapter designs a purification process in Aspen Hysys, in order to make a rough numerical estimate to the capabilities of the hydrogen gas sweetening and dehydration steps as explained above. The goal is to find out if it is possible to purify hydrogen up to ISO limits with reasonable (energy) costs. This report makes use of existing processes and sizing methods in literature. The constructed model does not make use of detailed-sizing or extensive cost analyses, but should be used as a ball-park estimate. An overview of the most important parameters are given in table 5.3 The process is designed in four steps:

1. Determine the set input parameters. These consist of stream characteristics as calculated by the dynamic model explained in chapter 4. The input parameters define the stream composition and characteristics as defined by cavern S43's limits.

2. Determine the limits that define the process. These limits influence tower specifications, by limiting the pressure or temperature. But also consist of restrictions set to the output gas: The ISO limits to the gas composition and the restrictions set by GTS for the pressure and temperature.

3. Step three is to determine process characteristics in order to fully define the process in Hysys. These are either calculated by sizing methods or standards available in literature. These parameters require more explanation, which is given in section 5.5.3 and 5.5.4.

4. With the most of the process defined, values like the height of the absorber tower are simulated in Aspen Hysys. This is also done to verify the absorbent inflow rates. The results of this step are found in section 5.5.5.

5. Lastly, there are the free variables, which are calculated by Aspen Hysys. Only limited by the limitations set in step 2.

5.5. Process design

The model built in Aspen Hysys for both the gas-sweetening process and the gas-dehydration step is displayed in figure 5.7. The parameters of the process are displayed in table 5.3 and are divided over the four design steps. The model is divided over three phases:

- Phase A: compression and cavern storage.
- Phase B: Gas sweetening.
- Phase C: Gas dehydration.

5.5.1. Step 1: Input variables

The gas enters the model with temperature and pressure defined by the averages of the GTS gas grid, 50 bar and 20 °C. The gas composition exiting the cavern is defined by the dynamic model demand case after 10 years of storage. This means a H2S concentration of 24 ppm and a H2O concentration of 643 ppm. The cavern operates at maximum pressure, 230 bar. And the gas exits the cavern at maximum flow rate: 5173 kmole/hr. Three other distinctions are made, the absorbent for the gas sweetening process is MDEA. The absorbent for the dehydration is TEG. The packing used in the absorber tower is Mellapak 250X, which is also used in the Lurgi plant. Mellapak 250X is a packing material produced by Sulzer and is used commonly used in CO2- and H2S-absorbers and strippers [65].

5.5.2. Step 2: Limits

Limitations to the gas outflow are set by ISO, 0.004 ppm H2S concentration and 5 ppm H2O concentration. The gas grid (GTS) has limits to the gas pressure (40-80 bar) and temperature (0 - 35 °C). There are temperature restrictions to the absorbents used to avoid degradation. Lastly, the MDEA has a minimum wetting rate to make sure the packing in the tower is sufficiently covered by a liquid film. This is defined by the minimum liquid loading which is 0.2 $\frac{m^3}{m^2 h}$ for Mellapak 250X. The minimum wetting rate in m^3/hr is then also dependant on the specific surface area, as well as the absorber tower dimensions.

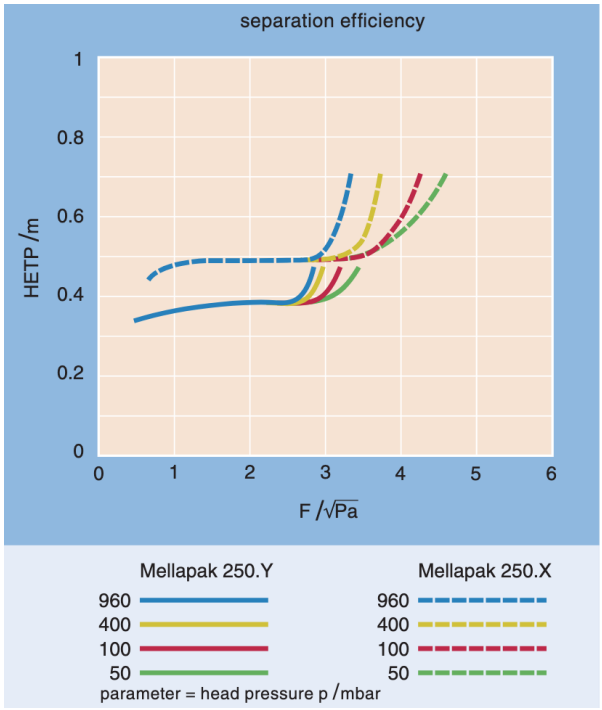

Figure 5.2: Purification efficiency of stripping factor (F) compared to HETP. [65]

5.5.3. Step 3: Sizing estimations: Phase B.

In order to run the model, more parameters should be determined in order to fully define the process in Aspen Hysys. First this report looks at the gas sweetening process.

Absorber tower dimensions

The diameter of the absorber tower is defined by analysing Purification efficiencies as described by Sulzer for their packing material Mellapak 250X. This is illustrated in a graph by made by Sulzer in figure 5.2. The gas load factor also known as the F-factor, is stable at 2 [$\sqrt{Pa}$], which will result in a Height Equivalent to a Theoretical Plate (HETP) of 0.5 m. The F factor is defined by equation 5.2. Here w_g is the gas velocity and ρ_G is the gas density. By knowing the actual volumetric flow ($Q_G = 0.81 m^3/s$), the column diameter is calculated to be 1 m which is done via equation 5.3. Using this method the diameter is dependant on the column pressure and temperature, the gas volumetric flow and density and on the packing type.

$$F = w_G * \sqrt{\rho_G} \tag{5.2}$$

$$D = \sqrt{\frac{Q_G * \sqrt{rho_G}}{\frac{1}{4}\pi * F}} \tag{5.3}$$

Absorber tower pressure

With the inputs and the limits defined, estimations can be made to the tower characteristics. The choice is made to let the gas operate at a pressure of 45 bar. This is only done so the gas does not have to compressed after the purification step and is by no means the most efficient absorber tower pressure.

Absorber tower temperature

The absorber process works best at low temperature, the limits found in literature [14] set the minimum limit at 25°C, which is used as the absorber tower temperature.

MDEA flow rate

An MDEA flow rate (Q_{MDEA}) is first calculated by equation 5.4 [63]. This equation estimates the rate necessary to absorb the specified H2S concentration. Here, the MDEA concentration is (C_{MDEA}), the H2S concentration

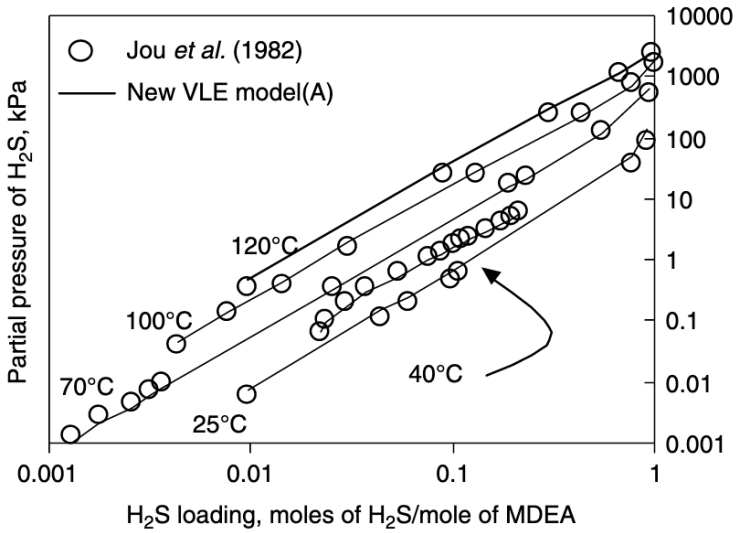

Figure 5.3: Partial pressure of H2S in 48.9 wt% aqueous MDEA solution at 25, 40, 70, 100 and 120°C. [71]

(C_{H2S}), the gas flow rate (Q_G in mol per hour) and the MDEA loading (L_{MDEA} in mol H_2S absorbed per mol MDEA). This last factor is dependant on the partial pressure. This relation is defined by figure 5.3.
For the concentration of 24 ppm, the MDEA flow rate is calculated to need at least 50 kgmole/hr. This can be seen as the estimated absorbent circulation rate. The actual MDEA circulation rate, has to be above a rate that agrees with the liquid loading limit of 0.2 $\frac{m^3}{m^2 h}$. This means that there should be a flow of 0.2 $\frac{m^3}{hr}$ per m^2 of packing surface area. The specific surface area of Mellapak 250X is specified in its name, 250 $\frac{m^2}{m^3}$. Since the diameter of the absorber column is defined, 1m, the maximum height of the tower for the estimated MDEA circulation rate is calculated to be 18m. When the tower is higher then 18 meters, the liquid flowrate should be increased.

$$Q_{MDEA} = \frac{C_{H2S} * Q_G * \rho_{MDEA}}{L_{MDEA} * C_{MDEA}} \tag{5.4}$$

Stripper characteristics
The stripper tower works with the same pressure characteristics as used in the Lurgi plant. The condenser works at 1 bar, and the reboiler at 3 bar. Two other parameters are set, first the temperature of the feed, which is set at 130 °C, also defined by the Lurgi plant. Secondly the condenser temperature, this is set at 195 °C, with a 10 °C margin, keeping it below the maximum degradation temperature of 205°C. The parameters copied from the Lurgi plant: reboiler pressure, condenser pressure and feed temperature, are considered independent of the factor that differentiates the stripper tower described in this model to that of the stripper tower used in the Lurgi plant: The liquid flow rate. They are therefore assumed to be suitable tower characteristics.

5.5.4. Step 3: Sizing estimations: Phase C.

Now estimations should be done to determine parameters for the dehydration step.

Absorber tower characteristics
Like with phase B, the absorber tower pressure is set at 45 bar to avoid an extra compression step. The tower temperature is also set at 25°C to avoid an extra heating step. Again, these are not the optimal tower settings for dehydration, but are a design choice. The TEG inflow rate is first estimated with a engineering rule of thumb of 3.5 gallons per pound of water. With 58 kg of water per hour this amounts to 1.7 m3/hr of TEG. This value is later verified graphically via Aspen Hysys in figure 5.5. The TEG inflow rate of is comparable to values used in the field and in literature in article [6] and [21]. The column diameter is determined from equation 5.5. where D is the internal diameter of the glycol contactor, m; Q_g gas volumetric flow rate, (m^3/hr); V_{max} is maximum superficial gas velocity, (m/hr); K_{SB} is the Souders and Brown coefficient which is 0.092 m/s at

40 bar [67]; ρ_L glycol density, (kg/m^3); and ρ_G gas density at column condition, (kg/m^3). This results in a diameter of 2m. Following the guidelines of Mokhatab's sizing handbook [67], the column has 10 trays with a tray spacing of 60 cm.

$$V_{max} = K_{SB}\left[\frac{\rho_L - \rho_G}{\rho_G}\right] = \left[\frac{4Q_G}{\pi D^2}\right] \tag{5.5}$$

Stripper tower characteristics
The stripper tower characteristics are limited to the maximum degradation value of TEG, the set value here is 187°C for the reboiler. And 98 °C for the condenser. The inside diameter of the stripper is defined with equation 5.6. The stripper tower works with 15 bubble trays with a 60 cm spacing. These values are also taken from the sizing handbook [67].

$$D_i = 0.2286(0.0060Q_{TEG})^{0.5}) \tag{5.6}$$

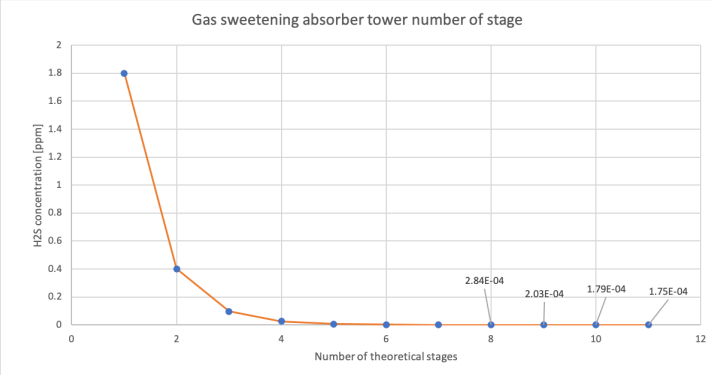

Figure 5.4: Graphical determination of number of stages in MDEA absorber.

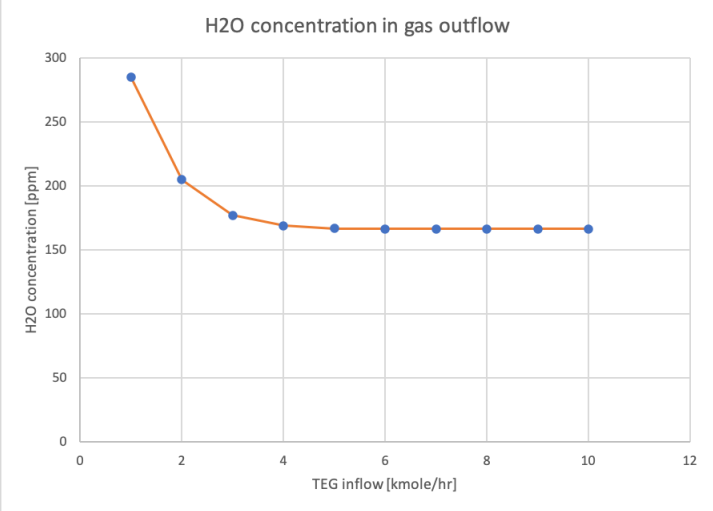

Figure 5.5: Graphical determination of TEG inflow rate.

5.5.5. Step 4: Graphical determination

With these estimations in place, the remaining variables that should be defined can be calculated using Aspen Hysys. The way this is done is by defining case studies in Aspen Hysys, allowing the program to change a variable while calculating a demanded output variable.

For the absorber tower, the demanded output variable is the H_2S concentration of the gas output. The values that are yet to be determined are: tower height, and number of theoretical stages. Lastly, the MDEA inflow rate should be checked. The tower height is defined by the number of theoretical stages times the HETP.

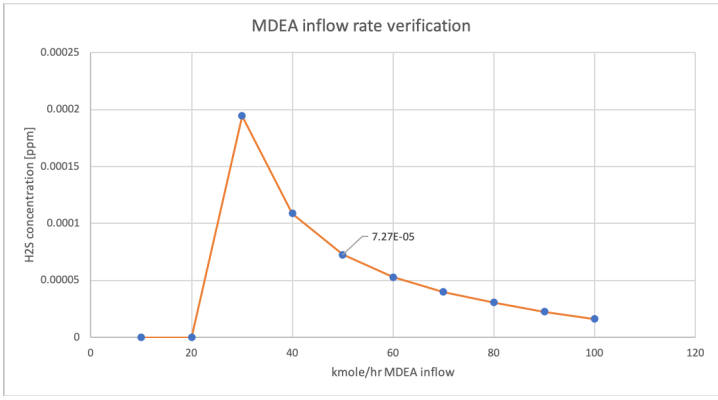

Figure 5.6: Graphical verification of MDEA inflow rate.

Since the HETP is defined as 0.5, the tower height can be defined by calculations in Aspen Hysys. This step can be seen in figure 5.4. The tower height is set at 4m, with 8 theoretical stage.

When verifying the estimated MDEA inflow rate, in figure 5.6. The first two values of 10 and 20 kmole/hr are below the minimum wetting rate. The estimated value of 50 kmole/hr, is proven to be suitable.

The TEG circulation rate is determined in figure 5.5. The maximum obtainable flow rate for water with this setup is still well above ISO standards. This will be discussed in the results.

5.6. Results

The results following this model should be seen as rough numerical estimates and should not be seen as a guideline to build a hydrogen purification plant. However, the model can make an estimate to the cost and energy required to purify the H_2S in the hydrogen stream up to ISO fuel cell standards.
An overview of the results can be found in 5.4

The goal to keep in mind when analysing these results is to find out if the concentrations in the gas flow are within the ISO limits and to analyse the energy requirements and financial requirements of both these Purification steps to see where the majority of the expenses en power is required. This is why first the different analysed cases are explained. After which this report highlights the projected hydrogen purity and the effectiveness of the purification. Then, the energy and financial requirements are analysed. This is done to find out how much energy and investments are required to power the purification step, compared to the original gas storage process.

5.6.1. Purity

Following the models results it can be concluded that a plant sized through methods explained above, with the cavern output gas flow and concentration, the MDEA flow rate adjusted for the gas flow characteristics at a working gas pressure of 45 bar, can theoretically purify the hydrogen gas from H_2S to a concentration below 4E-3 ppm. The H_2O concentration however is unable to reach the 5 ppm limit, this is because the stripper working with a maximum reboiler temperature is unable to adequately purify the H_2O from the TEG liquid stream, leaving a molar concentration of 21% H_2O. The impure TEG stream, has a significant effect on the H_2O concentrations in the gas stream. Further design optimisation is necessary. Investigation into the use of a different dehydration method, such as pressure swing adsorption is also an option. One of the downsides of using liquid absorbent for gas purification is the trace amounts of the absorbent in the gas stream. The concentration MDEA and TEG are 5E-4 ppm and 8E-3 ppm, respectively. These values are well below what is demanded by ISO standards.

5.6.2. Energy requirements

With the help of Aspen Hysys the power requirements for the plant are calculated per process step. Displayed in the appendix A.5. The largest power requirement (9.4MW) are required to compress the hydrogen gas before entering the cavern and by the cooler adjusting the temperature for the adiabatic pressure increase.

Gas sweetening			**Gas dehydration**		
Absorber column	Gas flow in [kmole/hr]	5173	***Absorber column***	Gas flow in [kmole/hr]	5173
	Gas flow out [kmole/hr]	5173		Gas flow out [kmole/hr]	5168
	liquid flow in [kmole/hr]	50		Liquid flow in [kmole/hr]	10
	liquid flow out [kmole/hr]	50		Liquid flow out [kmole/hr]	13
	H2S in [ppm]	24		H2O in [ppm]	624
	H2S out [ppm]	0.001		H2O out [ppm]	97
	MDEA loading in [mol/mol amine]	1.52E-05		H2O in TEG [mol%]	27%
	MDEA loading out [mol/mol amine]	1.89E-02		H2O out TEG [mol%]	40%
Stripper column	Liquid flow in [kmole/hr]	50	***Stripper column***	Liquid flow in [kmole/hr]	13
	Liquid flow out [kmole/hr]	8		Liquid flow out [kmole/hr]	10
	Vapor flow out [kmole/hr]	42		Vapor flow out [kmole/hr]	3
	H2S in [ppm]	2468		H2O in TEG [mol%]	40%
	H2S out [ppm]	2		H2O out TEG [mol%]	27%
	MDEA loading in [mol/mol amine]	1.89E-02			
	MDEA loading out [mol/mol amine]	1.52E-05			
	Gas in	**Gas out**		**Gas in**	**Gas out**
	ppm	*ppm*		*ppm*	*ppm*
H2	9.9932E+05	9.99E+05	*H2*	9.9931E+05	9.9931E+05
MDEA	0.00E+00	1.19E-02	*MDEA*	1.19E-02	4.69E-04
H2O	6.55E+02	6.24E+02	*H2O*	6.24E+02	1.66E+02
H2S	2.40E+01	1.03E-03	*H2S*	1.03E-03	3.26E-06
TEG	0.00E+00	0.00E+00	*TEG*	0.00E+00	8.03E-03

Table 5.4: Results of purification process.

When using the compressor calculated in chapter 3, this can be reduced to 7.6 MW. All in all the process has a 3% energy losses, excluding leakage losses, caused by the energy requirements of the purification process. The energy requirements are compared to the Gibbs free energy. The gas sweetening process only accounts for 6.6% of the power losses, this is due to relatively small MDEA flow required to filter the H2S. The absorber tower does not require power, so the only losses are caused by the heating, cooling and pressurising of the MDEA liquid. The TEG dehydration is a similar process, but requires a larger TEG inflow, this amounts to 5.2% of the total losses. The remaining 90.1 %, are required by the storage compression and cooling of stage A. The total energy requirements are calculated to be 3.8W per mole hydrogen.

5.6.3. Cost analysis of refitting storage plant

An analysis is done by Aspen Process Econopmic Analyzer for case 1 and case 4. Both the results of these approximations are found in the Appendix A.4. For case 1, 74% of the CAPEX is used for the gas compression and cooling of phase A. The sweetening and dehydration process, B and C, both take up around 11% of the CAPEX. The total cost is estimated to reach around €0.08 per Kg of hydrogen. This is limited only to the utility costs of the plant. The value is comparable to the value (€0.06) per Kg) calculated by the National Renewable Energy Laboratory [1] for storage costs of hydrogen gas in salt caverns.

5.7. Conclusion

In conclusion to the process model: The model is successful in filtering out the H_2S. The hydrogen flowing out of the process reaches a 99.993 % purity.
This happens with energy losses of 3%. Taking the total energy losses, only 6.6% is due to the gas sweetening process and 5.2% is caused by the gas dehydration. This means that the gas-sweetening process is a very energy efficient process, while keeping the operational costs down by recycling the relatively costly MDEA solution. The gas dehydration is less energy efficient and with the calculated specifications is not capable getting the H2O concentrations below the ISO limit. PEM fuel cells are considered to be a vital part of the future hydrogen economy.

Key takeaways: Chapter 5

This chapter designs a possible purification plant for hydrogen gas storage in salt caverns.

- The plant uses MDEA to purify the hydrogen gas from H_2S and uses TEG to purify the hydrogen gas from H_2O.
- Highly influential parameters for the MDEA absorption tower include pressure, temperature and MDEA inflow.
- The process is successful in filtering out the H_2S concentration with an MDEA absorber towers working at a pressure of 45 bar to below 0.004 ppm ISO limit.
- Water concentration in the cavern output exceeds the maximum allowable limit, therefore an extra dehydration step is added using TEG-absorption.
- The plant is unsuccessful in purifying the hydrogen gas stream to the 5 ppm ISO limit.
- The output hydrogen is calculated to have a 99.993 % purity, a minimum of 19MW is required to power the complete process, from grid to grid.
- The complete process has around 3% energy losses compared to the Gibbs energy of liquid water formation, of the total energy 6.6% is by gas sweetening, 5.3% is caused by the dehydration step
- Total CAPEX is calculated at €17 million, OPEX is calculated at €1260 per hr. For the case 1 74% of the CAPEX are required for phase A,11% for phase B and 11% for phase C.

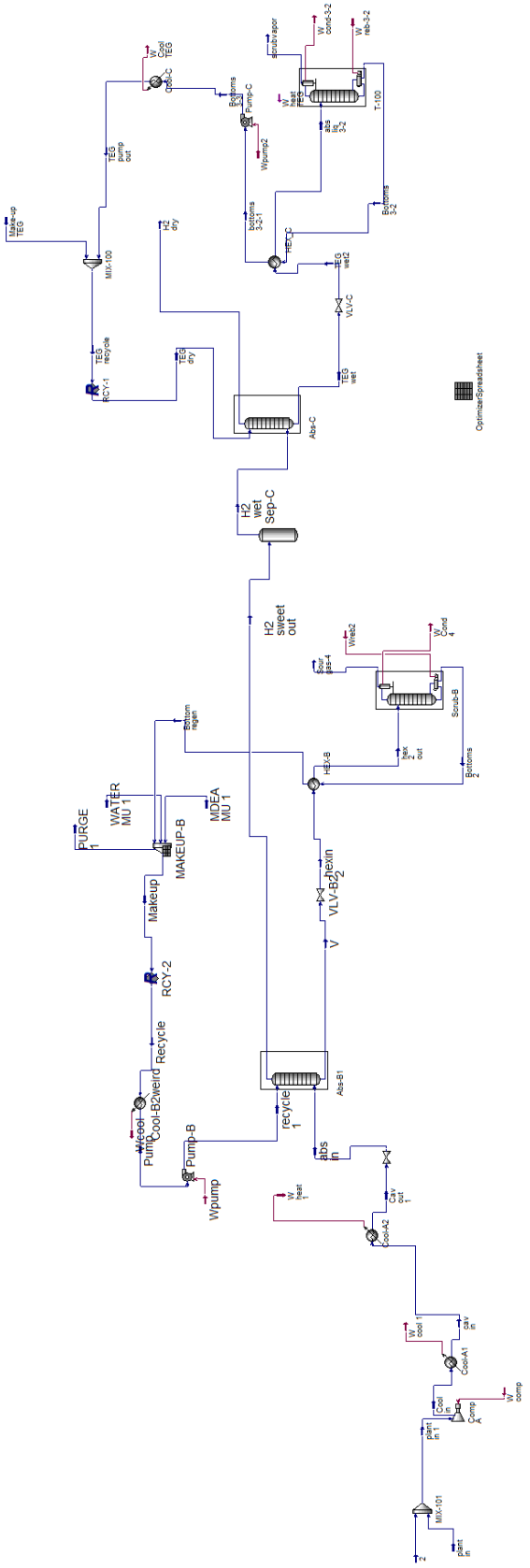

Figure 5.7: Aspen Hysys process setup. Including dehydration process.

6

Conclusions and recommendations

This report focuses on the compatibility of sub-surface salt caverns for long-term, large-scale hydrogen gas storage. First a literature review is done to review the salt cavern storage process and to find out what the high risk areas will be when implementing hydrogen gas. This is done to answer the first research question:

What are potential risks when storing hydrogen in salt caverns?

The risks are primarily found when the gas pressure increases. The most important risks when storing high pressure hydrogen in caverns are:

- Hydrogen gas leakage.
- Hydrogen diffusion and embrittlement.
- Hydrogen (auto-)ignition and flame detection.
- Hydrogen contamination .

After literature review, it was found that there was a hiatus in research done on the contamination risks of hydrogen in salt caverns. Hydrogen contamination is therefore the main focus of this thesis. Impurity limits for hydrogen are especially strict when the gas is used in fuel cells. Limiting H2O concentration to 5 ppm and H2S concentration to 0.004 ppm.

Are there substantial risks of contamination with salt-cavern storage? What are defining variables that contribute to said contamination?

The model constructed in PHREEQC works as a batch reactor, simulating values taken from the S43 cavern in the storage plant in Epe Germany operated by Vattenfall. H2S can be produced when a cavern is contaminated by Sulfate Reducing Bacteria. Results from this research method determine that values that influence the H2S production rate are (sorted by significance):

- Bacterial growth and reduction rate
- Brine volume and sulfate concentration.
- Brine pH and ionic strength.
- Cavern pressure and temperature.
- Fe2+ and Fe3+ concentration.

The cavern pressure, temperature, sulfate and iron concentration and brine volume, are all values that should be taken in to account when either building or choosing a cavern that is to be used for hydrogen storage. None are as important as the bacterial presence, the number of sulfate reducing bacteria (SRB) present in the cavern soil The SRB concentration should be tested before hand as this has an important effect on the H2S

production rate. If there are no SRB's, there will be no H_2S.

How do these impurities build up when the cavern is used?

The PHREEQC model determines what happens inside the cavern, but does not take into account any mass flows, in or out the cavern. Therefore, a dynamic model is constructed which determines the build up of H2S, as a function of time and a cavern demand-curve. Two cases are made: Case one, the cavern use is maximised, 1MPa/day pressure change throughout the year. Case two, the cavern demand curve is determined by the simulated hydrogen demand of a hydrogen gas turbine which uses the cavern for seasonal storage.
In case one, the H2S build up is limited however still exceeds the fuel cell guidelines. A shift is perceived in the H2S production after 1.75 years, the sulfate concentration in the brine is depleted. Now the sulfate has to be transported from the sump first, reducing the H2S production rate.
In case two, H2S concentration greatly increases throughout the year. Reaching peaks of 6.6 ppm in one year and 24 ppm in 10 years. In time it reaches a concentration equilibrium, which is far above any allowable ISO concentration.

How can the gas impurities be purified? What changes should be made to the current storage process?

With such a high H2S production it should not be used in a gas turbine or in fuel cells directly. This research continues by designing an above ground purification process in Aspen Hysys in order to find out if its possible purify the hydrogen gas within reasonable (energy) costs.
The accuracy of Aspen Hysys is validated by comparing simulations to empirical data from a specific natural gas sweetening plant operated by Lurgi. The choice for the gas sweetening step is made to use MDEA as a chemical absorbent. The choice for the dehydration is TEG, this is based on the dehydration step present in the storage plant in Epe. The model is successful in purifying the H_2S to within ISO limits. The model is unsuccessful in reaching the ISO limit for H_2O with 160 ppm remaining. The surplus of H_2O is caused by inefficient stripping of TEG. The energy cost for the MDEA absorption process is estimated to be non-substantial compared to the original storage process. This can therefore be seen as a suitable addition to the cavern storage plant.

What are key cavern conditions that influence the suitability of hydrogen storage in salt caverns and for what purpose can the storage plant be implemented?

To answer the main research question, the key cavern conditions that influence the suitability of hydrogen storage in salt cavern, based on the risk of contamination are the bacterial sulfate reduction rate and the pH of the aqueous environment. Caverns should be tested prior to use on the possibility of sulfate reducing bacteria. It is possible to reduce H_2S production by changing the pH or injecting aqueous iron, or by the way the cavern is used. The reduced production of H_2S after the sulfate has been depleted in the brine is a factor to this. But more significant is how much H_2S the cavern is allowed to build up. H_2S in gas outflow is estimated to have large peaks in outflow concentration due to possible H_2S build up in relatively empty caverns.

6.1. Recommendations

As mentioned in the first chapter, there are other aspects of the hydrogen storage process that can negatively impact the feasibility. One of the primary aspects is the hydrogen leakage rate when its at high pressure. The effects of hydrogen leakage is the subject of many studies, and is widely considered its greatest safety hazard. Both leakage and diffusion of hydrogen should be taken into account when equipping the storage plant. But further research should also be done on the permeability of the rocksalt cavern wall
Several studies are currently done to determine the diffusion rate of hydrogen in both the rocksalt and brine by the TU DELFT ADMIRE group.

This report assumes a homogeneously mixed cavern, in reality the due to the difference in weight, the concentration distribution of hydrogen is more favoured towards the top of the cavern. However, this is also heavily effected by fluid dynamics in the cavern caused by temperature differentiation and in and outflow of the cavern gas.

This research is based on the assumption that there are sulfate reducing bacteria present in the cavern. The H2S production is caused by these bacteria and it happens at a rate that is derived from literature study. However, an accurate prediction of the reduction rate should be made by testing cavern soil.

As explained in chapter 4, the possibility of sulfate reduction in the sump is ignored in this study, it is calculated that the hydrogen can reach the sump in under a year. This can prove to have additional adverse effects to the H_2S production.

This report does not take in to account thermal sulfate reduction as the cavern temperature does not reach the minimum temperature of this process. When using deeper caverns, this could be a factor.

Other contamination risks, like methanogenesis, are also not taken into account since it is assumed that the cavern lacks the necessary components for this reaction. This changes when there these components are available. For methanogenenis this is dependant on the amount of CO2 stored in the cavern, for example when its used as a cushion gas. Or when it is available through impurities of the gas input.

The cavern in this report is situated in a relatively highly pure halite salt slab in the Zechstein sea area. When building a cavern in other areas, the composition of the minerals in the salt slab could be very different, this might lead to different results. For example anhydrite rich areas could have a negative effect to the cavern suitability.

As discussed in chapter 4, the way the cavern is used will have a great effect on the H2S concentration of the cavern outflow. This report discusses a demand curve that supplies a hydrogen gas turbine for power production. In reality the use of the cavern can be very different then this scenario, therefore the build up in the cavern can be very different as well.

The process is designed following rough estimates and back of the envelope sizing guidelines. The process is designed as an indication of its possible capabilities and sequential (energy) costs. An improved design study is necessary to provide accurate data. Further investigation to the suitability of TEG dehydration of hydrogen gas is recommended. As is a design based on a different dehydration method such as pressure swing adsorption.

The process works at a pressure of 45 bar, based on the minimum grid pressure of 40 bar for natural gas. Further research is required to confirm the suitability of hydrogen gas processing at this pressure level in terms of leakage and suitability of package material.

Bibliography

[1] Wade A Amos. Costs of storing and transporting hydrogen. Technical report, National Renewable Energy Lab., Golden, CO (US), 1999.

[2] Andrzej Anderko and Malgorzata M Lencka. Computation of electrical conductivity of multicomponent aqueous systems in wide concentration and temperature ranges. *Industrial & engineering chemistry research*, 36(5):1932–1943, 1997.

[3] CAJ Appelo. Solute transport solved with the nernst-planck equation for concrete pores with 'free'water and a double layer. *Cement and Concrete Research*, 101:102–113, 2017.

[4] CAJ Appelo, David L Parkhurst, and VEA Post. Equations for calculating hydrogeochemical reactions of minerals and gases such as co2 at high pressures and temperatures. *Geochimica et Cosmochimica Acta*, 125:49–67, 2014.

[5] Gustave Erdman Archie. Introduction to petrophysics of reservoir rocks. *AAPG bulletin*, 34(5):943–961, 1950.

[6] Alireza Bahadori and Hari B Vuthaluru. Simple methodology for sizing of absorbers for teg (triethylene glycol) gas dehydration systems. *Energy*, 34(11):1910–1916, 2009.

[7] Albert-Laszlo Barabasi. Network science. *Philosophical Transactions of the Royal Society A: Mathematical, Physical and Engineering Sciences*, 371(1987):20120375, 2013.

[8] Edward P Bartlett. The concentration of water vapor in compressed hydrogen, nitrogen and a mixture of these gases in the presence of condensed water. *Journal of the American Chemical Society*, 49(1):65–78, 1927.

[9] JJ Baschuk and Xianguo Li. Modelling co poisoning and o2 bleeding in a pem fuel cell anode. *International Journal of Energy Research*, 27(12):1095–1116, 2003.

[10] Samia Ben Ahmed, Mohamed Mouldi Tlili, Mongi Amami, and Mohamed Ben Amor. Gypsum precipitation kinetics and solubility in the nacl–mgcl2–caso4–h2o system. *Industrial & Engineering Chemistry Research*, 53(23):9554–9560, 2014.

[11] Pierre Bérest, Arnaud Réveillère, David Evans, and Markus Stöwer. Review and analysis of historical leakages from storage salt caverns wells. *Oil & Gas Science and Technology–Revue d'IFP Energies nouvelles*, 74:27, 2019.

[12] O Bildstein, RH Worden, and E Brosse. Assessment of anhydrite dissolution as the rate-limiting step during thermochemical sulfate reduction. *Chemical Geology*, 176(1-4):173–189, 2001.

[13] HK Birnbaum and CA Wert. Diffusion of hydrogen in metals. *Berichte der Bunsengesellschaft für physikalische Chemie*, 76(8):806–816, 1972.

[14] Markus Bolhàr-Nordenkampf, Anton Friedl, Ulrich Koss, and Thomas Tork. Modelling selective h2s absorption and desorption in an aqueous mdea-solution using a rate-based non-equilibrium approach. *Chemical Engineering and Processing: Process Intensification*, 43(6):701–715, 2004.

[15] Markus Bolhàr-Nordenkampf, Anton Friedl, Ulrich Koss, and Thomas Tork. Modelling selective h2s absorption and desorption in an aqueous mdea-solution using a rate-based non-equilibrium approach. *Chemical Engineering and Processing: Process Intensification*, 43(6):701–715, 2004.

[16] Max Born. Volumen und hydratationswärme der ionen. *Zeitschrift für Physik A Hadrons and Nuclei*, 1 (1):45–48, 1920.

[17] CD Borsarelli. The partial molar volumes of hydrated proton and electron determined with time-resolved photoacoustic. In *Journal de Physique IV (Proceedings)*, volume 125, pages 11–13. EDP sciences, 2005.

[18] Elke Bozau, Steffen Häußler, and Wolfgang van Berk. Hydrogeochemical modelling of corrosion effects and barite scaling in deep geothermal wells of the north german basin using phreeqc and phast. *Geothermics*, 53:540–547, 2015.

[19] Franck Carbonero, Ann C Benefiel, Amir H Alizadeh-Ghamsari, and H Rex Gaskins. Microbial pathways in colonic sulfur metabolism and links with health and disease. *Frontiers in physiology*, 3:448, 2012.

[20] Kenneth L Cashdollar, Isaac A Zlochower, Gregory M Green, Richard A Thomas, and Martin Hertzberg. Flammability of methane, propane, and hydrogen gases. *Journal of Loss Prevention in the Process Industries*, 13(3-5):327–340, 2000.

[21] Rachid Chebbi, Muhammad Qasim, and Nabil Abdel Jabbar. Optimization of triethylene glycol dehydration of natural gas. *Energy Reports*, 5:723–732, 2019.

[22] Xuan Cheng, Zheng Shi, Nancy Glass, Lu Zhang, Jiujun Zhang, Datong Song, Zhong-Sheng Liu, Haijiang Wang, and Jun Shen. A review of pem hydrogen fuel cell contamination: Impacts, mechanisms, and mitigation. *Journal of Power Sources*, 165(2):739–756, 2007.

[23] D-T Chin and PD Howard. Hydrogen sulfide poisoning of platinum anode in phosphoric acid fuel cell electrolyte. *Journal of the Electrochemical Society*, 133(12):2447–2450, 1986.

[24] Ralf Cord-Ruwisch, W Kleinitz, F Widdel, et al. Sulfate-reducing bacteria and their activities in oil production. *Journal of Petroleum Technology*, 39(01):97–106, 1987.

[25] Fritz Crotogino. Traditional bulk energy storage—coal and underground natural gas and oil storage. In *Storing Energy*, pages 391–409. Elsevier, 2016.

[26] Fritz Crotogino. Larger scale hydrogen storage. In *Storing Energy*, pages 411–429. Elsevier, 2016.

[27] Christiane Dahl and Cornelius G Friedrich. *Microbial sulfur metabolism*. Springer, 2008.

[28] Manuel Antonio Díaz, Alfredo Iranzo, Felipe Rosa, Fernando Isorna, Eduardo López, and Juan Pedro Bolivar. Effect of carbon dioxide on the contamination of low temperature and high temperature pem (polymer electrolyte membrane) fuel cells. influence of temperature, relative humidity and analysis of regeneration processes. *Energy*, 90:299–309, 2015.

[29] H Djizanne, P Bérest, B Brouard, and A Frangi. Blowout in gas storage caverns. *Oil & Gas Science and Technology–Revue d'IFP Energies nouvelles*, 69(7):1251–1267, 2014.

[30] Hans Doornenbal and Alan Stevenson. *Petroleum geological atlas of the Southern Permian Basin area*. EAGE, 2010.

[31] J Dufour, DP Serrano, JL Galvez, J Moreno, and C Garcia. Life cycle assessment of processes for hydrogen production. environmental feasibility and reduction of greenhouse gases emissions. *International journal of hydrogen energy*, 34(3):1370–1376, 2009.

[32] Lars ErikØi. Comparison of aspen hysys and aspen plus simulation of co2 absorption into mea from atmospheric gas. *Energy Procedia*, 23:360–369, 2012.

[33] Stephen Foh, M Novil, E Rockar, and P Randolph. Underground hydrogen storage final report. *Inst. of Gas Tech., DOE, Brookhaven Natl Lab, Upton, NY (Dec. 1979)*, 1979.

[34] HD Frazier and AL Kohl. Selective absorption of hydrogen sulfide from gas streams. *Industrial & Engineering Chemistry*, 42(11):2288–2292, 1950.

[35] Yunjiao Fu, Wolfgang van Berk, and Hans-Martin Schulz. Hydrogen sulfide formation, fate, and behavior in anhydrite-sealed carbonate gas reservoirs: A three-dimensional reactive mass transport modeling approach. *AAPG Bulletin*, 100(5):843–865, 2016.

[36] MC Geluk. Late permian (zechstein) carbonate-facies maps, the netherlands. *Netherlands Journal of Geosciences*, 79(1):17–27, 2000.

[37] LH Gevantman and John Lorenz. *Physical properties data for rock salt*. Number 167. US Department of Commerce, National Bureau of Standards, 1981.

[38] Carlo Giavarini and Keith Hester. *Gas hydrates: Immense energy potential and environmental challenges*. Springer Science & Business Media, 2011.

[39] Gunther Glenk and Stefan Reichelstein. Economics of converting renewable power to hydrogen. *Nature Energy*, 4(3):216, 2019.

[40] Gerald James Spurgeon Govett. *Rock geochemistry in mineral exploration*. Elsevier, 2013.

[41] Hal Greenhouse. *Hermeticity of electronic packages*. Elsevier, 2000.

[42] Paul C Hanlon. *Compressor handbook*. McGraw-Hill„ 2001.

[43] Christina Hemme and Wolfgang van Berk. Potential risk of h2s generation and release in salt cavern gas storage. *Journal of Natural Gas Science and Engineering*, 47:114–123, 2017.

[44] Christina Hemme and Wolfgang Van Berk. Hydrogeochemical modeling to identify potential risks of underground hydrogen storage in depleted gas fields. *Applied Sciences*, 8(11):2282, 2018.

[45] Johannes Hierold and Peter Pilz. Physicochemical investigations of hydrogen storage in underground porous media–a contribution to the energy transition. In *EAGE/DGMK Joint Workshop on Underground Storage of Hydrogen*, volume 2019, pages 1–3. European Association of Geoscientists & Engineers, 2019.

[46] Thorsten Hörbrand, Thomas Baumann, and Helge C Moog. Validation of hydrogeochemical databases for problems in deep geothermal energy. *Geothermal Energy*, 6(1):20, 2018.

[47] IEA. The Future of Hydrogen. *International Energy Agency*, 2019.

[48] Pierre-André Jacques, Jari Ihonen, and Pauli Koski. Hycora–hydrogen contaminant risk assessment grant agreement no: 621223 review on the impact of impurities on pemfc and.

[49] Lara M Jochum, Xihan Chen, Mark A Lever, Alexander Loy, Bo Barker Jørgensen, Andreas Schramm, and Kasper U Kjeldsen. Depth distribution and assembly of sulfate-reducing microbial communities in marine sediments of aarhus bay. *Applied and environmental microbiology*, 83(23), 2017.

[50] Herrick L Johnston, Irving I Bezman, and Charles B Hood. Joule-thomson effects in hydrogen at liquid air and at room temperatures1. *Journal of the American Chemical Society*, 68(11):2367–2373, 1946.

[51] Makoto Kawase, Yoshihiro Mugikura, and Takao Watanabe. The effects of h 2 s on electrolyte distribution and cell performance in the molten carbonate fuel cell. *Journal of the Electrochemical Society*, 147(4): 1240–1244, 2000.

[52] Kavan Khaledi, Elham Mahmoudi, Maria Datcheva, and Tom Schanz. Stability and serviceability of underground energy storage caverns in rock salt subjected to mechanical cyclic loading. *International journal of rock mechanics and mining sciences*, 86:115–131, 2016.

[53] Nick Kimman. Power-to-gas efficiency of a hydrogen back-up system governed by interruptible sources and services. *http://resolver.tudelft.nl/uuid:46183251-f22a-42b5-a994-ed353d4338c0*.

[54] LE Klebanoff, JW Pratt, and CB LaFleur. Comparison of the safety-related physical and combustion properties of liquid hydrogen and liquid natural gas in the context of the sf-breeze high-speed fuel-cell ferry. *International Journal of Hydrogen Energy*, 42(1):757–774, 2017.

[55] Nikolay Ivanov Kolev. Solubility of o 2, n 2, h 2 and co 2 in water. In *Multiphase Flow Dynamics 4*, pages 209–239. Springer, 2011.

[56] Olaf Kruck, F Crotogino, R Prelicz, and T Rudolph. Overview on all known underground storage technologies for hydrogen. *Project HyUnder–Assessment of the Potential, the Actors and Relevant Business Cases for Large Scale and Seasonal Storage of Renewable Electricity by Hydrogen Underground Storage in Europe. Report D*, 3, 2013.

[57] S Shiva Kumar and V Himabindu. Hydrogen production by pem water electrolysis–a review. *Materials Science for Energy Technologies*, 2(3):442–454, 2019.

[58] Anna S Lord. Overview of geologic storage of natural gas with an emphasis on assessing the feasibility of storing hydrogen. *SAND2009-5878, Sandia National Laboratory, Albuquerque, NM*, 2009.

[59] Anna S Lord, Peter H Kobos, and David J Borns. Geologic storage of hydrogen: Scaling up to meet city transportation demands. *International journal of hydrogen energy*, 39(28):15570–15582, 2014.

[60] MR Louthan Jr, GR Caskey Jr, JA Donovan, and DE Rawl Jr. Hydrogen embrittlement of metals. *Materials Science and Engineering*, 10:357–368, 1972.

[61] X Luo, JN Knudsen, D De Montigny, T Sanpasertparnich, R Idem, D Gelowitz, R Notz, S Hoch, H Hasse, E Lemaire, et al. Comparison and validation of simulation codes against sixteen sets of data from four different pilot plants. *Energy Procedia*, 1(1):1249–1256, 2009.

[62] K.H. Lux. 2005.

[63] Douglas H MacKenzie, Francis Chiraka Prambil, CHRISTINA A Daniels, and Jerry A Bullin. Design & operation of a selective sweetening plant using mdea. *Energy Progress*, 7(1), 1987.

[64] Roy S Marlow et al. Cement bonding characteristics in gas wells. *Journal of petroleum technology*, 41 (11):1–146, 1989.

[65] MELLAPAK. Mellapak brochure, 2020. URL `http://web.ist.utl.pt/ist11061/de/Equipamento/Structured_Packings.pdf`.

[66] Industrial Metallurgists. Hydrogen embrittlement of steel, 2020. URL `https://www.imetllc.com/training-article/hydrogen-embrittlement-steel/`.

[67] Saeid Mokhatab, William A Poe, and John Y Mak. *Handbook of natural gas transmission and processing: principles and practices*. Gulf professional publishing, 2018.

[68] Mahesh Murthy, Manuel Esayian, Woo-kum Lee, and JW Van Zee. The effect of temperature and pressure on the performance of a pemfc exposed to transient co concentrations. *Journal of The Electrochemical Society*, 150(1):A29–A34, 2003.

[69] Richard A Oriani. The diffusion and trapping of hydrogen in steel. *Acta metallurgica*, 18(1):147–157, 1970.

[70] D Parkhurst and CAJ Appelo. Phreeqc (version 3)–a computer program for speciation. *Batch-Reaction, One-Dimensional Transport, and Inverse Geochemical Calculations (Denver, Colorado, USA, US Geological Survey, Water Resources Division)*, 2013.

[71] Prashant Patil, Zeeshan Malik, and Megan Jobson. Prediction of co2 and h2s solubility in aqueous mdea solutions using an extended kent and eisenberg model. In *Institution of Chemical Engineers Symposium Series*, volume 152, pages 498–510, 2006.

[72] John Polasek and J Bullin. Selecting amines for sweetening units. *ENERGY PROGRESS.*, 4(3):146–149, 1984.

[73] Donovan Porter, Alakendra N Roychoudhury, and Donald Cowan. Dissimilatory sulfate reduction in hypersaline coastal pans: activity across a salinity gradient. *Geochimica et Cosmochimica Acta*, 71(21): 5102–5116, 2007.

[74] Robert J Remick. Effects of h2s on molten carbonate fuel cells. *Progress Report, 1 Apr.-30 Jun. 1984 Institute of Gas Technology, Chicago, IL.*, 1985.

[75] Theo Bosma Rob van Gerwen, Marcel Eijgelaar. HYDROGEN IN THE ELECTRICITY VALUE CHAIN. *DNV GL*, 2019.

[76] Ian M Robertson, Petros Sofronis, A Nagao, ML Martin, S Wang, DW Gross, and KE Nygren. Hydrogen embrittlement understood. *Metallurgical and Materials Transactions A*, 46(6):2323–2341, 2015.

[77] Louis Schlapbach and Andreas Zuttel. Hydrogen-storage materials for mobile applications. In *Materials for sustainable energy: a collection of peer-reviewed research and review articles from nature publishing group*, pages 265–270. World Scientific, 2011.

[78] Zsolt Schléder, János L Urai, Sofie Nollet, and Christoph Hilgers. Solution-precipitation creep and fluid flow in halite: a case study of zechstein (z1) rocksalt from neuhof salt mine (germany). *International Journal of Earth Sciences*, 97(5):1045–1056, 2008.

[79] Vijay A Sethuraman and John W Weidner. Analysis of sulfur poisoning on a pem fuel cell electrode. *Electrochimica Acta*, 55(20):5683–5694, 2010.

[80] Zheng Shi, Datong Song, Jiujun Zhang, Zhong-Sheng Liu, Shanna Knights, Rajeev Vohra, NengYou Jia, and David Harvey. Transient analysis of hydrogen sulfide contamination on the performance of a pem fuel cell. *Journal of The Electrochemical Society*, 154(7):B609–B615, 2007.

[81] Zhuofan Shi, Kristian Jessen, and Theodore T Tsotsis. Impacts of the subsurface storage of natural gas and hydrogen mixtures. *International Journal of Hydrogen Energy*, 45(15):8757–8773, 2020.

[82] Min Sub Sim, David T Wang, Grant M Zane, Judy D Wall, Tanja Bosak, and Shuhei Ono. Fractionation of sulfur isotopes by desulfovibrio vulgaris mutants lacking hydrogenases or type i tetraheme cytochrome c3. *Frontiers in microbiology*, 4:171, 2013.

[83] Prabhu Soundarrajan and Frank Schweighardt. Hydrogen sensing and detection, 2008.

[84] F Strozyk, L Reuning, M Scheck-Wenderoth, and DC Tanner. The tectonic history of the zechstein basin in the netherlands and germany. In *Permo-Triassic Salt Provinces of Europe, North Africa and the Atlantic Margins*, pages 221–241. Elsevier, 2017.

[85] Jósef Szarawara and Andrzej Gawdzik. Method of calculation of fugacity coefficient from cubic equations of state. *Chemical Engineering Science*, 44(7):1489–1494, 1989.

[86] Radosław Tarkowski and Grzegorz Czapowski. Salt domes in poland–potential sites for hydrogen storage in caverns. *International Journal of Hydrogen Energy*, 2018.

[87] N Tarom, Md Mofazzal Hossain, and Azar Rohi. A new practical method to evaluate the joule–thomson coefficient for natural gases. *Journal of Petroleum Exploration and Production Technology*, 8(4):1169–1181, 2018.

[88] J Ter Meer, J Gerritse, C Di Mauro, MP Harkes, HHM Rijnaarts, AC Cinjee, Ir HC van Liere, Ir H Slenders, and RFW Baartmans. Hydrogen as indicator for in-situ redox condition and dechlorination. *Natural Attenuation of Environmental Contaminants*, pages 1–125, 1999.

[89] Nederlandse Gas Unie. Physical properties of natural gases. *N.V. Nederlandse Gasunie*, 1980.

[90] M Vanpee and RJ Mainiero. The spectral distribution of the blue hydrogen flame continuum and its origin in hydrogen nitric oxide flames. *Combustion and Flame*, 34:219–230, 1979.

[91] PTHM Verhallen, LJP Oomen, AJJMvd Elsen, J Kruger, and JMH Fortuin. The diffusion coefficients of helium, hydrogen, oxygen and nitrogen in water determined from the permeability of a stagnant liquid layer in the quasi-s. *Chemical Engineering Science*, 39(11):1535–1541, 1984.

[92] IEA WEO. International energy agency, world energy outlook 2016. *Paris Google Scholar*, 2016.

[93] Jiujun Zhang, Haijiang Wang, David P Wilkinson, Datong Song, Jun Shen, and Zhong-Sheng Liu. Model for the contamination of fuel cell anode catalyst in the presence of fuel stream impurities. *Journal of Power Sources*, 147(1-2):58–71, 2005.

[94] G Zimmermann, G Jacob, KH Lautenschläger, G Richter, and J Teschner. Wissensspeicher, 1986.

A

Appendix A: General Appendix

A.1. Hydrogen production

A.1.1. Production of hydrogen

Hydrogen can be produced through various processes, they are often categorised in to three colour groups; green, blue and grey. Grey hydrogen is produced with fossil fuels, with Steam Methane Reforming (SMR) the most common production process. Blue hydrogen follows the same process but with the addition of a CO_2 capturing and storing process, preventing it from reaching the atmosphere. Lastly, green hydrogen considers the production of hydrogen via green processes such as gasifying biomass, or through the electrolysis of water. Analysing the production processes does not fit directly in to the scope of this research, but is none the less essential as it establishes possible impurities in the hydrogen gas input.

Grey hydrogen

Most hydrogen today is produced using SMR. In this process high temperature steam (700 °C - 1000 °C) is used to produce hydrogen from methane. This happens at the presence of a catalyst under high pressure (3-25 bar). In this endothermic reaction; hydrogen and carbon monoxide are formed, as is seen in reaction A.1. Subsequently carbon monoxide and steam are reacted using a catalyst in what is called a water-gas shift reaction (A.2). In a final process step impurities and unwanted products are separated using pressure swing adsorption, essentially leaving pure hydrogen as the final product.

$$CH_4 + H_2O(+heat) \rightarrow CO + 3H_2 \tag{A.1}$$

$$CO + H_2O \rightarrow CO_2 + H_2(+heat) \tag{A.2}$$

Another grey hydrogen process is the gasification of coal. Coal gasification is a complex process of parallel-consecutive chemical reactions at high temperature with the organic part of coal and a gasification agent such as steam and oxygen. No combustion takes place at this temperature as the oxygen input is limited. The reaction generates carbon monoxide and hydrogen. Like with SMR, the reaction is followed by a water-gas shift reaction to transform a large portion of the remaining carbon monoxide to hydrogen. These two reactions are given in equations A.3 and A.4.

$$3C(Coal) + O_2 + H_2O \rightarrow 3CO + H_2 \tag{A.3}$$

$$CO + H_2O \rightarrow CO_2 + H_2 \tag{A.4}$$

Blue hydrogen

As mentioned in the introduction, blue hydrogen is simply the production of hydrogen through grey production methods and then capturing the carbon dioxide using Carbon Capture and Storage (CCS). There are three different types of CCS. Post combustion, by scrubbing a plants exhaust fumes. Pre-combustion by first converting the fossil fuel into a clean-burning gas and stripping out the CO_2 released by the process. Lastly, oxyfuel, uses pure oxygen in a combustion process, resulting in an exhaust gas that is almost pure CO2. All CCS processes have maximum trapping range of up to 90% of the carbon dioxide emissions. For hydrogen production this value is often lower as the carbon capturing happens post combustion, making the trapping process more difficult. Trapping is done via pressure swing absorption, membrane filtration, cryogenic separation or amine scrubbing [31]. Once the CO_2 is captured it is liquefied, transported and buried so that it does not escape into the atmosphere and contribute to climate change.

Green hydrogen

Green hydrogen is produced through a carbon neutral process. The primary green method of producing hydrogen is using electrolysis, a process that has been invented in 1800, but has been primarily used to reduced metals from salts, creating hydrogen as a by-product.

With new insights on hydrogen as an energy carrier, scientific priorities are turned giving rise to vast rising scientific research on the subject. Electrolysis of acidified water concerns the decomposition of water in to oxygen and hydrogen as given by equation A.7. The principal of alkalyne electrolysis of water is as followed: A DC electrical power source is connected to two electrodes, a cathode and an anode. The electrons from the electric current cause an oxidation/ reduction reactions. At the cathode, the electrons pass into the solution, the electrolyte, and cause a reduction. At the anode, the electrons leave the electrolyte and cause an oxidation. The reduction reaction is given in equation A.5, the oxidation reaction is given in A.6. Material choices of both the electrolye and the cathode and anode are highly influential on the reaction characteristics, as are

temperature, PH and applied voltage.
Another example is production using bio-mass. Although this process discharges CO_2, the production is considered carbon-neutral as the CO_2 that will be exhausted has been absorbed by the biomass from the atmosphere in the first place.

$$4H_2O + 4e^- \rightarrow 2H_2 + 4OH^- \tag{A.5}$$

$$4OH^- \rightarrow O_2 + 2H_2O + 4e^- \tag{A.6}$$

$$2H_2O(+electrical\ energy) \rightarrow O_2 + 2H_2 \tag{A.7}$$

A.2. Map of Zechstein sea, depth to base of Zechstein Z1 layer

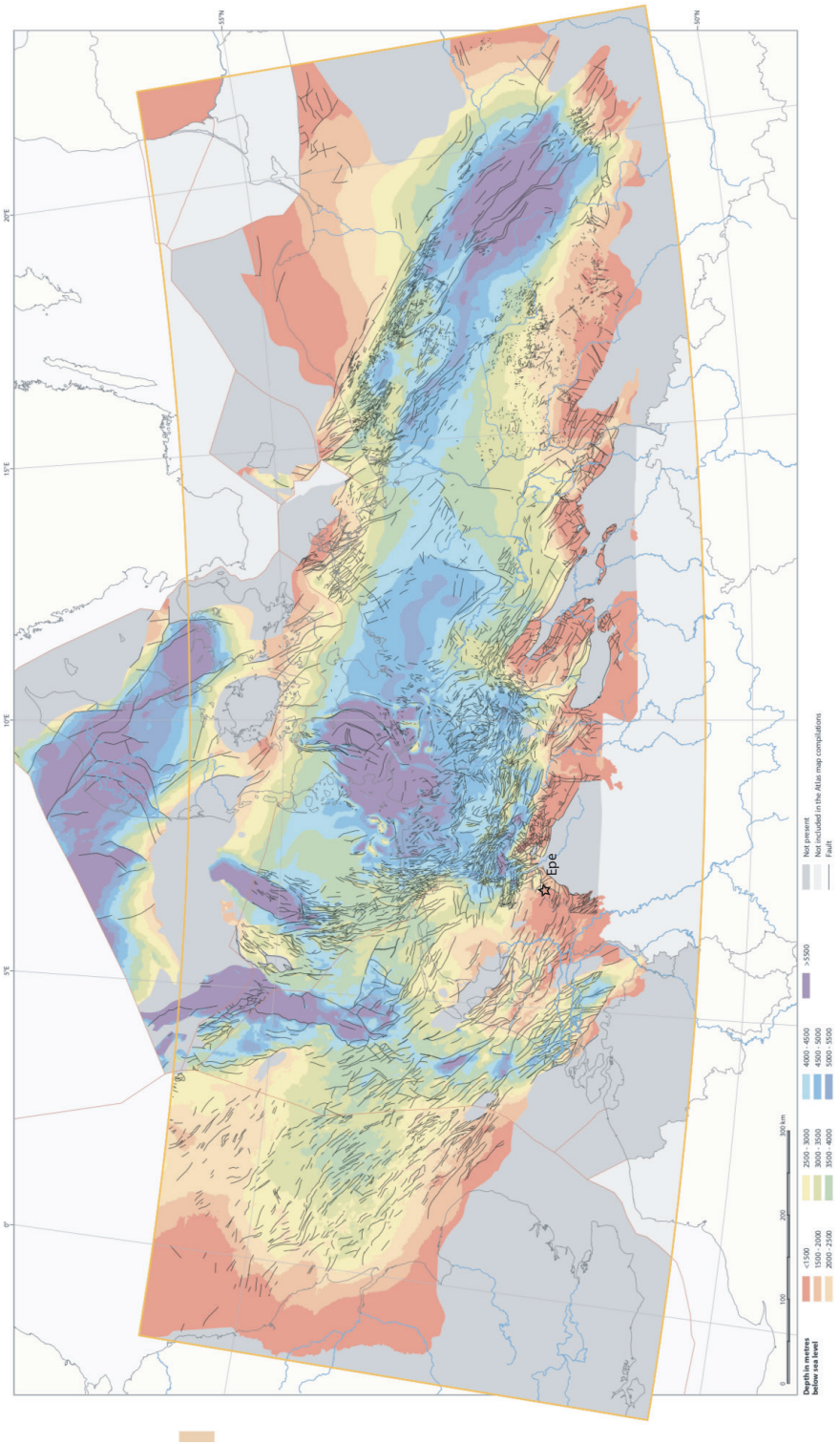

Figure A.1: Depth to base of Zechstein layer [30]

A.3. Leakage cases

A.3.1. Leakage cases historical analysis

Site	Time span between creation and failure	Leak mechanism
Elk City, Oklahoma	19 years?	Breach somewhere between 365 m and 35.5 m, upward in the cement, horizontal in the Doxey Formation
Conway/ Yoder, Kansas	5–60 years	Gas leaking from several faulty wells
Mont Belvieu,Texas	17 years	The leak was likely to be at caprock depth
Mineola, Texas	50 years	A breach in the casing originating from a pressure surge in a neighboring cavern
Hutchinson,Kansas	20 years	Gas migration through fractured channels to the brine aquifer below
Epe, Germany	34 years	Casing overstretching due to caverns convergence
Magnolia,Louisiana	33 years	Flaw in the casing at a,440-m depth, attributed to poor welding job.
Eminence,Mississippi	37–40 years	Fast cavern closure rate (40% in one year) frequent re-brining
Teutschenthal	c. 17 years	Ethylene accumulated in permeable layer, layer uplift led to overstretching of casing.
Boling, Texas	c. 22 years	Casing overstretch and failure, dragged down by the salt
Clute, Texas	c. 27 years	Effects of salt-dome internal movements

Table A.1: Main characteristics of salt cavern failures, including well ages in hydrocarbon storage leakage events.

A.3.2. Failures in Salt cavern storage

After the cavern is leached a number of tests are required prior to the first filling. It is necessary to carry out 3D seismic tests to ascertain the structural and sedimentary characteristics of the salt bed. Next to the seismic tests, sonar surveys are carried out to determine the overall cavern geometry as well as to supply detailed measurements of the sensitive and relatively narrow cavern neck and open borehole. Lastly, tightness tests are required to survey the sealability of the caverns as well as the borehole. Only when the seal requirements are met can the gas storage process be implemented by gas injection and brine discharge.
There are some intrinsic safety advantages concerning underground gas storage. For example, the lack of oxygen underground prevents explosions, the high fluid pressure is the normal state underground, and the cavern is naturally shielded against acts of violence. However to avoid future incidents and to get a complete analysis of critical areas, this sector will analyse historical leakages from salt cavern storage wells.[11] The leakage of gas will result in catastrophic influences on the environment and energy reserves. The cases analysed concern hydrocarbon storage facilities located at various depths around the world. Salt caverns are almost perfectly tight, therefore, the tightness fault in these historical cases is often found within the piping connecting the cavern to the surface. Causal distinction is made between the casing, the tubing and the cementation of the wells.

Well leakage

In most incidents a breach in the lowest part of the steel casing of the well causes the leakage. The breach can be created by internal or external corrosion, poor welding connection of different pipe segments, or excessive deformation of the rock formation. The age of the well is highly influential to the frequency of leakage occurring. This is caused by the time it takes for corrosion, excessive strains, tensile and shear stresses to build and take effect. Overview of different analysed salt cavern gas leak and the time between cavern creation and date of leakage is given in appendix A.3.
Due to the high viscosity of the rock salt and due to tectonic forces as explained in 2.3.2, the ground layers enclosing the salt caverns are slowly displacing and shifting, pressuring the well casing. The tensile strain that is

created by salt creep dragging down the casing, creating vertical forces, can lead to the casing overstretching and failure.
Important to note is that a breach in the steel casing in itself is insufficient to cause a full-blown leak. A leak can only develop when a pathway to an outlet exists, or is created. This outlet can be the surface, a porous or permeable ground layer, or a fault or jointed rock mass. When there is no pathway, or the cement job is sufficient, a breach in the casing will not lead to a leak. In many cases when a breach is created in the casing and the gas has an outlet through the cement the gas will find an underground receptor along the well casing. Especially when the enclosing rock is tight but the cementation is poor, the gas will mitigate upwards through the cemented annulus until it encounters a permeable layer. The underground receptor is often a permeable or porous zone, such as an aquifer, with a volume large enough to host the fleeing gas. The pressure differentiation created between the stored gas and the new found permeable receptor is the driving force of the leak. When the cavern is full and gas pressure is at a maximum, the pressure of the stored gas is significantly higher then the geostatic pressure at almost any possible leak location. Pressure effects of casing leaks is illustrated in figure A.2, the gas finds an aquifer where the hydrostatic pressure lower then the stored gas pressure, creating the driving force for the gas seepage.

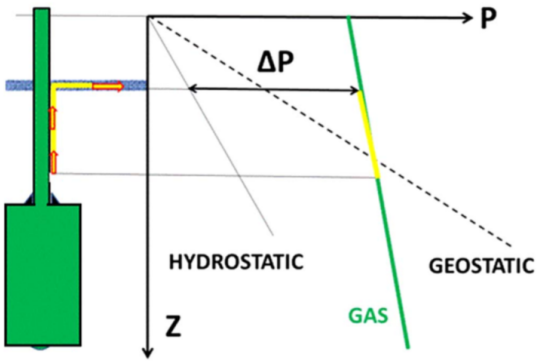

Figure A.2: A gas leaks from a breach in the casing. Gas migrates through the cement and reaches a shallower aquifer layer, at which point its pressure is much higher than in situ groundwater pressure and even, in many cases, higher than geostatic pressure. [11]

A.4. Dehydration graphs

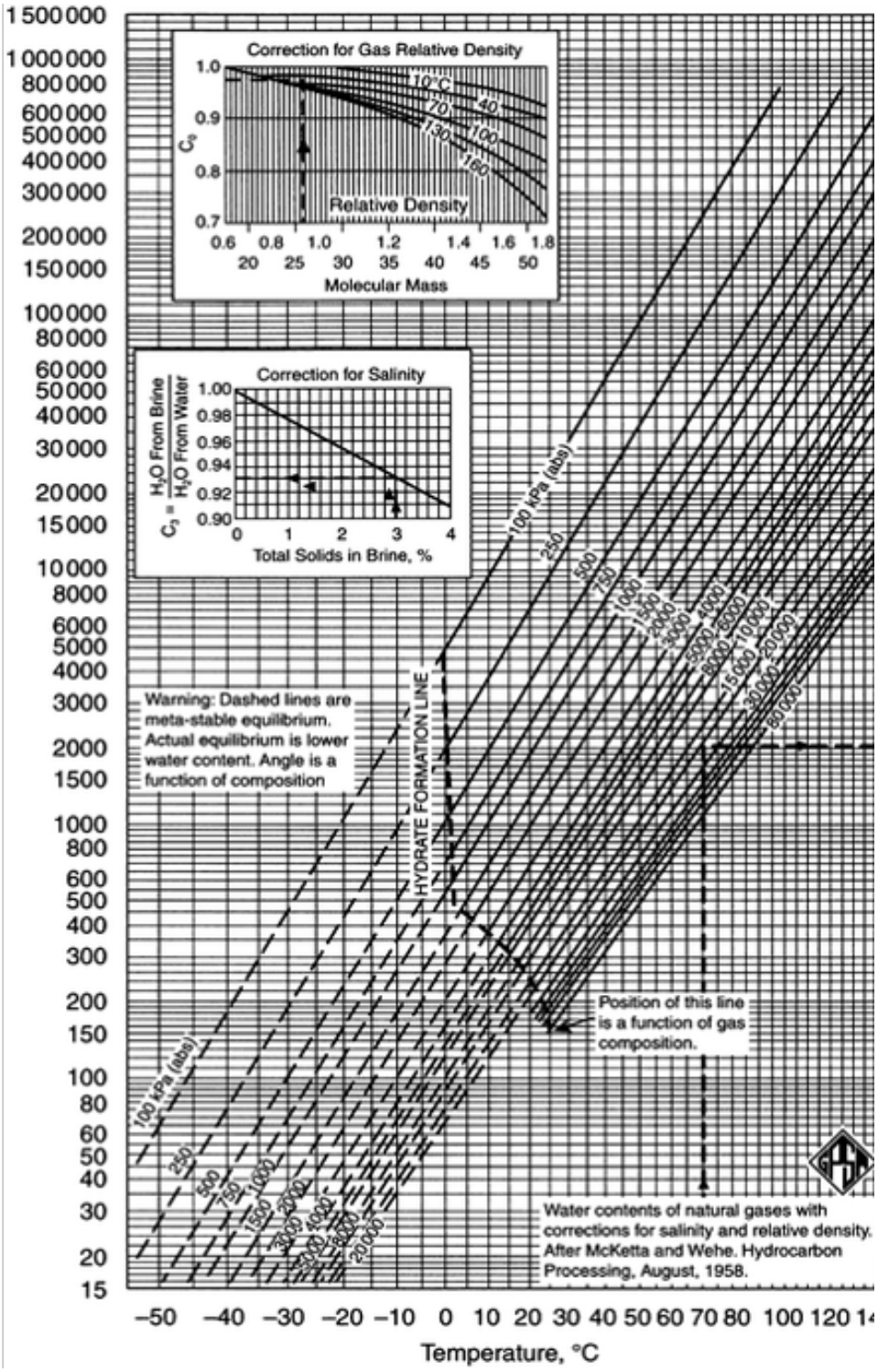

Figure A.3: Water content of natural gas as a function of pressure and temperature (Mc Ketta-Wehe chart) [38]

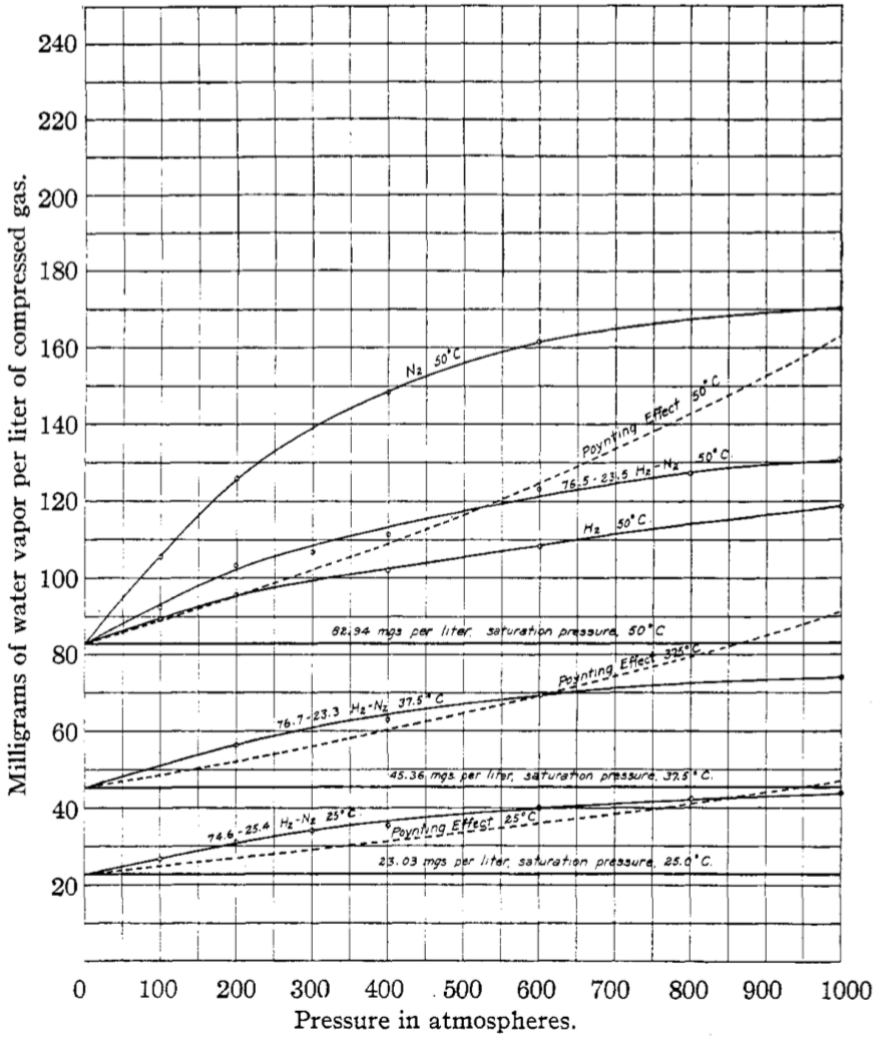

Figure A.4: Water-vapor content of compressed hydrogen gas in contact with liquid water, 25.0°, 37.5°, 50.0°. [8]

A.5. Phreeqc model explanation

All of the equations in this section are credited to the creators of PHREEQC, Parkhurst and Apello.

Gas-liquid equilibrium reactions

An important factor to calculating the conversion of hydrogen gas to other substances is finding the amount of hydrogen that will dissolve in the brine water. This is dependant to the solubility of hydrogen in the brine solution. Solubility m_i, or molality (mol per kilogram water), is dependant on a variety of parameters and in this case can not be taken as a constant taken from literature considering the conditions of the storage atmosphere. Solubility can be calculated from the fugacity, the molar volume in aqueous solution, and the equilibrium constant (Henry's constant). Solubility and aqueous diffusion calculations are explained in more detail by Parkhurst and Apello in articles [4], [70], [3] also in the phreeqc.dat file itself. To make conclusions on the effects of differentiation of variables in the model made with PHREEQC a summary is made on the leading calculations used in the program/ database combination.
The solubility of a gas is calculated in phreeqc.dat via equation A.8. Here, P_i the pressure and P_0 the standard state pressure (both in bar), ϕ is the fugacity coefficient, m_0 is the molality (in $molkgw$) for the gas in

standard state ($1atm$), and γ is the activity coefficient in water and K_H is Henry's constant .

$$m_i = \frac{\frac{P_i}{P_0}\phi_i}{\frac{\gamma_i}{m_0}K_H} \tag{A.8}$$

Where Henry's constant, which defines the ratio between the aqueous and gas fraction of a chemical species at equilibrium, is defined for each species with either a temperature independent constant log(K_H) or with the temperature dependant analytical expression A.9.

$$log_{10}K_H = A_1 + \frac{A_2}{T} + A_4 log_{10}T + \frac{A_5}{T^2} \tag{A.9}$$

$A_{1...5}$ are gas dependant constants defined in the database.
To calcluate the activity coefficient, the database will use extended Debye-Hückel equation A.11. This uses the two Debye-Hückel constants (a^0 and b_γ), I is the ionic strength, z the charge number of the ion, and A and B are constants dependant to the temperature used in the model.

$$log(K_p) = log(K_{P=1atm}) - \frac{\Delta V_r}{2.303 \times RT}(P-1) \tag{A.10}$$

To adjust the equilibrium constant for pressure, equation A.10 is used, which uses ΔV_r which is the molar volume change of the reaction in cm^3/mol. The molar volume is defined for each solid-liquid reaction separately in phreeqc.dat. The default is 0 cm^3/mol, when undefined, which would result in no change as a result of pressure differentiation.

$$log\gamma_i = \frac{-Az_i^2\sqrt{I}}{1+Ba^0\sqrt{I}} + b_\gamma I \tag{A.11}$$

The fugacity constant (ϕ) is determined by the excess free energy which can be determined using the equation of state (EOS), phreeqc.dat uses the well-known Peng-Robinson cubic EOS, which is given in equation A.12. The Peng-Robinson formulas enable an accurate estimate of the $P - V_m$ relationship for a gas.

$$P = \frac{RT}{V_m - b} - \frac{a\alpha}{V^2 + 2bV_m - b^2} \tag{A.12}$$

Here, R is the ideal gas constant, V_m is the molar volume in $\frac{cm^3}{mol}$, b is the gas' minimal volume, a is the van Der Waal attraction and α is a correction taken from the acentric factor; a is given in equation A.13, b is given in equation in equation A.14 and α is given in A.15.

$$a = 0.456235\frac{(RT_c)^2}{P_c} \tag{A.13}$$

$$b = 0.077796\frac{RT_c}{P_c} \tag{A.14}$$

$$\alpha = (1 + (0.37464 + 1.54226\omega - 0.26992\omega^2)(1 - \sqrt{(\frac{T}{T_c})}))^2 \tag{A.15}$$

In these equations P_c and T_c are the critical pressure and temperature respectively. ω is the molecule dependant acentric factor acentric factor. When P_c and T_c are not defined in the database phreeqc.dat, PHREEQC will use the ideal gas law. When considering gas mixtures, Peng and Robinson used the weighted sum of a, b and ω:

$$b = b_{sum} = \sum y_i b_i \tag{A.16}$$

and

$$a\alpha = a\alpha_{sum} = \sum_i (\sum_j (y_i y_j (a_i\alpha_i * a_j\alpha_j)^{0.5}))(1 - k_{ij}) \tag{A.17}$$

Where y_i is the mole fraction of gas i in the mixture, and k_{ij} is a binary interaction parameter for gas i and j. The fugacity can be calculated via the Peng Robinson EOS which is showed in equation A.18. This is further explained in article [85].

$$ln(\phi) = (\frac{PV_m}{RT} - 1) - ln(\frac{P(V_m - b)}{RT} + \frac{a\alpha}{2.828bRT}\dot{l}n(\frac{V_m + 2.414b}{V_m - 0.414b}) \tag{A.18}$$

Gas	Equilibrium reaction	log K_H	T_C	P_C	ω
H_2 (g)	$H_{2(g)} = H_{2(aq)}$	-3.1050	33.2	12.8	0.225
O_2 (g)	$O_{2(g)} = O_{2(aq)}$	-2.8983	154.6	49.8	0.021
N_2 (g)	$N_{2(g)} = N_{2(aq)}$	-3.1864	126.2	33.5	0.039
H_2S (g)	$H_2S = H^+ + HS^-$	-7.9759	373.2	88.2	0.1
CH_4 (g)	$CH_{4(g)} = CH_{4(aq)}$	-2.8	190.6	45.3	0.008
NH_3 (g)	$NH_{3(g)} = NH_{3(aq)}$	1.7966	405.6	111.3	0.25

Table A.2: Important gas equilibrium -reactions, -constants at 25°C 1atm, the critical pressure and temperature and acentric factor.

For the calculation of fugacity and for the Peng Robinson equation it is required to find the apparent molar volumes, for which PHREEQC uses the Helgeson–Kirkham–Flower-modified-Redlich–Rosenfeld (HKFmoRR) equation as given in equations A.19 and A.20.

$$V_{m,i} = V^0_{m,i} + A_v 0.5 z_i^2 \frac{I^{0.5}}{1 + a_i^o b_\gamma I^{0.5}} + (b_{1,i} + \frac{b_{2,i}}{T - 228} + b_{3,i}(T - 228) I^{b_{4,i}} \tag{A.19}$$

$$V^0_{m,i} = 41.84(0.1 a_{1,i} + \frac{100 a_{2,i}}{2600 + P_{bar}} + \frac{a_{3,i}}{T - 228} + \frac{10^4 a_{4,i}}{(2600 + P_{bar})(T - 228)} - \omega \frac{\delta \epsilon_r^{-1}}{\delta P_{bar}}) \tag{A.20}$$

In these two formulas $a_{1..4}$ and ω are parameters for individual solutes given in phreeqc.dat $b_{1..4}$ are adjustable coefficients for fitting experimental data also defined for relevant ions in phreeqc.dat. Sources of the data are given by Apello and Parkhurst in article [4]. I is the ionic strength, ϵ_r is the relative dielectric constant of pure water, z_i is the charge number of the ion. a^o and B_γ are the Debye-Hückel parameters also used for the activity calculations. $\omega \frac{\partial \epsilon_r^{-1}}{\partial P_{bar}}$ is the energy of solvation, calculated from ω and the pressure dependence of the Born equation [16]. The molar volume of a salt then becomes

$$V_m = \sum \upsilon_i V_{m,i} \tag{A.21}$$

Here υ_i is the stoichiometric coefficient of element i in the salt.
The coefficients of the HKFmoRR are described in article [4] and are relative to H^+, which means the molar volume of H^+ is considered 0. The actual partial molar volume of a proton, and thus of H^+, is empirically determined to be around $-5.6 cm^3/mol$ [17], but it's pressure cancels in the calculation of the pressure-dependent solubility. This is because for a solid, dissolving in water, the aqueous volume is
$V_{m,real} = \sum \upsilon_i (V_{m,i} - z_i V_{m,H^+})$. So as z_{H^+} is 1, $V_{m,real,H+}$ will be 0.

Diffusion rate of aqueous species in brine solution
Another important factor that effects both equilibrium and kinetic reactions present in the model is the diffusion coefficient of the available substances.

PHREEQC gives the option to define a standard singular diffusion coefficient. Or, in combination with phreeqc.dat, to enable multi component diffusion. With multi component diffusion, each solute can be given, or is given, its own diffusion coefficient, allowing it to diffuse at its own rate. With this function enabled, the diffusive flux is calculated via equation A.22.

$$J_i = -(D_{w,i} \times \epsilon^n) \left(\frac{\partial ln(\gamma_i)}{\partial ln(c_i)} + 1 \right) grad(c_i) + CBt_i \tag{A.22}$$

In the equation i indicates the species; J is the flux in $mol \cdot m^{-2} s^{-1}$ and $D_{w',i}$ is the species dependant corrected diffusion coefficient in $\frac{m^2}{s}$; ϵ is the porosity, which in our model is taken from literature to be 20% for the sump [43]; n is an empirical component from Archie's law [5], expected to be around 1; c_i is the concentration in mol/m^3; $grad(c_i)$ is the concentration gradient in mol/m^4. Lastly CBt_i is the charge balance term, which is either defined in the model or (re-)calculated by PHREEQC.

The diffusion coefficient is given as a constant $D_{w,0}$ (for the species in pure water at 25 °Celsius, for H_2 this is taken as 9.31e-9) and is then corrected twice. Once for the temperature (as proposed by Smolykov [2] in equation A.23) and once for the ionic strength of the brine as by equations A.24 and A.25. This further explained by Apello in article [3].

$$D_{w,TK} = D_{w,0} \times exp\left(\frac{c_1}{T} - \frac{c_1}{T_{atm}}\right)\frac{\eta_0 T}{T_{atm}\eta} \tag{A.23}$$

$$D_{w,I} = D_{w,TK} \times exp\left(\frac{c_2 a^o |z_i| \sqrt{I}}{1+\kappa\alpha}\right) \tag{A.24}$$

$$\kappa\alpha = (10^{10} \times \kappa)^{-1}\frac{c_3}{1+I^{0.75}} \tag{A.25}$$

Here $c_1 ... c_3$ are substance dependant coefficients defined in the phreeqc.dat database, a^o is a Debye Hückel parameter in $\frac{mol}{dm^3}^{-0.5}$, η is the viscosity and η_0 is the viscosity of pure water at 25 °C (both in $Pa \cdot s$).

Solid-liquid equilibrium reactions

Table A.3 defines the solid-liquid equilibrium reactions that are taken into account, as inputs or as possible secondary phases, in both chemical models. It also defines the equilibrium constants that are defined in phreeqc.dat. The equilibrium constants are defined for 25 °C at 1 atm, however these can be adjusted for temperature and pressure. The database phreeqc.dat gives the standard equilibrium constants. For most substances it will also give the standard enthalpy of reaction, making it possible to adjust the equilibrium constant for temperature using the van 't Hoff equation A.26. Here K_1 is the equilibrium constant at the temperature T_1, which is 25 °C, while K_2 is the equilibrium constant at the temperature defined in the input model, T_2.

$$ln\frac{K_2}{K_1} = \frac{-\Delta V_r}{R}\left(\frac{1}{T_2} - \frac{1}{T_1}\right) \tag{A.26}$$

For the most common or defining reactions equation A.27 is used to get an accurate equilibrium constant dependant on temperature. Where $A_{1...5}$ are analytical constants defined in the database.

$$log_{10}(K_p) = A_1 + \frac{A_2}{T} + A_4 log_{10} T + \frac{A_5}{T^2} \tag{A.27}$$

Equilibrium phase	**Equilibrium reaction**	**log K**
Halite	$NaCl \rightleftharpoons Cl^- + Na^+$	1.570
Anhydrite	$CaSO_4 \rightleftharpoons Ca^{2+} + SO_4^{2-}$	-4.39
Siderite	$FeCO_3 \rightleftharpoons Fe^{2+} + CO_3^{2-}$	-10.89
Goethite	$FeO(OH) + 3H^+ \rightleftharpoons Fe^{+3} + 2H_2O$	-1.0
Pyrite	$FeS_2 + 2H^+ + 2e^- \rightleftharpoons Fe^{+2} + 2HS^-$	-18.479
Mackinawite	$FeS + H^+ \rightleftharpoons Fe^{2+} + HS^-$	-4.648
Sulfur	$S + 2H^+ + 2e^- \rightleftharpoons H_2S$	4.882
Gypsum	$CaSO_4 : 2H_2O \rightleftharpoons Ca^{2+} + SO_4^{2-} + 2H_2O$	-4.58
Calcite	$CaCO_3 \rightleftharpoons CO_3^{2-} + Ca^{2+}$	-8.48
H_2S	$H_2S \rightleftharpoons HS^- + H^+$	-6.994
HS^-	$H_2S \rightleftharpoons S^{-2} + H^+$	-12.918

Table A.3: Important equilibrium -phases, -equations and -constants (log K, at 25°C and 1atm) taken in to account. Data from phreeqc.dat

A.6. 3D representation cavern S43

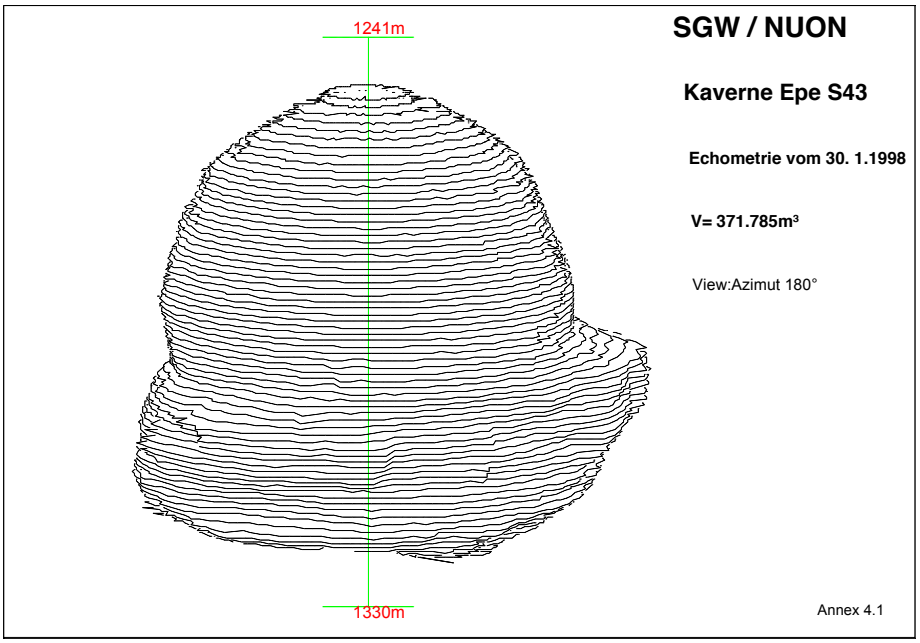

A.7. Drilling log cavern S43

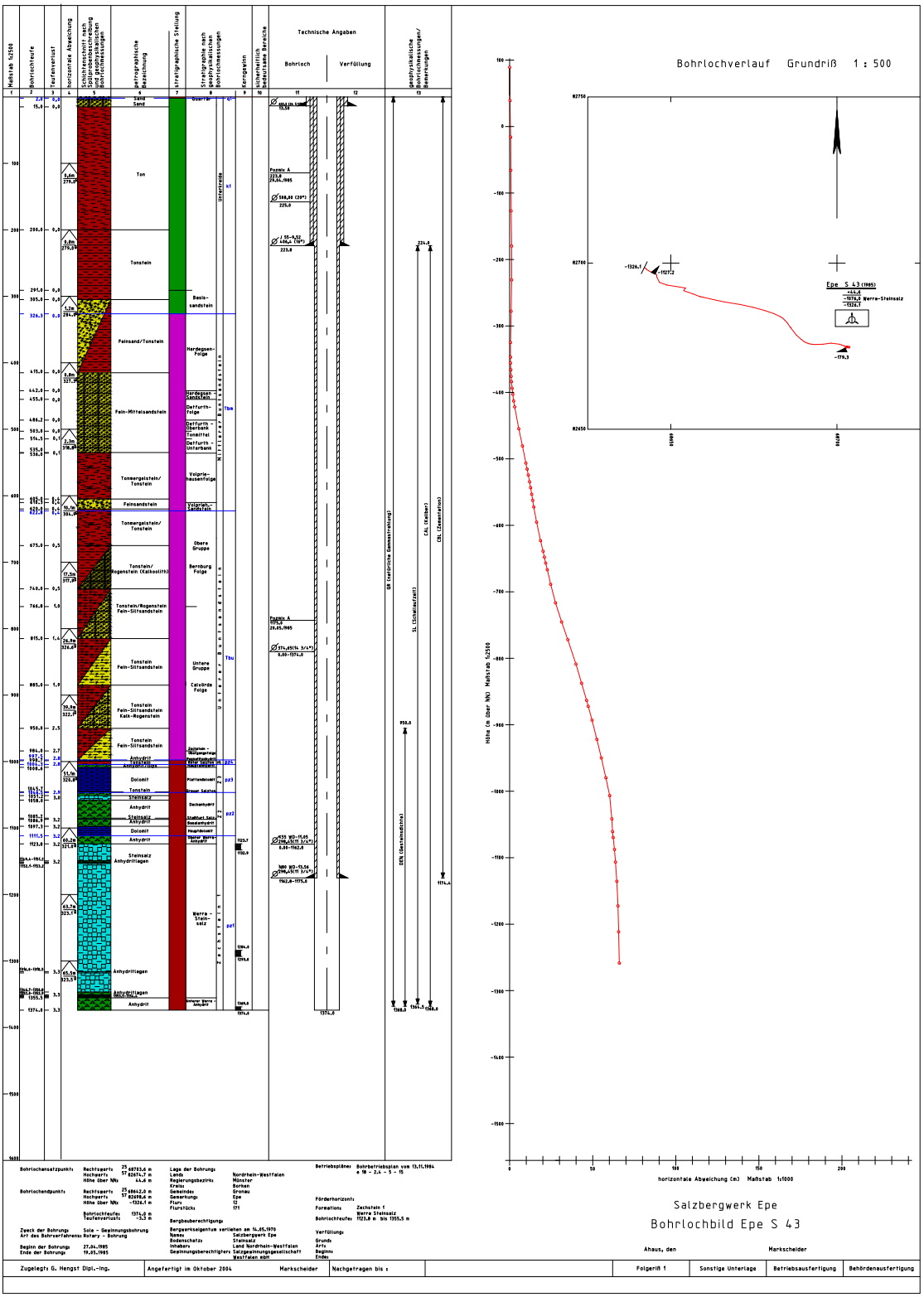

A.8. Soil testing on Cavern S43

Open Grid Europe GmbH Kompetenzcenter Gasqualität

Open Grid Europe
The Gas Wheel

Laborprobenummer	**19-0146**
Probenahmeort	**Epe**
Betrieb/Anlage	**Fa. Nuon**
Probestelle	**Feststoffprobe**
Auftragsnummer	**CA-18-6392**
Charge/Information	**K. S43 Klumpen auf USAV**
Probenahmedatum	**14.01.2019 14:46**
Probeneingang	**14.01.2019**
Probenstatus	**Archiv (Prüfbericht)**

Originalprobe		
Leco CS 300	Kohlenstoff	**0,43** Masse %
	Schwefel	**< 0.5** Masse %
Soxleth	Extraktionsmittel	**Dichlormethan**
	Extrahierbare Anteile	**9,8** Masse %
Extraktionsrückstand		
Sensorisch	Farbe	**braun**
Sensorisch	Konsistenz	**feinpulverig**
Leco CS 300	Kohlenstoff	**< 0.02** Masse %
DIN EN 15309	Silizium	**< 0.01** Masse %
DIN EN 15309	Aluminum	**0,01** Masse %
DIN EN 15309	Eisen	**1,94** Masse %
DIN EN 15309	Titan	**< 0.01** Masse %
DIN EN 15309	Calcium	**0,04** Masse %
DIN EN 15309	Magnesium	**0,14** Masse %
DIN EN 15309	Barium	**< 0.01** Masse %
DIN EN 15309	Strontium	**< 0.01** Masse %
DIN EN 15309	Mangan	**0,02** Masse %
DIN EN 15309	Natrium	**39,1** Masse %
DIN EN 15309	Kalium	**< 0.01** Masse %
DIN EN 15309	Schwefel	**0,42** Masse %
DIN EN 15309	Phosphor	**< 0.01** Masse %
DIN EN 15309	Chlor	**57,31** Masse %
DIN EN 15309	Fluor	**< 0.01** Masse %
DIN EN 15309	Brom	**< 0.01** Masse %
DIN EN 15309	Zink	**< 0.01** Masse %
DIN EN 15309	Kupfer	**< 0.01** Masse %
DIN EN 15309	Nickel	**< 0.01** Masse %
DIN EN 15309	Chrom	**0,04** Masse %
DIN EN 15309	Kobalt	**< 0.01** Masse %
DIN EN 15309	Blei	**< 0.01** Masse %

Quelle: Open Grid Europe GmbH Kompetenzcenter Gasqualität, LISA-Datenbank (Archiv)
Ersteller: Dominique Dominique (D6591) am: 24.01.2019 15:59:46

A.9. Cost analysis by Aspen Economic Analyzer

Compression (A)	*Capital Cost*	*Installation Cost*
Compressor A	€ 2,487,408	€ 2,773,848
Cooler A1	€ 356,752	€ 725,208
Cooler A2	€ 202,576	€ 879,472
Gas sweetening (B)		
Absorber B	€ 57,376	€ 200,464
Heat Exchanger B	€ 7,304	€ 54,208
Make-up B	€ 15,612	€ -
Scrubber B	€ 45,672	€ 171,072
Condenser B	€ 6,776	€ 41,008
Reboiler B	€ 70,161	€ 239,367
Cooler B1	€ 8,712	€ 77,528
Pump B	€ 3,872	€ 25,608
Gas dehydration (C)		
Separator drum C	€ 19,712	€ 90,200
Pump C	€ 43,208	€ 68,024
Heat exchanger C	€ 7,216	€ 47,520
Absorber C	€ 59,048	€ 192,984
Cooler C	€ 9,592	€ 90,200
Make up C	€ 3,578	€ -
Scrubber C	€ 40,200	€ 179,300
Reboiler C	€ 11,000	€ 76,400
Condenser C	€ 8,600	€ 60,100
	€ -	
Total	€ 9,456,885	
Total A	€ 7,425,264	79%
Total B	€ 1,024,740	11%
Total C	€ 1,006,882	11%
OPEX	€ 1,260	

Table A.4: Cost estimation by Aspen Economic Analyser.

A.10. Energy analysis by Aspen Hysys

Compression (A)	**Power [MW]**
Compressor 1	9.40E+00
Cooler 1	- 7.80E+00
Cavern	-
Cooler 2	- 1.40E+00
Gas Sweetening (B)	
Heat exchanger	6.30E-02
Cooler	- 5.00E-02
Pump	2.30E-03
Condenser	4.9E-01
Reboiler	6.5E-01
Dehydration (C)	
Heat exchanger	4.00E-02
Cooler	- 8.30E-02
Pump	1.80E-03
Condenser	- 4.9E-01
Reboiler	2.9E-01
Total power [MW]	11.4
Total gas flow [kmole/hr]	5173
Total Gibbs energy [MW]	340.8
Energy losses total [%]	3.06%
Energy losses by cavern storage [%]	2.76%
Energy losses by gas sweetening	0.2%
Energy losses by dehyfration	0.16%

Table A.5: Energy costs as required by the specified purification process.